

NEW EXTENDED DEUTERIUM FRACTIONATION MODEL: ASSESSMENT AT DENSE ISM CONDITIONS AND SENSITIVITY ANALYSIS

T. ALBERTSSON^{1,*}, D. A. SEMENOV¹, A. I. VASYUNIN², TH. HENNING¹, AND E. HERBST²

(1) Max-Planck-Institut für Astronomie, Königstuhl 17, 69117 Heidelberg, Germany

(2) Departments of Chemistry and Astronomy, University of Virginia, Charlottesville, VA 22904, USA

* Visiting scientist at University of Virginia, Charlottesville

Draft version February 25, 2024

ABSTRACT

Observations of deuterated species are useful in probing the temperature, ionization level, evolutionary stage, chemistry, and thermal history of astrophysical environments. The analysis of data from ALMA and other new telescopes requires an elaborate model of deuterium fractionation. This paper presents a publicly available chemical network with multi-deuterated species and an extended, up-to-date set of gas-phase and surface reactions. To test this network, we simulate deuterium fractionation in diverse interstellar sources. Two cases of initial abundances are considered: i) atomic except for H₂ and HD, and ii) molecular from a prestellar core. We reproduce the observed D/H ratios of many deuterated molecules, and sort the species according to their sensitivity to temperature gradients and initial abundances. We find that many multiply-deuterated species produced at 10 K retain enhanced D/H ratios at temperatures $\lesssim 100$ K. We study how recent updates to reaction rates affect calculated D/H ratios, and perform a detailed sensitivity analysis of the uncertainties of the gas-phase reaction rates in the network. We find that uncertainties are generally lower in dark cloud environments than in warm IRDCs and that uncertainties increase with the size of the molecule and number of D-atoms. A set of the most problematic reactions is presented. We list potentially observable deuterated species predicted to be abundant in low- and high-mass star-formation regions.

Subject headings: astrochemistry – molecular processes – methods: numerical – ISM: clouds, molecules – stars: circumstellar matter, protostars

1. INTRODUCTION

The life cycle of molecules covers a wide range of environments, starting from the sparse interstellar medium (ISM), which eventually evolves into stars and planets. As molecular hydrogen cannot be easily observed in the cold interstellar medium, other molecular tracers are employed to probe the relevant physical conditions and chemical composition. More than 170 molecules have been observed in the interstellar medium to date¹, ranging from diatomic species to the fullerenes C₆₀ and C₇₀ (Cami et al. 2010) and including deuterated species. A variety of deuterated species have been detected in various astrophysical environments, including molecular clouds: DCO⁺ (van der Tak et al. 2009; Guélin et al. 1977), DNC (van der Tak et al. 2009; Turner & Zuckerman 1978), H₂D⁺ (Parise et al. 2011; Stark et al. 1999), HDCO (Loren & Wootten 1985), D₂CO (Turner 1990), HD₂⁺ (Parise et al. 2011), HDO (Phillips et al. 1973); pre-stellar cores: D₂CO (Bacmann 2004), H₂D⁺ (Caselli et al. 2003; Vastel et al. 2006; Caselli et al. 2008), HD₂⁺ (Vastel et al. 2012), N₂D⁺ (Miettinen et al. 2012), NHD₂ (Roueff et al. 2000); hot cores/corinos: D₂CO, HDCO (Bergman et al. 2011), DCOOCH₃ (Demyk et al. 2010; Margulès et al. 2010), HD₂⁺ (Vastel et al. 2004), HDO, NH₂D (Jacq et al. 1990); warm protostellar envelopes: DCO⁺, HDCO (Parise et al. 2009), HDO (Jørgensen & van Dishoeck 2010; Liu et al. 2011), OD (Parise et al. 2012); protoplanetary disks: DCN, DCO⁺ (van Dishoeck et al. 2003; Guilloteau et al. 2006; Qi et al. 2008) and comets: CH₃D (Bonev et al. 2009; Gibb et al. 2012), HDCO (Kuan et al. 2008), HDO (Villanueva et al. 2009; Hartogh et al. 2011;

Gibb et al. 2012). For comprehensive reviews, we refer to Roueff & Gerin (2003) and Bergin et al. (2007). The study of deuterium chemistry has proven useful to constrain the ionization fraction, density and thermal history of the ISM and protoplanetary disks (e.g., Geiss & Reeves 1981; Aikawa & Herbst 2001; Crapsi et al. 2005; Willacy 2007; Öberg et al. 2012).

Still, many more deuterated species of key importance remain to be detected. Upon the completion of the high-sensitive, high-resolution Atacama Large Millimeter Array (ALMA), we will be able to, for the first time, detect and spatially resolve emission lines of numerous new complex and rare-isotope molecules. In order to analyze these rich observational data, new astrochemistry models including isotope-exchange reactions and state-to-state processes will be required. The main goal of the present paper is to present and provide a new extended, public deuterium fractionation model, and to explore its validity and accuracy.

The implementation of deuterium chemistry is a challenging task though because of a limited number of accurately determined rate coefficients of relevant reactions, and the sheer number of hydrogen-dominated reactions in astrochemical networks. Previous studies used the available limited set of reaction data, substituted with “educated guesses” for missing reaction rates, and cloned data from similar reactions involving hydrogen-bearing species (e.g., Herbst 1982; Brown et al. 1988; Rodgers & Millar 1996; Charnley et al. 1997; Turner 2001; Aikawa et al. 2003, 2012; Sipilä et al. 2013). In many cases only mono- and double-deuterated species were considered. We follow the general approach, but abandon the restriction on the total number of deuterons in chemical species.

The redistribution of elemental deuterium, initially locked mainly in HD, is initiated by fast ion-molecule reactions with

¹ [http://www.astrochymist.org/astrochymist\\$_mole.html](http://www.astrochymist.org/astrochymist$_mole.html)

polyatomic ions, such as H_3^+ (and H_2D^+ , HD_2^+ , D_3^+). Due to zero-point vibrational energy differences between modes with D and H, and the lack of a ground rotational state for H_3^+ , the backward reactions between H_2 and H_3^+ isotopologues are endothermic, with barriers of $\sim 100\text{--}300\text{ K}$, leading to the initial enrichment of abundances of the H_3^+ isotopologues at $\lesssim 20\text{--}30\text{ K}$. In a similar way, other ions such as CH_2D^+ and C_2HD^+ allow deuterium fractionation to proceed effectively at warmer temperatures of $\lesssim 30\text{--}80\text{ K}$ because of larger endoergicities for the backward reactions (e.g., Millar et al. 1989; Roueff et al. 2005; Parise et al. 2009). These deuterated ions react further with abundant molecules such as CO and N_2 , transferring deuterium atoms to new molecules. These findings have been proven both observationally and theoretically (see, e.g., Bacmann et al. 2002, 2003; Roberts et al. 2003; van der Tak 2006; Roberts & Millar 2006; Caselli et al. 2008). The initial gas-phase deuterium enrichment of H_3^+ is even more pronounced in cold, dense regions, where some destructive neutral species, especially CO, become severely depleted onto dust grain surfaces. The dissociative recombination of abundant H_3^+ isotopologues leads to a high flux of D atoms ($\lesssim 10\text{--}30\%$ compared to H) sticking to dust grains, which further react with surface species such as CO forming abundant multi-deuterated complex (organic) ices such as formaldehyde and methanol. These molecules can later desorb into the gas-phase due to non-thermal desorption or due to the gradual warm-up of the environment by a forming protostar.

The physical environment plays an important role in deuterium fractionation. In one of the first theoretical studies of deuterium fractionation, Solomon & Woolf (1973) estimated the D/H ratio for HCN in Orion, albeit erroneously assuming that fractionation is driven solely by neutral-neutral processes involving HD and atomic D. The ion-molecule fractionation route was first proposed by Watson (1974) and Watson (1976), who used it to constrain the interstellar D/H elemental ratio. Guelin et al. (1977) used observations of DCO^+ to constrain the electron abundance in dark clouds, while Herbst (1982) showed that the $\text{DCO}^+/\text{HCO}^+$ ratio can be used as a sensitive measure of the gas kinetic temperature in the ISM. Dalgarno & Lepp (1984) studied the D/H ratio of HCO^+ , considering cold and warm ISM conditions, and illustrated the role of depletion (and thus the density of the environment) for deuterium fractionation processes.

The first complete gas-phase model of deuterium chemistry in a dense cold cloud was undertaken by Millar et al. (1989), while Brown & Millar (1989) explored grain-surface deuteration processes. More recently, Roberts & Millar (2000b) studied deuterium chemistry over a wide range of physical parameters, by varying density, temperature, initial abundances and freeze-out. They found that if freeze-out is present, molecular D/H ratios can become very high; e.g., $\gtrsim 1\text{--}10\%$, and gas-phase chemistry can produce abundant mono- and multi-deuterated molecules.

Not only are the current physical properties of the environment important for chemical evolution, but also is the evolutionary history. Taquet et al. (2012) have considered a two-stage model to study deuterium chemistry in prestellar cores, with a gas-phase steady-state phase followed by the formation and evolution of grain mantles and surface deuterium fractionation. With such a simple approach they have reproduced high observed abundances of the isotopologues of formaldehyde and methanol. Taquet et al. have concluded that D and H abstraction and substitution reactions on dust surfaces are cru-

cial for attaining the observed high D/H ratios. The role of abstraction reactions for deuterium fractionation has been intensively investigated in the laboratory (see e.g., Nagaoka et al. 2005; Hidaka et al. 2009; Hama et al. 2012).

Cazaux et al. (2011) have studied the chemistry of formaldehyde and water by modeling the formation of ices in translucent clouds, and later following the chemical evolution as the cloud collapses to eventually form a Class I protostellar object. Their results show that the degree of deuteration of formaldehyde is sensitive to the initial D/H ratios of gaseous molecules attained before the collapse phase, while the degree of deuteration of water depends strongly on the dust temperature during the water ice formation. Intriguingly, Coutens et al. (2012) have observed deuterated water vapor in the low-mass protostar IRAS 16293-2422 and found that the water D/H ratio is lower than for other deuterated species detected in the same source. This observational trend continues toward more evolved hot cores/corinos (e.g., Parise et al. 2004; Bacmann et al. 2012) and suggests that the water may have formed relatively early, in a warm dilute ISM environment, while the depletion of CO at a later, cold and dense core stage allows for efficient surface synthesis of highly deuterium-enriched complex ices. An alternative explanation could be efficient abstraction and substitution reactions of H atoms by D atoms for organic ices like formaldehyde and methanol during cold prestellar cloud phase, which would not be as effective for water ice. A detailed one-dimensional chemical-hydrodynamical model of the prestellar core collapse and the formation of a protostar, coupled to the gas-grain chemistry and deuterium fractionation, has been developed by Aikawa et al. (2012). They have found that due to initially high D/H ratios accumulated in the cold phase, large (organic) molecules and carbon chains remain strongly deuterated even at later, warmer conditions.

While physical properties, such as temperature and density, and surface chemistry can have a significant effect on deuterium fractionation, smaller effects can derive from other global properties such as metallicity and ionization fields. In order to understand the influence of metallicity and ionization one needs to study deuterated species on a more global scale. Bayet et al. (2010) have conducted an observational survey of deuterated species in extragalactic star-forming regions and studied the influence of density, temperature, far-UV radiation field, cosmic-ray ionization and metallicity on the D/H ratios for ~ 20 deuterated species. Without modeling any particular source, they have compared the predicted column densities with those derived from the current limited set of observational data in external galaxies and found an overall reasonable agreement. Bayet et al. (2010) have provided a list of key deuterated species in extragalactic environments to be searched for with ALMA.

ALMA is a truly revolutionary observational facility not only for extragalactic and cosmological studies, but also for observations of the Milky Way ISM, the analysis of which requires better chemical tools. In this paper we present a new up-to-date, extended, multi-deuterated chemical network and assess its reliability by modeling the deuterium fractionation in various phases of the ISM and comparing the results with observed D/H ratios of a variety of mono-, doubly-, and triply-deuterated species in distinct astrophysical environments. A list of the most promising, deuterated species potentially detectable with ALMA in the local Milky Way ISM is provided. Also, we report a detailed sensitivity analysis to understand and to quantify the intrinsic error bars in calculated abun-

dances of deuterated species in several representative astrophysical environments. We isolate the most problematic gas-phase reactions with uncertain rate coefficients to be studied in the laboratory or theoretically, and quantify the associated uncertainties in modeled abundances. The User Manual and the new deuterium network are freely available on the Internet².

The remainder of the paper is structured as follows. In Section 2 we present our new deuterium chemistry model. We give a detailed description of the construction of our deuterium network and our choice of the relevant reaction rates and branching ratios. We also discuss error propagation based on uncertainties in rate coefficients. In Section 3 this model is used to calculate abundances and D/H ratios under a wide range of physical conditions. We discern general trends in D/H ratios with temperature, density, and initial abundances, and divide the species according to whether temperature or initial abundance influences D/H ratios more strongly. A sensitivity analysis is performed to quantify intrinsic uncertainties in modeled abundances due to uncertainties in reaction rate data. A list of the most problematic reactions for deuterium chemistry is presented. We then discuss our results and compare them with recent observations and theoretical studies in Section 4. Conclusions follow in Section 5. Appendices are only available as online material. Appendix A contains updated and added reactions, Appendix B shows dominant reaction pathways for selected deuterated species, and Appendix C lists deuterium fractionation rate coefficients in cold dark environments.

2. MODEL

2.1. Parameter space

In this work we are primarily concerned with providing a new extended deuterium network and assessing its capacity to model chemistry under both static cold and warm conditions in the ISM. We do not consider evolutionary models such as those pertaining to low-mass and high-mass star formation separately, although the static conditions we consider arise from evolutionary processes. The evolution of the interstellar medium begins from fragmentation of turbulent, mainly atomic clouds with kinetic temperatures up to ~ 100 K and densities of $\sim 10\text{--}100\text{ cm}^{-3}$. The denser clumps evolve into starless molecular cores (Bergin & Tafalla 2007) with temperatures of $8\text{--}15$ K and densities of $\sim 10^4\text{--}10^6\text{ cm}^{-3}$ (Snow & McCall 2006; André et al. 2009; Launhardt et al. 2010; Nielbock et al. 2012). Some of these gravitationally-bound cores may begin contracting, first isothermally, and then with increasing internal densities and temperatures. Then a central hydrostatic object forms, which starts heating up the surrounding gas. Protostars with a mass greater than 8 solar masses are generally referred to as \O High-mass protostellar objects (HMPOs). The collapsing envelope material can then reach temperatures of several hundred K closer to the central star, and peak densities of $\sim 10^8\text{ cm}^{-3}$, conditions which define a “hot core” or, for low-mass protostars, a hot “corino” (van Dishoeck 2006). In this paper we concentrate on the evolutionary stages ranging from a cold molecular cloud to the warm envelopes of protostars. We choose a wide parameter space with a grid of 1 000 points covering temperatures between $5\text{--}150$ K and densities of $10^3\text{--}10^{10}\text{ cm}^{-3}$, and

assume the standard ISM dust and a fixed $A_V = 10$ mag, meaning that the photochemistry is only driven by secondary UV photons. Assuming a fixed A_V reduces the problem to two dimensions, which is easier to analyze and visualize.

2.2. Chemical model

We have utilized the gas-grain chemical model “ALCHEMIC” developed by Semenov et al. (2010), where a detailed description of the code and its performance is presented. The code is optimized for modeling the time-dependent evolution of large chemical networks, including both gas-phase and surface species. In this paper we added a large set of reactions involving deuterated species. A few features of the “ALCHEMIC” model are summarized below.

The self-shielding of H_2 from photodissociation was calculated using Equation (37) from van Dishoeck & Blake (1998). The shielding of CO by dust grains, H_2 , and its self-shielding was calculated using the precomputed table of Lee et al. (1996, Table 11). We consider cosmic rays (CRP) as the only external ionizing source, using a CRP ionization rate for H_2 , $\zeta_{\text{CR}} = 1.3 \times 10^{-17}\text{ s}^{-1}$ (Herbst & Klemperer 1973), appropriate for molecular cloud environments and which has been utilized in several previous studies (such as Wakelam et al. 2006; Vasyunin et al. 2008; Druard & Wakelam 2012). The gas-grain interactions include dissociative recombination and neutralization of ions on charged grains, sticking of neutral species and electrons to uniformly-sized $0.1\text{ }\mu\text{m}$ dust grains with a sticking coefficient of 1 and release of ices by thermal, CRP-, and UV-induced desorption, such that at high temperatures the surface population will be low as thermal desorption takes over. We do not allow H_2 and its isotopologues to stick to grains. We assume a UV photodesorption yield of 10^{-3} (e.g., Öberg et al. 2009a,b). With our fixed visual extinction, the photon field derives from secondary electron excitation of molecular hydrogen followed by fluorescence.

We assume that each $0.1\text{ }\mu\text{m}$ spherical silicate grain provides $\approx 1.88 \times 10^6$ sites (Biham et al. 2001) for surface recombination that proceeds solely through the classical Langmuir-Hinshelwood mechanism (e.g. Hasegawa et al. 1992). The grain surface topology, the presence of high- and low-energy binding sites, grain sizes and shapes are all separate parameters that may severely impact the chemistry. An accurate study of this impact will require a detailed treatment of the microscopic physics of molecules on various solid surfaces, which is far beyond the scope of the present study. For further reading we recommend papers by Perets & Biham (2006); Cuppen et al. (2009); Vasyunin & Herbst (2013a,b), where some of these issues are already addressed.

Upon a surface recombination, we assume there is a 5% probability for the products to leave the grain due to the conversion of some of the exothermicity of reaction into breaking the surface-adsorbate bond (Garrod et al. 2007). We do not find significant differences (less than a factor of 2) in D/H ratios and abundances of essential species, such as H_3^+ , water, ammonia from varying this probability between 1–10%. However, we found a significant variation in ice abundances of formaldehyde and methanol of up to a factor of 6 at lower temperatures ($\lesssim 25$ K) when considering higher desorption probabilities $\gtrsim 5\%$. Interestingly, ice abundances increase with the desorption probability and we find that this is due to a much more efficient formation of formaldehyde and methanol at intermediate times. Due to more intense gas-grain interactions precursor species of H_2CO and CH_3OH are able to form

² <http://mpia.de/PSF/codes.php>

more readily in the gas phase and later stick to grains. Consequently, formaldehyde and methanol are formed faster via surface processes. Following experimental studies on the formation of molecular hydrogen on dust grains by Katz et al. (1999), we adopt the standard rate equation approach to the surface and ice chemistry without quantum-mechanical tunneling through the potential walls of the surface sites. We also do not consider competition kinetics between activation and diffusive barriers (Garrod & Pauly 2011).

A typical run, with relative and absolute tolerances of 10^{-5} and 10^{-25} , utilizing the original gas-grain network without deuterium chemistry ($\sim 7\,000$ reactions, ~ 700 species) takes 1–5 s for 1 Myr of evolution with a Xeon 3.0 GHz CPU. With our new, almost tenfold larger deuterium network, the same run takes approximately an order of magnitude longer to calculate. The linear dependence of the CPU time vs. species number in the model is due to the advanced numerical scheme implemented in the *ALCHEMIC* code, which generates and uses sparse Jacobi matrices.

2.3. Initial abundances

As input data, reaction rate coefficients and physical properties need to be specified, as do initial abundances. We have chosen to implement two different initial abundance sets and calculate the chemical evolution with the new deuterium network for 1 Myr.

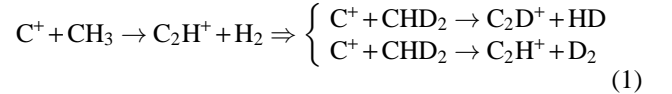
For the first set, hereafter referred to as the “Primordial” model, we utilized the “low metals” abundances of Graedel et al. (1982) and Lee et al. (1998). Initially all deuterium is located in HD, with $D/H = 1.5 \times 10^{-5}$ (Stancil et al. 1998; Linsky 2003), see Table 1. The abundances in the second set, the “Evolution” model, were calculated with our deuterium chemistry model, assuming a TMC1-like environment: $T = 10$ K and $n_H = 10^4$ cm $^{-3}$, at $t = 1$ Myr. Under such conditions elemental deuterium from HD is efficiently redistributed to other molecules, leading to their high initial D/H fractionation. These final abundances at 1 Myr are used as input in the “Evolution” model (see Table 2). The “Evolution” model serves as a simple example of a two-stage chemical model with physical conditions that can change dramatically at 1 Myr, unless the evolutionary model is run strictly under TMC-1 conditions.

2.4. Deuterium fractionation chemistry

As a first step toward creating a consistent network with deuterium fractionation, we undertook a thorough search in the literature for updates to the reaction rates of the original non-deuterated network. We utilized the latest *osu.2009* gas-phase chemical network and incorporated all essential updates as of December 2012, adopted from Horn et al. (2004), Chabot et al. (2010), Hamberg et al. (2010a), Wakelam et al. (2010b), Laas et al. (2011), as well as those reported in the *KInetic Database for Astrochemistry* (KIDA)³. Further, to allow for the synthesis of the few complex molecules in our network such as methanol (CH₃OH), methyl formate (HCOOCH₃), and dimethyl ether (CH₃OCH₃), an extended list of surface reactions and photodissociation of ices was adopted from Garrod & Herbst (2006). Several tens of gas-phase photoreaction rates were updated using the new calculations of van Dishoeck et al. (2006)⁴.

Next, we applied a cloning routine to this updated network (as described in Rodgers & Millar 1996), and added all additional primal isotope exchange reactions for H₃⁺ as well as CH₃⁺ and C₂H₂⁺ from Roberts & Millar (2000b); Gerlich et al. (2002); Roberts et al. (2004); Roueff et al. (2005). In this cloning routine all reactions bearing hydrogen atoms are considered to have deuterated analogues, and “cloned” accordingly (assuming the same rate coefficient if no laboratory data are available). In cases where the position of the deuterium atom is ambiguous, we apply a statistical branching approach. In the resulting network we do not yet distinguish between the ortho/para states of molecules, and leave this for a separate paper.

A typical example of the outcome of the cloning procedure is presented for the reaction between C⁺ and CH₃:



The single ion-molecule reaction of C⁺ with CH₃ is cloned into two separate channels for CHD₂. Moreover, the branching of these two new channels is not equal. To visualize this, we label the two deuterium atoms in CHD₂ D_a and D_b. For the first reaction, which forms C₂D⁺, D_a can be placed on either product and D_b on the other, hence we have two possibilities: C₂D_a⁺ + HD_b or C₂D_b⁺ + HD_a. For the second channel, which forms C₂H⁺, both deuterons have to be placed on D₂ and we only have one possibility. This analysis assumes that the deuterons on D₂ are indistinguishable, which is in agreement with the Pauli Exclusion Principle. Alternatively, we could initially assume that they are distinguishable, but because half of the D₂ rotational-nuclear spin states are missing, the simple argument about 2/3 and 1/3 branching ratios remains valid.

To limit the size of the network we have restricted the cloning process to avoid any -OH endgroups. Observations of deuterated species suggest that fractionation of species with -OD endgroups is less important in low-mass protostars, but may still be important for high-mass protostars. For example, Parise et al. (2006) conducted a survey of deuterated formaldehyde and methanol in a sample of seven low-mass class 0 protostars, and found CH₃OD / CH₂DOH $\lesssim 0.1$. A hypothesis of rapid conversion of CH₃OD into CH₃OH in the gas-phase due to protonation reactions that would affect only species for which deuterium is bound to the electronegative oxygen has been suggested by Charnley et al. (1997) and Osamura et al. (2004). We conducted a small study using a version of our deuterium network where -OH endgroups were cloned and found no significant changes in the resulting time-dependent molecular abundances.

Full tables of added and updated reactions are found in Tables A1 and A2 in Appendix A of the online material. The resulting chemical network consists of $\sim 55\,000$ reactions connected by $\gtrsim 1\,900$ species, to our knowledge the most extended network for deuterium chemistry to date⁵.

2.5. Analysis of reaction updates

Given the large size of the network with uncertainties in the adopted rate coefficients, reaction barriers, and branching ratios, it is educational to estimate how these uncertainties propagate in time-dependent modeled abundances. Before performing a detailed sensitivity analysis, as in our study of disk

³ <http://kida.obs.u-bordeaux1.fr/> as of [2012-12-26]

⁴ <http://www.strw.leidenuniv.nl/~ewine/photo/>

⁵ Publicly available at: <http://mpia.de/PSF/codes.php>

Table 1
Initial abundances for the “Primordial” model with respect to n_{H} .

Species	H_2	H	HD	He	C	N	O
	0.499	2.00×10^{-3}	1.50×10^{-5}	9.75×10^{-2}	7.86×10^{-5}	2.47×10^{-5}	1.80×10^{-4}
Species	S	Si	Na	Mg	Fe	P	Cl
	9.14×10^{-8}	9.74×10^{-9}	2.25×10^{-9}	1.09×10^{-8}	2.74×10^{-9}	2.16×10^{-10}	1.00×10^{-9}

Table 2
Initial abundances of major species for the “Evolution” model with respect to n_{H} .

Species	H_2	He	H	HD	C	N	O
	0.500	9.76×10^{-2}	2.32×10^{-4}	9.57×10^{-6}	1.02×10^{-8}	8.75×10^{-8}	1.45×10^{-6}
Species	S	Si	Na	Mg	Fe	P	Cl
	2.00×10^{-9}	7.00×10^{-11}	6.37×10^{-11}	3.70×10^{-10}	6.07×10^{-11}	5.72×10^{-12}	1.64×10^{-10}
Species	$\text{H}_2\text{O (ice)}$	CO (ice)	CO	$\text{CH}_4 \text{ (ice)}$	$\text{NH}_3 \text{ (ice)}$	O_2	N_2
	9.90×10^{-5}	3.91×10^{-5}	1.85×10^{-5}	1.66×10^{-5}	1.30×10^{-5}	7.04×10^{-6}	3.78×10^{-6}
Species	$\text{O}_2 \text{ (ice)}$	D	$\text{N}_2 \text{ (ice)}$	HDO (ice)	$\text{C}_3\text{H}_2 \text{ (ice)}$	HNO (ice)	D_2
	2.29×10^{-6}	1.81×10^{-6}	1.26×10^{-6}	1.08×10^{-6}	7.68×10^{-7}	7.25×10^{-7}	7.07×10^{-7}

Table 3
Species showing variations in D/H ratios by more than a factor of 5 due to the updates in the reaction network.^a

Species	$R(\text{D}/\text{H})$	Species	$R(\text{D}/\text{H})$
HD_2O^+	24.3	CHD_3	8.5
CH_2D_2	8.5	CH_3D	8.1
CH_4D^+	7.9	$\text{C}_2\text{H}_2\text{D}_2$	7.3
CD_4	7.0	H_2DO^+	5.9
HD_2CS^+	5.4	D_2CS	5.3

^a Includes only species with fractional abundances $> 10^{-25}$

chemistry uncertainties (Vasyunin et al. 2008), it is of interest to characterize the influence of the reaction rate updates on the calculated abundances and the D/H ratios. This may help us to highlight the significance of recent laboratory astrochemistry activities, both for deuterated and un-deuterated species, in providing more accurate astrochemical data to the community.

First, we studied the effects of introducing deuterium chemistry into our model on abundances of un-deuterated species by comparing abundances throughout the parameter space to a non-deuterated version of the network. We found that species with relative abundance $> 10^{-25}$ show mean values in abundance variations between the two networks within a factor 0.95 - 1.05. Since we did not find any particularly large variations in abundances for H-bearing species, we conclude that the results from our updated analysis are a pure effect of updated reaction rates and not caused by the additional pathways created by the cloning routine.

In order to separate the effect that recent updates have had on abundances, we generated an additional network by cloning an outdated network restricted to the reaction rate updates up until 2005. We then studied the impact of updated reaction rate coefficients by comparing the calculated time-dependent abundances between the “old” chemical network and the “new” network in the 2D-parameter space discussed in Sect. 2.1. In addition to the D/H abundance ratios, we will emphasize the differences in these ratios between the models, which we calculated by dividing the respective D/H ratios in the updated 2012 network by those from the outdated 2005 network, and will denote this ratio as $R(\text{D}/\text{H})$. The results have been obtained with the “Primordial” model only. In

this comparison, we have excluded minor species with relative abundances below 10^{-25} . It should be noted that the $R(\text{D}/\text{H})$ ratios may remain unchanged when absolute abundances of species and their isotopologues in the updated and outdated networks increase in unison.

We list in Table 3 the arithmetic mean value calculated over the parameter grid ($T = 5 - 150$ K, $n_{\text{H}} = 10^3 - 10^{10} \text{ cm}^{-3}$) of $R(\text{D}/\text{H})$ ratios for all species with fractional abundances $\geq 10^{-25}$ for which the mean value of $R(\text{D}/\text{H})$ ratios have changed by more than a factor of 5. Among the listed species, we find light hydrocarbons (e.g., CHD_3 , CH_2D_2), ions (CH_4D^+ , HD_2O^+), and simple organic molecules (e.g. DCOOH , D_2CO), as well as key molecules such as doubly-deuterated water and ammonia. Multi-deuterated species appear to be more affected by the updates than their singly-deuterated analogues, as there are more intermediate pathways involved in their chemistry, as is most evident by comparing HD_2O^+ and H_2DO^+ in Table 3.

There are also several species affected by the abundances that do not show any variance in D/H ratios, i.e. both deuterated and undeuterated species are similarly affected by updates. The abundances of CH_2D^+ and CHD_2^+ provide good examples of such behavior. These species show a coherent increase (within a factor of 1.1 between un-deuterated species and isotopologues) in their gas-phase abundances at 1 Myr and at high temperatures ($\gtrsim 100$ K) and densities ($n_{\text{H}} \gtrsim 10^7 \text{ cm}^{-3}$). As a result, their $R(\text{D}/\text{H})$ values remain close to unity. We identified the coherent increase in abundance as originating from an update taken from KIDA in the rate coefficient for the slow radiative association reaction forming CH_5^+ via CH_3^+ colliding with H_2 . The rate coefficient of this reaction was lowered by almost two orders of magnitude, from $1.30 \times 10^{-14} \text{ cm}^3 \text{ s}^{-1}$ to $4.10 \times 10^{-16} \text{ cm}^3 \text{ s}^{-1}$ (at room temperature; see Wakelam et al. 2010b). We note that the older value was based on a misinterpretation of the original literature, which used 300 K in the formula for the rate coefficient but was intended only for temperatures up to 50 K (Herbst 1985). The same D/H ratio variation is transferred to HD_2O^+ and H_2DO^+ through the ion-neutral reaction with CH_5^+ and its isotopologues reacting with free oxygen atoms. The abundances of the CH_4 isotopologues derive from the dissociative recombination of CH_5^+ (and its isotopologues) as

well as from ion-molecule reactions with CO, so CH₄ is directly affected by the updated reaction rate. It then transfers its D/H ratio variation into C₂H₂D₂ through CH₂D₂ reacting with CH. Another route involves the intermediary reaction between CH₂D₂ and S⁺ to form HD₂CS⁺, which later dissociatively recombines into D₂CS, which in turn reacts with CH₂D₂.

On the other hand, the deuterated analogue of this radiative association reaction does not occur; instead CH₃⁺ + HD produces CH₂D⁺ and H₂, and the corresponding rate constant is the same in the outdated and new networks (Millar et al. 1989). This slows down production of the key ion, CH₃⁺, while deuterated isotopologues of CH₃⁺ and CH₅⁺ are produced with almost the same rate, consequently affecting D/H ratios of the gas-phase species listed in Table 3. It does not affect abundant organic species such as methanol and formaldehyde however, as they are mainly formed by surface hydrogenation of CO ice.

We find that there is a particularly large variance in abundances for the two sulphur-bearing species, C₂S and C₂S⁺, which show an increase in abundance by a factor of 187 and 26, respectively, compared with the non-deuterated network. We are not concentrating on the chemistry of sulphur-bearing molecules in this study because their chemistry is still poorly understood and often restricted to a few pathways. But the additional pathways that the cloning routine generates has a stronger effect on these two species as pathways reducing their abundances proceed much slower than their formation pathways.

2.6. Error propagation in deuterium fractionation chemistry

We studied the impact of uncertainties in reaction rate coefficients on the resulting chemical abundances, and how they propagate throughout the chemical evolution. Two separate environments were chosen for this study, representing dark clouds ($T = 10$ K, $n_{\text{H}} = 10^4$ cm⁻³; Nielbock et al. 2012) and lukewarm infrared dark clouds ($T = 25$ K, $n_{\text{H}} = 10^5$ cm⁻³; Vasyunina et al. 2012). In these and all subsequent runs mentioned in this paper, we use the “Primordial” initial conditions unless stated to the contrary. We chose to concentrate on the uncertainties of the rate coefficients of the gas-phase reactions. Including variations in surface chemistry rates is a tricky problem as these depend on surface mobility, binding and diffusion energies of reactants, and properties of the surface itself (porosity, irregularities, etc.). Recently, Taquet et al. (2012) have studied the importance of deuterium fractionation on dust surfaces, using a multi-layered ice mantle model and quantified some of the associated errors in the calculated abundances due to the uncertainties in the surface chemistry, so we do not repeat such a study here.

Our analysis is based on the same method as employed by Vasyunin et al. (2004) and Vasyunin et al. (2008). We performed computations for a large set of models, using identical physical conditions and initial abundances, and the same chemical network but with randomly varied rate coefficients within their uncertainty limits. The rate uncertainties were taken from the KIDA database. Most of the reactions with deuterated species were created by the cloning procedure, and hence have unknown uncertainties. For these reactions we used the high standard error value in KIDA⁶, with a normal logarithmic error distribution of a factor of two.

⁶ <http://kida.obs.u-bordeaux1.fr/>

With this method, we generated 10000 networks with the new rate coefficients $k(T)$ randomly distributed as follows:

$$k(T) = \exp(\ln k_0(T) + \ln F \times N[0, 1]), \quad (2)$$

where $k_0(T)$ is the measured, calculated, or estimated rate coefficient at temperature T , F is the statistical distribution of the uncertainty, and $N[0, 1]$ is a random value drawn from a standard Gaussian distribution with mean $\mu = 0$ and variance 1. The time needed for a full run consisting of 10000 networks for a specified temperature and density takes approximately one day of computational time on a Xeon 3.0 GHz CPU (with relative and absolute tolerances of 10^{-4} and 10^{-20} , respectively).

The huge size of our new deuterium chemical network makes it a challenging task to find a very precise correlation between the rate uncertainties and uncertainties in the molecular abundances of a particular species. Since for many deuterated species the set of primal pathways easily exceeds several reactions, the relative contribution of each individual reaction to the final uncertainty is likely to be small, $\lesssim 10\%$. To isolate the most problematic reactions for several key observed species, we conducted a sensitivity analysis using the same cross-correlation method as implemented by Vasyunin et al. (2008). We selected a handful of molecules, including their isotopologues and isomers; viz., H₃⁺, H₂O, HCN, HCO⁺, and CH₃OH, and for each of these species we calculated time-dependent linear correlation coefficients between the abundances and the rate coefficients for all the 10000 network realizations and for each of our 30 logarithmically taken time steps. The linear correlation coefficients $c_L(i, j, t)$ at specific density, i , and temperature, j , points and at time t are calculated by:

$$c_L(i, j, t) = \frac{\sum_l (x_l^s(i, j, t) - \overline{x^s(i, j, t)}) (\alpha_l^j - \overline{\alpha^j})}{\sum_l (x_l^s(i, j, t) - \overline{x^s(i, j, t)})^2 \sum_l (\alpha_l^j - \overline{\alpha^j})^2} \quad (3)$$

with $x_l^s(i, j, t)$ being the molecular abundance for species s and iteration l , and $\overline{x^s(i, j, t)}$ and $\overline{\alpha^j}$ signifying the standard (mean) abundances and rate coefficients for species s , respectively. Because key reactions can vary through time evolution, we calculate and use cumulative correlation coefficients in our results, for which we integrated the absolute values of time-dependent linear correlation coefficients over the 30 logarithmic taken time steps taken over 1 Myr. In our results in the next section, we restrict discussion to the cumulative correlation coefficients, designated as c .

3. RESULTS

3.1. Sensitivity analysis

We have determined that 10000 realizations of the network may not be adequate for results of our sensitivity analysis to fully converge. For correlation coefficients $c < 0.1$ we sometimes still see small variations when we compare our results with a model containing only 9000 realizations. Therefore, we also ran a separate set of simulations with 20000 realizations for a dark cloud environment, but found the same result with only minor deviations for the reactions with low correlation coefficients, $c < 0.1$. All correlation coefficients should stop fluctuating with size as soon as the number of the network realizations exceeds the number of reactions in the network, which is ~ 50000 . Running the sensitivity analysis code with so many realizations, however, would be pro-

hibitively time consuming. Therefore, below we consider reactions with $c > 0.1$ in our discussion.

Table 4 lists the subset of reactions with cumulative correlation coefficients $c > 0.1$, which are the most problematic for the chemical evolution of the following species (and their isotopologues and isomers): H_3^+ , HCO^+ , HCN , H_2O , CH_3OH , H_3O^+ , CH_3^+ , C_2H_2^+ and CO . Because there are several additional key reactions with $0.05 < c < 0.1$, we list a more extensive table in the online material (Table A3 of Appendix A), including also reactions with $c > 0.05$ for the same set of species.

As can clearly be seen, ion-neutral processes dominate Table 4, accompanied by a few dissociative recombination and neutral-neutral reactions as well as cosmic ray ionization of the two critical species: H_2 and He . The last process may require more detailed description in astrochemical models, such as recently presented in Rimmer et al. (2012) and Glassgold et al. (2012), so we assigned a relatively large uncertainty of a factor of 2 for this group of processes. Approximately half of the bimolecular reactions are connected to the chemical evolution of water and light hydrocarbons in the gas. Abundances of species mostly produced on grains, such as methanol, will not be strongly affected by the uncertainties. However, a small fraction of these species is still present in the gas in the center of dense cores, for which uncertainties in the gas-phase chemistry may become important. Many of the deuterated reactions in the table are produced by our cloning procedure, so their error coefficients are only an approximation, and can, in fact, be larger than estimated. Also, isomerization reactions for HOC^+ and DOC^+ with reaction rate uncertainties of a factor of two possess strong correlation coefficients (0.3–0.4).

We find it clear that fractionation channels of the H_3^+ and CH_3^+ isotopologues require further study, as do reactions involving the isotopologues of H_3^+ reacting with CO , water, OH and their isotopologues, forming the initial steps towards more complex molecules. Reactions with H_3^+ and H_2D^+ are both well represented in the list and initiate the ion-molecule chemistry, while HD_2^+ and D_3^+ are often not abundant enough to have a significant effect in our models. H_3^+ and H_2D^+ react with CO to form the isotopologues of HCO^+ , with OH and OD to form ionized water (H_2O^+ , HDO^+) as well as the water isotopologues, which strongly affect water abundances and D/H ratios. We also see many other interconnecting reactions among our set of key species. Several dissociative recombination reactions, which proceed very rapidly, show strong correlations. While their reaction rates can be accurately determined (Florescu-Mitchell & Mitchell 2006) the products and branching ratios of these reactions are not precisely known (see e.g. Hamberg et al. 2010b; Geppert et al. 2006).

3.2. Uncertainties

After calculating time-dependent abundances for all the realizations of the chemical network with varied reaction rate coefficients, and for each considered physical model, we fit Gaussians to the resulting abundance distributions at 1 Myr for all species. We carefully checked that such an approximation could be applied to the abundance distributions and found it to be the case for almost all species. In Figure 1, we show examples of abundance distributions, with their Gaussian fits, for H_2D^+ and DCOOH in dark cloud and warm infrared dark cloud environments, respectively, both showing good fits. From the Gaussian fits, we then determined the full width half-maximum value (FWHM, 2.35σ) of these dis-

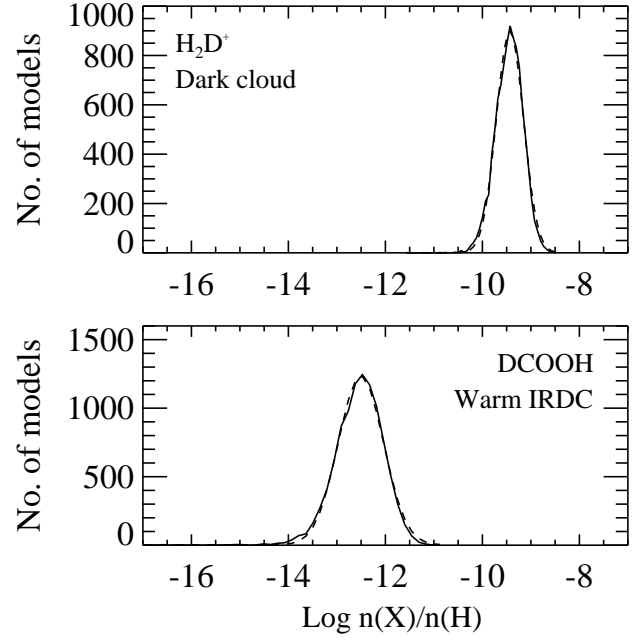


Figure 1. Distributions of abundances from 10000 chemical runs for H_2D^+ in dark clouds (top) and DCOOH in warm IRDCs (bottom). Plots also show fitted Gaussian distributions (dashed lines).

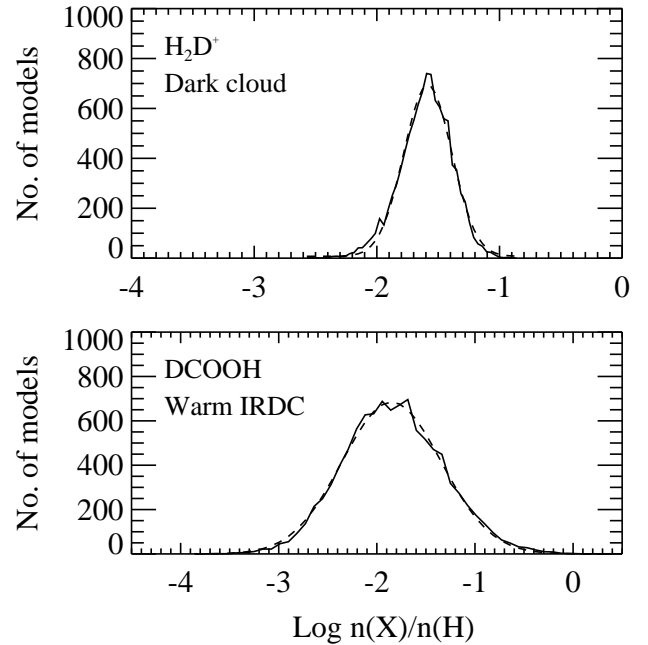


Figure 2. Distributions of D/H ratios from 10000 chemical runs for H_2D^+ in dark clouds (top) and DCOOH in warm IRDCs (bottom). Plots also show fitted Gaussian distributions (dashed lines).

tributions and used the 1σ values to quantify the spread in abundances, which we henceforth refer to as the abundance uncertainties. We also applied the same procedure for the calculated D/H ratios, and show examples of the resulting D/H ratio distributions in Figure 2 for water and formic acid in the same two regions. We find good fits to all these distributions with estimated 1σ values of factors of 1.9 and 2.9 for the abundance distribution of water and formic acid, respectively, while the values for D/H ratios are a factor of 1.4 and 3.2, respectively.

In Figure 3, we plot the 1σ abundance uncertainties for

Table 4
40 most problematic reactions (with cumulative correlation coefficients $c > 0.1$) and their associated (real) uncertainty factors.

Reaction	Uncertainty	Reaction	Uncertainty
$\text{H}_2 + \text{CRP} \rightarrow \text{H}_2^+ + \text{e}^-$	2.00	$\text{He} + \text{CRP} \rightarrow \text{He}^+ + \text{e}^-$	2.00
$\text{H}_3^+/\text{H}_2\text{D}^+ + \text{HD} \rightarrow \text{H}_2\text{D}^+/\text{HD}_2^+ + \text{H}_2$	1.25	$\text{H}_3^+ + \text{D}_2 \rightarrow \text{HD}_2^+ + \text{H}_2$	2.00
$\text{H}_2\text{D}^+/\text{HD}_2^+ + \text{H}_2 \rightarrow \text{H}_3^+/\text{H}_2\text{D}^+ + \text{HD}$	2.00	$\text{H}_3^+/\text{H}_2\text{D}^+ + \text{D} \rightarrow \text{H}_2\text{D}^+/\text{HD}_2^+/\text{D}_3^+ + \text{H}$	2.00
$\text{HD}_2^+ + \text{D} \rightarrow \text{D}_3^+ + \text{H}$	2.00	$\text{H}_3/\text{H}_2\text{D}^+ + \text{e}^- \rightarrow \text{H}/\text{D} + \text{H} + \text{H}$	2.00
$\text{H}_3^+ + \text{CO} \rightarrow \text{HCO}^+/\text{HOC}^+ + \text{H}_2$	1.25	$\text{H}_2\text{D}^+ + \text{CO} \rightarrow \text{DCO}^+/\text{DOC}^+ + \text{H}_2$	1.25
$\text{H}_3^+ + \text{OH}/\text{OD} \rightarrow \text{H}_2\text{O}^+/\text{HDO}^+ + \text{H}_2$	2.00	$\text{H}_2\text{D}^+ + \text{OH}/\text{OD} \rightarrow \text{HDO}^+/\text{D}_2\text{O}^+ + \text{H}_2$	2.00
$\text{HD}_2^+ + \text{OH}/\text{OD} \rightarrow \text{D}_2\text{O}^+ + \text{H}/\text{D}$	2.00	$\text{H}_3^+ + \text{H}_2\text{O}/\text{HDO} \rightarrow \text{H}_3\text{O}^+/\text{H}_2\text{DO}^+ + \text{H}_2$	1.25
$\text{H}_3^+ + \text{HDO} \rightarrow \text{H}_3\text{O}^+ + \text{HD}$	1.25	$\text{H}_3^+ + \text{DNC} \rightarrow \text{H}_2\text{CN}^+ + \text{HD}$	2.00
$\text{H}_2\text{D}^+ + \text{HNC} \rightarrow \text{HDCN}^+ + \text{H}_2$	2.00	$\text{OH} + \text{D} \rightarrow \text{OD} + \text{H}$	2.00
$\text{H}_3\text{O}^+ + \text{e}^- \rightarrow \text{OH} + \text{H} + \text{H}$	1.25	$\text{H}_3\text{O}^+/\text{H}_2\text{DO}^+ + \text{e}^- \rightarrow \text{H}_2\text{O}/\text{HDO} + \text{H}$	1.25
$\text{HD}_2\text{O}^+ + \text{e}^- \rightarrow \text{D}_2\text{O} + \text{H}$	1.25	$\text{HDO}^+/\text{D}_2\text{O}^+ + \text{H}_2 \rightarrow \text{H}_3\text{O}^+/\text{H}_2\text{DO}^+ + \text{D}$	1.25
$\text{H}_2\text{CN}^+/\text{HDCN}^+ + \text{e}^- \rightarrow \text{CN} + \text{H}/\text{D} + \text{H}$	2.00	$\text{H}_2\text{CN}^+ + \text{e}^- \rightarrow \text{HCN}/\text{HNC} + \text{H}$	2.00
$\text{HDCN}^+ + \text{e}^- \rightarrow \text{HCN}/\text{HNC} + \text{D}$	2.00	$\text{HDCN}^+ + \text{e}^- \rightarrow \text{DCN}/\text{DNC} + \text{H}$	2.00
$\text{H} + \text{OD} \rightarrow \text{HDO}$	2.00	$\text{D} + \text{OH} \rightarrow \text{HDO}$	2.00
$\text{HCO}^+/\text{DCO}^+ + \text{e}^- \rightarrow \text{CO} + \text{H}/\text{D}$	1.25	$\text{HCO}^+ + \text{D} \rightarrow \text{DCO}^+ + \text{H}$	2.00
$\text{HOC}^+ + \text{H}_2 \rightarrow \text{HCO}^+ + \text{H}_2$	2.00	$\text{DOC}^+ + \text{H}_2 \rightarrow \text{HCO}^+/\text{DOC}^+ + \text{HD}$	2.00
$\text{HCO}^+ + \text{HCN} \rightarrow \text{H}_2\text{CN}^+ + \text{CO}$	2.00	$\text{DCO}^+ + \text{HCN} \rightarrow \text{HDCN}^+ + \text{CO}$	2.00
$\text{HCO}^+/\text{DCO}^+ + \text{H}_2\text{O} \rightarrow \text{H}_3\text{O}^+/\text{H}_2\text{DO}^+ + \text{CO}$	1.50	$\text{HCO}^+ + \text{HDO} \rightarrow \text{H}_2\text{DO}^+ + \text{CO}$	1.50
$\text{HCO}^+ + \text{OD} \rightarrow \text{HDO}^+ + \text{CO}$	2.00	$\text{HCO}^+ + \text{CH}_2\text{DOH} \rightarrow \text{CH}_2\text{DOH}^+ + \text{CO}$	2.00
$\text{HCO}^+ + \text{CH}_3\text{OH} \rightarrow \text{CH}_3\text{OH}_2^+ + \text{CO}$	2.00	$\text{C}^+ + \text{H}_2\text{O} \rightarrow \text{HCO}^+/\text{HOC}^+ + \text{H}$	2.00

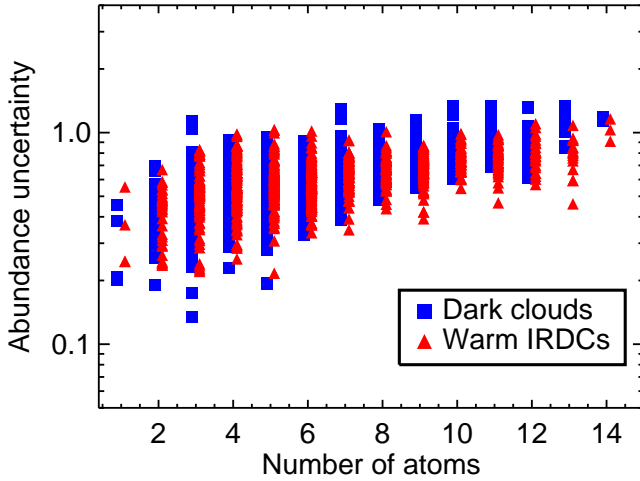


Figure 3. The 1σ abundance uncertainties in orders of magnitude for up to triply-deuterated species as a function of the number of atoms in a molecule. The dark cloud model results are denoted by squares and the warm infrared dark cloud model by triangles. A colored version of the plot is available in the online version.

deuterated species with up to three D-atoms at 1 Myr as a function of the number of atoms for both environments. There are two major trends visible in this plot. First, the abundance uncertainties are in general lower in the case of the IRDCs models compared with cold dark clouds.

At such a low temperature (10–20 K) many reactions with barriers cannot proceed, lowering the overall chemical complexity and thus the cumulative rate uncertainties. One would expect uncertainties to be the lowest for dark clouds, but we suggest that as D/H ratios and abundances of deuterated species are also higher in colder environments, more reactions can occur to increase uncertainties. Second, there is a strong trend of increasing abundance uncertainties with the number of atoms in species. This is obvious as the more atoms a species has, the more reaction pathways lead to its production

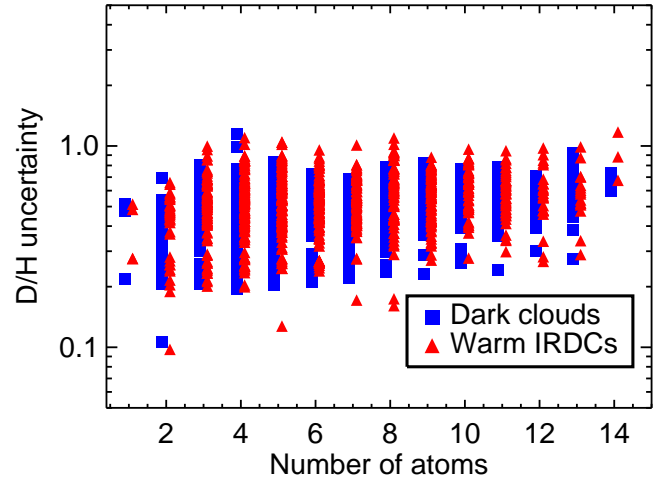


Figure 4. The 1σ uncertainties of the calculated D/H ratios in orders of magnitude for up to triply-deuterated species as a function of the number of atoms in a molecule. The dark cloud model results are denoted by squares and the warm infrared dark cloud model by triangles. A colored version of the plot is available in the online version.

and destruction from initial composition, and thus the higher is the accumulating effect of their uncertainties on modeled abundances (see also the discussion in Vasyunin et al. 2008).

In general, using the 1σ confidence level, the abundances and column densities of species made of $\lesssim 3$ atoms (e.g., CO, HCO^+ , DCO^+) are uncertain by factors 1.5–5, those for species made of 4–7 atoms are uncertain by a factor of 1.5–7, and those for more complex species made of > 7 atoms are uncertain by a factor of 2–10. The uncertainties for D- and H-bearing species are very similar in dark cloud environments. In warm IRDCs the typical uncertainties of larger H-bearing species (> 4 atoms) are approximately a factor of two lower compared to D-bearing species, as de-fractionation begins at these elevated temperatures (25 K). Our estimates for the abundance uncertainties for deuterated species are

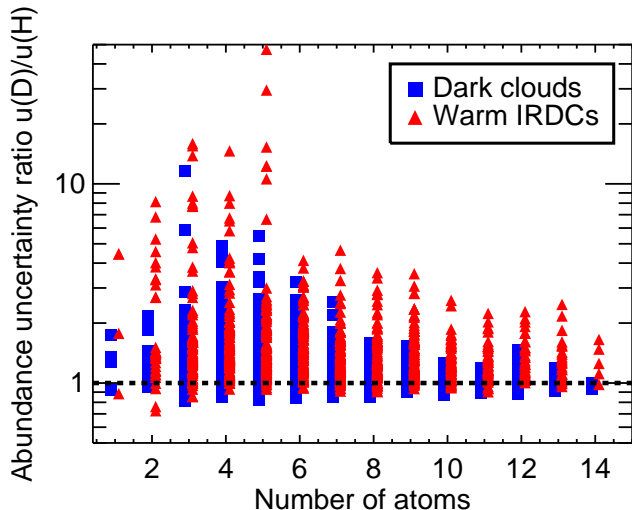


Figure 5. Ratios of abundance uncertainties between un-deuterated and deuterated species with up to three D-atoms, as a function of the number of atoms in a molecule. The dark cloud model results are denoted by squares and the warm infrared dark cloud model results by triangles. The dashed line is added to identify where ratios are close to unity. A colored version of the plot is available in the online version.

comparable to the abundance uncertainties of un-deuterated species in protoplanetary disks (Vasyunin et al. 2008), as well as diffuse and dark dense clouds (e.g., Vasyunin et al. 2004; Wakelam et al. 2010a). Chemically simple species containing Mg, Na, and Si tend to have high uncertainties reaching up to 3 orders of magnitude in abundances because their chemical pathways remain poorly investigated. Also large molecular species, be they rather abundant hydrocarbons (C_nH_m with $n, m \gtrsim 4$), with fractional abundances up to $10^{-9} - 10^{-7}$, or complex and less abundant organic species (e.g. methyl formate, dimethyl ether), have large error bars in the computed abundances. For this latter group, the uncertainties can reach more than one order of magnitude.

In addition to the abundance uncertainties, we also determine uncertainties in the resulting D/H ratios, as shown in Figure 4. Overall, the uncertainties in D/H ratios are lower when compared with the uncertainties of the corresponding H- and D-bearing isotopologues. This is because abundances of the individual isotopologues are often affected by the rate uncertainties in the same way, given that a majority of the deuterium fractionation processes are cloned, thus inheriting the rate of the ‘ancestor’ reaction. We find the same trends as for the abundance uncertainties, but only a hint of increasing uncertainties with number of atoms. Uncertainties for D/H ratios are generally about half of one order of magnitude, but may vary between a factor of 2 and 10. As in the case of the abundance uncertainties, we find the largest D/H uncertainties for large hydrocarbons (C_nH_m , with $n, m \gtrsim 4$), complex organics and species containing Mg, Na, and Si.

The question remains how the uncertainties compare between deuterated and un-deuterated species. To illustrate the overall relative uncertainties between deuterated species and their un-deuterated analogues, we plot in Figure 5 the ratios of abundance uncertainties of up to triply-deuterated species and their un-deuterated analogues as a function of the number of atoms. Note that these relative uncertainties are not the same as the uncertainties in D/H ratios; the former can be labeled as $u(D)/u(H)$, while the latter can be labeled as $u(D/H)$, where u stands for uncertainty. Hence, the $u(D)/u(H)$ ratio al-

lows us to compare the relative errors between deuterated and un-deuterated species.

A majority of deuterated species show larger abundance uncertainties with respect to their un-deuterated analogues. There are two major reasons for this behavior. First, the majority of reactions with deuterated species originate from our cloning procedure, and thus have larger assumed uncertainties. Second, to produce a deuterium isotopologue of a molecule additional chemical pathways (e.g., isotope exchange processes) are required, increasing the accumulation of rate uncertainties. For many hydrocarbons (C_nH_m , $C_nH_m^+$ with $m, n = 2, 3$) the abundance uncertainties of their deuterated isotopologues are comparable to those of the main isotopologues (with ratios of $\sim 0.7 - 2$). These hydrocarbons form through ions of hydrocarbons reacting with H_2 or smaller neutral hydrocarbons, such as CH_4 and C_2H_3 , and their reactions originate purely from the cloning procedure.

For a limited number of species, the abundance uncertainties of their deuterated isotopologues are even smaller than for the main isotopologues (with ratios of $\sim 0.7 - 0.9$; see Figure 5), e.g., C_2D^+ and D^- . These are simple radicals and ions produced by a limited set of reactions, with relatively well-known rate coefficients and thus small uncertainties. The relevant deuterium fractionation chemistry is also limited and has comparably low uncertainties ($\sim 0.7 - 1.1$). Note that the spread in abundance uncertainties ratios appears to decrease with increasing number of atoms in species, getting closer to unity. This effect in Fig. 5 occurs because we plot only species with relative abundances exceeding 10^{-25} (with respect to hydrogen), whose numbers decrease substantially with size. If we also add species with such low abundances, this feature disappears and the trend in the uncertainties between small and large molecules is similar.

For HD and D_2 , we find that the ratio of their abundance uncertainties to that of H_2 can reach very large values, ~ 1000 and ~ 10000 , respectively. This effect occurs because abundances of H_2 are very well constrained (uncertainties are $\sim 10^{-5}$), while HD and D_2 have typical values of abundance uncertainties up to one order of magnitude.

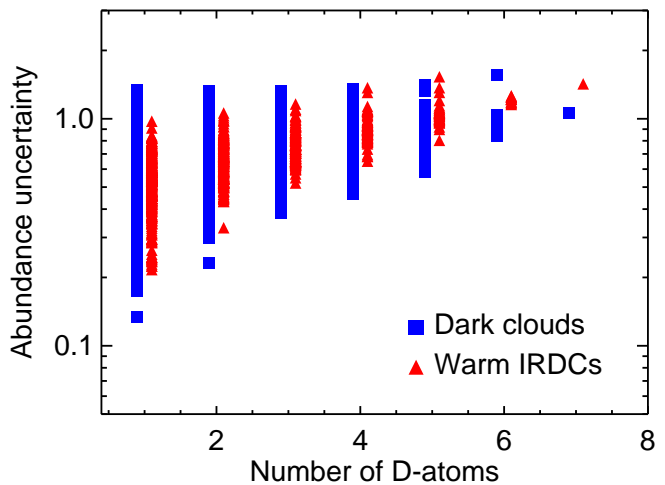


Figure 6. Abundance uncertainties in orders of magnitude for deuterated species as a function of number of D-atoms. The dark cloud model results are denoted by squares and the warm infrared dark cloud model results by triangles. A colored version of the plot is available in the online version.

Finally, in Figure 6 we plot the abundance uncertainties of deuterated species as a function of number of D-atoms, once

again restricted to species with relative abundances $> 10^{-25}$. We see an increase in uncertainty with number of D-atoms, as expected from the increasing number of reactions involved for subsequently adding more D-atoms. We also notice a wider spread in uncertainties for species with lower levels of deuteration because smaller species, such as OD, HDO, DCO^+ , often have lower uncertainties because there are not as many steps involved in their formation compared to larger species. Larger multiply-deuterated species cannot have these low uncertainties as there are too many steps involved in their formation. Once again we also find that dark clouds have a larger spread in uncertainties than warm IRDCs. Again we argue that this difference occurs because dark cloud environments overall have higher abundances of deuterated species which are processed through more reactions.

3.3. General trends in D/H distributions

In this section, we discuss general trends in the modeled D/H ratios in our 2D-parameter space (see Section 2.1). The computed D/H fractionation ratios at the final time of 1 Myr are shown in Figure 7 for the “Primordial” (left panels of each separate block) and “Evolution” model (right panels of each separate block), which were introduced in Section 2.3, as functions of density and temperature for the following key gaseous molecules: H_2DO^+ , H_2D^+ , HDO, D_2O , ND, ND_3 , DCOOH and DCN . For most species, the D/H ratios can reach high values of $\gtrsim 10^{-3}$ at $T \lesssim 30\text{--}80$ K. At higher temperatures, $\gtrsim 100$ K, the computed D/H ratios begin to approach the elemental ratio of $\approx 1.5 \times 10^{-5}$. The higher D/H ratios of $\gtrsim 0.1$ have been observed for many species in the ISM, such as CH_2DOH , D_2CO (Ceccarelli 2002), D_2O (Butner et al. 2007), H_2D^+ (Caselli et al. 2003), HDO (Liu et al. 2011), NH_2D (Hatchell 2003; Roueff et al. 2005), NHD_2 (Roueff et al. 2005). For comparison of our model results with observations, see Section 4.1.

We isolate species that are either mostly sensitive to kinetic temperature or initial abundances, the former referring to the standard temperature dependence for deuterium fractionation, and the latter referring to the difference between the initial abundances in the “Primordial” and evolutionary models. We note that usually species for which D/H ratios depend more strongly on the initial abundances also show (a weaker) temperature dependence, because the release of CO and other radicals decreases the abundances of the H_3^+ isotopologues which lowers the efficiency of transferring D atoms to other species. These two groups are listed in Table 5. The temperature-dependent species can be further divided into two subgroups by the temperature where D/H ratios decrease most sharply, and hence where deuterium fractionation becomes less pronounced: (1) at low temperatures, $T \sim 20\text{--}40$ K (related to the fractionation via H_3^+ isotopologues) and (2) at higher temperatures $T \sim 80$ K (related to the fractionation via CH_2D^+ and C_2HD^+).

The left two columns of Figure 7 show species that demonstrate a strong dependence of D/H ratios on the initial abundances while the right two columns show species with a strong temperature gradient for D/H ratios and no distinct dependence on initial abundances. We define here a strong dependence on the initial abundance as an overall variation by a factor of 5 in D/H ratios at temperatures > 100 K for the final time step. For the case of HDO in Figure 7, D/H ratios are approximately 2 orders of magnitude higher in the “Evolution” model compared to the “Primordial” model at temper-

atures > 100 K and hence its D/H ratios are considered to depend strongly on the initial abundance. Frozen molecules show D/H distributions similar to their gas-phase analogues as we do not specifically consider selective substitution of H by D in surface species (yet we do consider production of deuterated molecules by surface chemistry). Therefore, we do not discuss the distribution of D/H for ices separately.

The placement of species in different groups can be explained by the relative pace of their chemical evolution. If steady-state abundances are reached by 1 Myr in the “Primordial” stage, then they remain at steady state throughout the evolutionary model unless the physical conditions are changed. In Figure 8 we show the evolution of D/H ratios at three separate times of $10^4, 10^5, 10^6$ years, and at a density $n_{\text{H}} = 10^4 \text{ cm}^{-3}$ as a function of temperature for H_2D^+ , CH_2D^+ and HDO. We discuss the specific case for the evolution of HDO later and begin with the two ions (two top panels) which are highly reactive, with fast chemical timescales associated with ion-neutral reactions and dissociative recombinations. Thus, the chemical “memory” of the pristine state of the fast-evolving deuterated species is completely lost at the final considered time of 1 Myr, with no apparent differences between abundances computed with the two distinct initial abundance sets.

We find that the majority of neutral species, which includes several H-, C-, O-, N- and S-bearing species, show a dependence on the initial abundance as their evolution is significantly slower compared to ions. These are predominantly neutral species unless they are strongly associated with one of the major ions (such as H_3^+ , CH_3^+ , HCO^+ and their isotopologues). This is illustrated in Figure 8 for HDO (bottom panel), where we see differences in D/H ratios of ~ 3 orders of magnitude between the two models at higher temperatures approaching 100 K. In the “Primordial” model we start with atomic abundances and the water D/H ratios are lower for ices than for gas vapor because. This is because the formation of key ingredients for HDO ice through $\text{OD} + \text{H}$ or $\text{OH} + \text{D}$ is slower gas-phase fractionation via ion-molecule processes. In contrast, the “Evolution” model starts with high abundances and D/H ratios of water, mostly frozen onto grains. At low temperatures < 30 K water quickly reach the steady-state abundances while at higher temperatures, because gas-phase fractionation is not efficient, the D/H ratios of water vapor decreases with increasing temperature. Desorption play an important role at temperatures above 20–30 K where, even in highly obscured regions, CRP-driven desorption occurs. At temperatures $\gtrsim 100$ K we see a drop in D/H ratios down to similar values of water ice because desorption replenishes the water vapor constantly and the water vapor also inherits the same D/H ratios as the ice ($\sim 10^{-2}$).

H_2DO^+ was the only ion we found showing a significant difference in the distribution between the two sets of initial abundances, which is related to the protonation of HDO by H_3^+ and which thus behaves chemically similar to HDO (see above). Complex neutral species, which are not a direct outcome of fast dissociative recombination reactions, evolve more slowly via neutral-neutral and surface processes, and thus show a dependence on the adopted initial abundances. The high initial abundances of deuterated species accumulated at 10 K in the “Evolution” model enable rich deuterium chemistry during the entire time span of 1 Myr even at warm temperatures of $T \lesssim 50\text{--}100$ K. As a result, some species show almost uniformly high D/H ratios of $\gtrsim 10^{-3}$ at

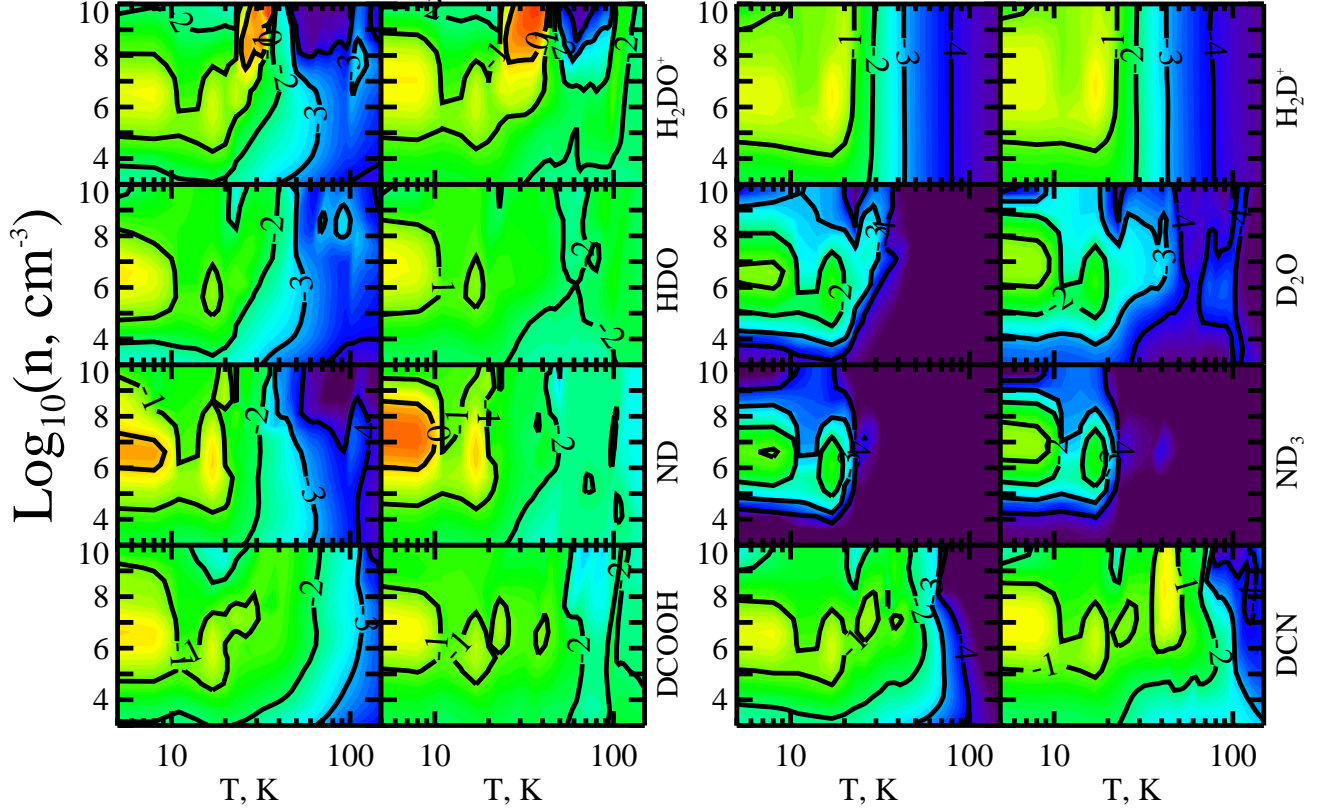


Figure 7. Plots of the D/H distributions at 1 Myr for our models. Each panel is a contour plot displaying the distribution of specific logarithmic D/H ratios. In the online version, fractionation levels with elemental (low), intermediate, and high D/H fractions are indicated with a continuous scale starting with dark blue ($< 10^{-5}$), green (10^{-2}), yellow (10^{-1}), and red (≥ 1) colors. If we label the columns as 1, 2, 3, and 4 from left-to-right, columns 1 and 3 show results from the “Primordial” model, while columns 2 and 4 show results from the evolutionary model. Columns 1 and 2 show ratios with significant differences from the norm in their strong dependence on initial abundance, where significant differences of more than one order of magnitude are also visible at high temperatures > 100 K. Columns 3 and 4 show species with an unusually strong dependence on temperature (with elemental D/H ratio of $\sim 1.5 \cdot 10^{-5}$ achieved either at low, ~ 20 – 40 K or high, ~ 80 K, temperatures).

Table 5
Species showing strong dependences on initial abundances or temperature

Initial abundances	Temperatures	
	~ 30 K	~ 80 K
C ₂ HD, C ₃ HD, C ₆ D, CD, CD ₂ , CD ₃ OH CH ₂ D ₂ , CH ₂ DCN, CH ₂ DOH, CHD ₂ OH CHDCO, D ₂ CO, D ₂ CS, DC ₃ N, DC ₅ N DCOOCH ₃ , DCOOH, DCS ⁺ , DNCO, H ₂ DO ⁺ HDCO, HDO, HDS, ND, NH ₂ D, NHD ₂ , OD	C ₂ D ₂ , C ₂ HD ⁺ , CD ₄ CHD, CHD ₃ , N ₂ D ⁺ D ₂ O, D ₂ S, D ₃ ⁺ , D ₃ O ⁺ , DCN, DCO ⁺ , DNC, DOC ⁺ , H ₂ D ⁺ HD ₂ ⁺ , HD ₂ O ⁺ , N ₂ D ⁺ , ND ₃	C ₂ HD ⁺ , CH ₂ D ⁺ , CHD ₂ ⁺ CH ₃ D

$T = 10$ – 150 K (see Figure 7, left column). On the other hand, the same species in the “Primordial” model (with only HD available initially) show a significant decrease in the final D/H ratios toward warmer temperatures ($\gtrsim 40$ – 80 K). The effect is strong for saturated species that are at least partly formed on dust surfaces, and thus are sensitive to the choice of the initial abundances (and temperature), such as water or ammonia isotopologues. Also, most multiply-deuterated species, whose formation involves several isotope exchange reactions, show strong dependence on the initial abundances.

Ions constitute the majority of species for which calculated D/H ratios are only dependent on temperature (see Figure 7, right two columns). Species such as the H_3^+ isotopologues that are sensitive to freeze-out (or specifically, the freeze-out of CO), “daughter” molecules such as DCO⁺, as well as (ionized) light hydrocarbons related to CH₂D⁺ and C₂HD⁺, all show a strong temperature dependence. From the exact

gas kinetic temperature, labeled the critical temperature, at which the D/H ratios start to approach the elemental value, we can separate these species into two subgroups. The deuterated species formed via low-temperature fractionation channels involving isotopologues of H_3^+ have a critical temperature of 20 – 30 K, whereas other deuterated species synthesized via high-temperature fractionation channels involving CH₂D⁺ and C₂HD⁺ show a higher critical temperature of ~ 80 K (Parise et al. 2009). Most multi-deuterated species belong exclusively to the low-temperature group as do the majority of ions, which inherit the temperature dependence from the H_3^+ isotopologues via proton/deuteron transfer reactions. The best example of such species is H₂D⁺, shown in Figure 7. It shows a D/H turnover point at 20 K, after which the fractionation ratios decrease smoothly and reach levels of $\sim 10^{-5}$ at temperatures of ~ 100 K.

There are only a few species that show a dependence on

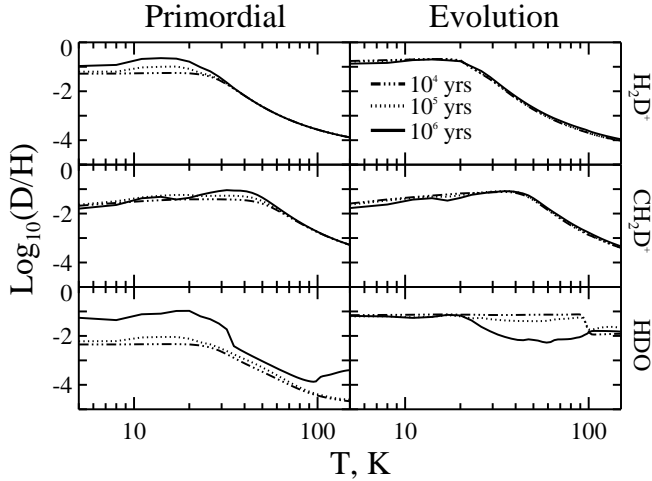


Figure 8. D/H ratios for H_2D^+ , CH_2D^+ and HDO as a function of temperature at a density $n_{\text{H}} = 10^4 \text{ cm}^{-3}$ and for three specific times: $10^4, 10^5, 10^6$ years.

temperature where deuterium fractionation is reduced at $T \sim 80 \text{ K}$. Those are directly synthesized from deuterated light hydrocarbon ions such as CH_2D^+ , which retain high D/H ratios at elevated temperatures, e.g. DCN and CH_2D_2 . HDCS is unique in showing no clear difference between the two models at least within our defined temperature range, as its chemical evolution depends almost equally on the two distinct deuterium fractionation routes (via H_3^+ and light hydrocarbon isotopologues) via the formation of the ion H_2DCS^+ .

Also, we find that the overall sensitivity of the calculated D/H ratios to density is weak, except for species sensitive to the freeze-out of CO and other radicals, i.e. H_2D^+ , HD_2^+ , and their direct dissociative recombination products. These species experience a rapid decrease in fractionation ratios toward lower densities of $< 10^4 \text{ cm}^{-3}$, at which CO cannot severely deplete onto the dust grains even after 1 Myr of evolution. However, if we would follow the evolution of our chemical model beyond 1 Myr, at some moment the CO depletion can become severe enough for low-density regions to allow high D/H ratios for the H_3^+ isotopologues (if the adopted non-thermal desorption rate is not too high).

To understand in more detail the differences between the evolution of deuterated molecules, we have analyzed the chemistry of several key isotopologues. We considered four distinct astrophysical environments: densities of 10^4 and 10^8 cm^{-3} , and temperatures of 10 and 80 K for both the “Primordial” and “Evolution” initial abundance sets. We list key formation and destruction pathways for the assorted species and their main reactants as online material (see Appendix B).

4. DISCUSSION

In recent years, it has been realized that the ortho/para ratio of H_2 and other species in a source can strongly affect the degree of deuterium fractionation. For example, the backward endothermic reaction between o- H_2 and H_2D^+ can proceed far more rapidly at low temperatures such as 10 K than the corresponding reaction involving p- H_2 , and so reduce the degree of deuterium fractionation if there is a sufficient amount of o- H_2 (e.g., Flower & Pineau-Des-Forêts 1990; Pagani et al. 1992; Flower et al. 2006; Sipilä et al. 2010; Pagani et al. 2013). The fraction of H_2 in its ortho levels is small but not well known, however, and can only be obtained by careful analysis of reduced fractionation levels in specific sources. Given the com-

plexity and huge size of our chemical network, with many reactions containing ortho and para reactants, we chose not to include the different states of deuterated and non-deuterated species for the moment, and leave this to a separate study. Thus, our network is rather accurate for modeling dense, cold ISM phases, where H_2 mainly exists in its para state (e.g., Pagani et al. 2009) and higher temperature phases where the degree of fractionation is in any case low.

Another important effect concerning deuterium fractionation that is not fully treated by our approach is the evolution of physical conditions, such as a steady warm-up phase of a protostellar envelope leading to the formation of a hot core/corino. Our simple evolutionary model, where we simulate a TMC-1 environment for 1 Myr and use these final abundances as the initial abundances for the modeling is only a “poor man’s” approach for such a study (see, e.g., Cazaux et al. 2011; Aikawa et al. 2012). Certainly this abrupt change from TMC-1 temperature and density to other temperatures and densities does not catch the gradual evolution of the physical conditions from one phase to the next. As we showed in Section 3, D/H ratios for a large number of the deuterated species are mainly dependent on temperature, while density has an effect on the evolution of a limited number of species. The gradual increase in temperature throughout the collapse of a dark cloud and the formation of a (proto)star will undoubtedly affect the evolution of some deuterated species in ways uncatchable by our approach. Examples include the release of key ice species into the gas-phase or the steady increase in mobility of surface radicals, which produce complex organic molecules (Garrod et al. 2008). However, the effects on predicted D/H ratios are likely to be only minor as the final stages of collapse are rapid, so that deuterium fractionation of the gas-phase species stays until the material winds up in the actual protostar or in the protoplanetary disk surrounding it (Aikawa et al. 2008, 2012).

4.1. Observations

We have listed in Tables 6-8 we list the the most abundant, (potentially) observable deuterated species with ALMA in dark clouds, infrared dark clouds (IRDCs), and high-mass protostellar objects (HMPOs), respectively. In order to predict the observability of molecules in these different environments we use the Cologne Database of Molecular Spectroscopy (CDMS; Müller et al. 2001, 2005) to calculate line fluxes under local thermal equilibrium conditions (LTE) for various deuterated molecules with transitions observable by ALMA. For these estimates we assume the following parameters for the different environments: for dark clouds temperature 10 K, number density 10^4 cm^{-3} and H_2 column density 10^{22} cm^{-2} (Launhardt et al. 2013), for warm IRDCs 25 K, 10^5 cm^{-3} and H_2 column density 10^{24} cm^{-2} (e.g. Rathborne et al. 2008), and for HMPOs 75 K, 10^5 cm^{-3} and column density 10^{24} cm^{-2} (e.g. Beuther et al. 2007; Rodón et al. 2008). There are known differences in H_2 column densities between interferometry and single-dish observations (Vasyunina et al. 2009). While we concentrate here on the higher end of column densities for our calculations, the calculated line fluxes can be adopted to the lower column densities by simply dividing them by 10.

For dark clouds and warm IRDCs we implement the atomic initial abundances, while for HMPOs we implemented instead the “Evolution” model (with initially high D/H ratios). Line intensities for a few molecules (e.g. DCO^+) can also

Table 6
Observable deuterated species with ALMA in dark clouds.

Species	$n(x)/n(H_2) [\times 10^{-11}]$	Line	Frequency [GHz]	Line flux [mK]	ALMA band
D_2CO	1.05	3 0 3 \rightarrow 2 0 2	174.413	33.48	5
		4 0 4 \rightarrow 3 0 3	231.410	28.48	6
		5 0 5 \rightarrow 4 0 4	287.486	14.99	7
D_2O	53.6	1 1 0 \rightarrow 1 0 1	316.800	1899.80	7
		2 0 2 \rightarrow 1 1 1	468.247	853.66	8
		2 1 1 \rightarrow 2 0 2	403.562	198.18	8
D_2S	0.0634	2 2 0 \rightarrow 1 1 1	669.787	1.40	9
DCN^*	5.21	1 \rightarrow 0	115.271	6648.00	3
		2 \rightarrow 1	230.538	5272.00	6
		3 \rightarrow 2	345.796	3860.00	7
DCO^+	16.04	2 \rightarrow 1	144.077	2196.40	4
		4 \rightarrow 3	288.144	2054.53	7
		5 \rightarrow 4	360.170	801.50	7
DNC	11.01	2 \rightarrow 1	152.610	1047.68	4
		4 \rightarrow 3	305.207	866.60	7
		6 \rightarrow 5	457.776	66.33	8
H_2DO^+	29.93	1 0 1 1 \rightarrow 2 1 1 0	250.914	9.84	6
$HDCO$	24.69	4 0 4 \rightarrow 3 0 3	256.586	616.96	6
		2 0 2 \rightarrow 1 0 1	128.813	513.23	4
		3 1 2 \rightarrow 2 1 1	201.341	313.03	5
$HDCS$	0.7897	5 0 5 \rightarrow 4 0 4	154.885	4.12	4
		3 0 3 \rightarrow 2 0 2	92.982	3.12	3
		6 0 6 \rightarrow 5 0 5	185.693	3.01	5
HDS	1.630	2 0 2 \rightarrow 1 0 1	477.764	25.62	8
		1 0 1 \rightarrow 0 0 0	244.556	18.22	6
		1 1 0 \rightarrow 1 0 1	195.559	9.05	5
ND	27.03	1 0 1 2 \rightarrow 0 1 2 3	491.934	294.70	8
		1 0 1 2 \rightarrow 0 1 1 2	491.969	124.38	8
		1 0 1 1 \rightarrow 0 1 2 2	491.917	123.84	8
ND_3	0.96	2 0 0 \rightarrow 1 0 1	614.933	73.05	9
		2 1 1 \rightarrow 1 1 0	618.125	60.59	9
		2 1 0 \rightarrow 1 1 1	614.968	59.74	9
NH_2D	296.70	1 1 0 1 \rightarrow 0 0 0 0	494.455	10000.00	8
		1 1 1 0 \rightarrow 1 0 1 1	85.926	870.34	3
		1 0 1 1 \rightarrow 0 0 0 1	332.782	732.35	7
NHD_2	14.60	2 1 1 0 \rightarrow 1 0 1 1	699.224	874.07	9
		2 1 1 1 \rightarrow 1 0 1 0	709.350	456.67	9
		1 1 1 0 \rightarrow 0 0 0 0	335.514	40.68	7

The table is limited to species with relative abundances $> 10^{-12}$.

Species detected unambiguously or in a preliminary manner in the specific environments are marked in boldface.

Parameters for line flux calculations: 10 K , 10^4 cm^{-3} , 10^{22} cm^{-2}

* DCN should be observable, but is not listed in CDMS or RADEX, instead calculated RADEX values for HCN are listed.

be estimated using the non-LTE molecular radiative transfer tool RADEX (van der Tak et al. 2007). Because RADEX and our calculations using CDMS gave different results we scaled our CDMS calculations to match RADEX values for linear molecules (e.g. DCO^+). We look for transitions in bands 3 - 9 for ALMA (84 - 720 GHz with gaps between bands, see science.nrao.edu/facilities/alma/observing) and consider a line sensitivity limit of 1 mK for all bands. In Tables 6-8 are only the three strongest transitions listed, while a full list is available upon request from the authors.

Amongst these listed species are tracers (through D/H ratios) of initial abundances (e.g. D_2CO , HDO , NH_2D , CH_2D^+) and temperature (D_2O , DCO^+ , DCN , D_2S) as we have listed in Table 5. A few ions are observable with ALMA, such as DCO^+ , H_2DO^+ , CH_2D^+ . We find that the tracer of ionization in the cold ISM regions with high depletion, H_2D^+ and HD_2^+ , will be hard to detect with ALMA, as found by Chapillon et al. (2011) for protoplanetary disks. We note that all isotopologues of ammonia are easily observable in the all three ISM environments. The metastable doublet lines of NH_3 are used to constrain gas temperature (e.g. Ho & Townes 1983; Maret et al. 2009). We think that using the relative abundances of the minor NH_3 isotopologues one could also discern the previous temperature history of the environment. We determine that several sulphur-bearing species, such as $HDCS$, D_2CS , HDS , should be observable by ALMA, and as sulphur chemistry is not well understood yet, observations of these species could serve as proxies for future studies. Finally

Table 7
Observable deuterated species with ALMA in infrared dark clouds.

Species	$n(x)/n(H_2) [\times 10^{-11}]$	Line	Frequency [GHz]	Line flux [mK]	ALMA band
C_4D	0.039	11 12 \rightarrow 10 11	97.140	2.36	3
		12 13 \rightarrow 11 12	105.971	2.35	3
		10 11 \rightarrow 9 10	88.308	2.25	3
CH_2D^+	0.045	2 1 2 \rightarrow 1 1 1	490.012	44.05	8
		1 0 1 \rightarrow 0 0 0	278.692	10.68	7
		2 1 1 \rightarrow 2 1 2	201.754	1.62	5
CH_2DCN	0.0038	9 0 9 \rightarrow 8 0 8	156.281	7.47	4
		10 0 10 \rightarrow 9 0 9	173.639	6.73	5
		6 0 6 \rightarrow 5 0 5	104.198	6.00	3
D_2CO	0.011	5 0 5 \rightarrow 4 0 4	287.486	63.48	7
		6 0 6 \rightarrow 5 0 5	342.522	48.67	7
		3 0 3 \rightarrow 2 0 2	174.413	45.25	5
D_2O	3.10	1 1 0 \rightarrow 0 0 0	317.800	30000.00	7
		2 0 2 \rightarrow 1 0 1	468.247	30000.00	8
		2 1 1 \rightarrow 1 0 0	403.562	24681.37	8
DCN^*	0.38	1 \rightarrow 0	88.634	21800.00	3
		2 \rightarrow 1	177.258	20590.00	5
		3 \rightarrow 2	265.886	19040.00	6
DCO^+	47.09	5 \rightarrow 4	360.170	30000.00	7
		3 \rightarrow 2	216.113	30000.00	6
		6 \rightarrow 5	432.189	30000.00	8
DNC	0.81	3 \rightarrow 2	228.910	24216.75	6
		6 \rightarrow 5	457.776	14474.58	8
		2 \rightarrow 1	152.610	11600.74	4
DOC^+	0.00062	3 \rightarrow 2	229.149	15.36	6
		5 \rightarrow 4	318.885	15.26	7
		6 \rightarrow 5	458.237	9.15	8
H_2DO^+	3.39	1 0 1 1 \rightarrow 2 1 1 0	250.914	2582.00	6
		3 3 10 \rightarrow 2 2 1 1	649.653	368.10	9
		3 3 00 \rightarrow 2 2 0 1	632.902	342.59	9
$HDCO$	0.10	5 0 5 \rightarrow 4 0 4	319.770	629.27	7
		3 0 3 \rightarrow 2 0 2	192.893	502.15	5
		4 1 3 \rightarrow 3 1 2	268.292	426.06	6
$HDCS$	0.0065	7 0 7 \rightarrow 6 0 6	216.662	6.88	6
		5 0 5 \rightarrow 4 0 4	154.885	6.46	4
		8 0 8 \rightarrow 7 0 7	247.488	5.69	6
HDS	0.018	1 1 1 \rightarrow 0 0 0	389.041	70.17	8
		2 0 2 \rightarrow 1 0 1	477.764	62.06	8
		3 0 3 \rightarrow 2 0 2	691.498	45.74	9
ND	0.16	1 0 1 2 \rightarrow 0 1 2 3	491.934	357.79	8
		1 0 1 2 \rightarrow 0 1 1 2	491.969	150.99	8
		1 0 1 1 \rightarrow 0 1 2 2	491.917	150.36	8
ND_3	0.0080	2 1 1 \rightarrow 1 1 0	618.125	125.84	9
		2 1 0 \rightarrow 1 1 1	614.968	124.41	9
		1 0 1 \rightarrow 0 0 0	309.909	68.34	7
NH_2D	27.15	1 1 0 1 \rightarrow 0 0 0 0	494.455	30000.00	8
		2 0 2 1 \rightarrow 1 0 1 1	649.916	17102.87	9
		1 1 1 0 \rightarrow 1 0 1 1	85.926	16766.37	3
NHD_2	0.45	1 1 0 1 \rightarrow 0 0 0 0	388.652	4199.24	8
		2 1 1 1 \rightarrow 1 0 1 0	709.350	3793.42	9
		2 0 2 0 \rightarrow 1 1 0 1	410.491	296.35	8

The table is limited to with relative abundances $> 10^{-12}$.

Species detected unambiguously or in a preliminary manner in the specific environments are marked in boldface.

Parameters for line flux calculations: 25 K , 10^5 cm^{-3} , 10^{24} cm^{-2}

* DCN should be observable, but is not listed in CDMS or RADEX, instead calculated RADEX values for HCN are listed.

we note that the HDO lines are expected to be observable with ALMA, but it is not included into CDMS, and we could not calculate its line intensities assuming LTE. On the other hand, water has a complex level structure, with some of the lines that are masing and many that become highly optically thick, and the escape probability non-LTE method of RADEX is not capable of modeling its line intensities reliably. For estimation of the water line fluxes one has to perform a full line radiative transfer modeling for each individual object.

For deuterated ices we only list the most abundant species in Table 9 and do not try to predict their observability. Amongst the deuterated ices we find several polyynes (C_nH_2 , with $n > 4$) are abundant, especially at temperatures $> 10\text{ K}$. These species have been observed in the Solar system such as in Titan's atmosphere (e.g. Teanby et al. 2009), but should also be abundant in ices in interstellar space. Several organics such as deuterated formic acid and hydroxylamine (both singly- and doubly-deuterated) are abundant, even among the

Table 8
Observable deuterated species with ALMA in high-mass protostellar objects.

Species	$n(x)/n(H_2) [\times 10^{-11}]$	Line	Frequency [GHz]	Line flux [mK]	ALMA band
C_4D	0.95	23 24 \rightarrow 22 23	203.104	28.13	5
		22 23 \rightarrow 21 22	194.275	27.98	5
		24 25 \rightarrow 23 24	211.932	27.96	6
C_6D	0.018	42 -1 43 \rightarrow 41 1 42	112.462	1.97	3
		41 -1 42 \rightarrow 40 1 41	109.856	1.97	3
		41 1 42 \rightarrow 40 -1 41	109.816	1.97	3
D_2CO	0.0017	8 0 8 \rightarrow 7 0 7	499.596	2.44	8
		11 0 11 \rightarrow 10 0 10	605.672	2.21	9
		7 0 7 \rightarrow 6 0 6	396.517	2.18	8
D_2CS	0.000658	12 0 12 \rightarrow 11 0 11	337.599	1.79	7
		14 0 14 \rightarrow 13 0 13	392.631	1.78	8
		11 0 11 \rightarrow 10 0 10	309.916	1.71	7
D_2O	1.87	2 1 1 \rightarrow 2 0 2	403.562	5768.78	8
		4 2 2 \rightarrow 3 1 1	692.244	3398.71	9
		2 0 2 \rightarrow 1 0 1	468.247	3334.45	8
DCN*	0.21	1 \rightarrow 0	88.634	71760.00	3
		2 \rightarrow 1	177.258	70430.00	5
		3 \rightarrow 2	265.886	68680.00	6
DCO ⁺	23.91	9 \rightarrow 8	648.193	75000.00	9
		6 \rightarrow 5	432.189	75000.00	8
		5 \rightarrow 4	360.170	75000.00	7
DCS ⁺	0.0023	12 \rightarrow 11	432.338	5.49	8
		10 \rightarrow 9	360.307	5.27	7
		13 \rightarrow 12	468.347	5.23	8
DNC	0.41	9 \rightarrow 8	686.553	7042.88	9
		6 \rightarrow 5	457.776	6233.04	8
		4 \rightarrow 3	305.206	3003.38	7
H_2DO^+	2.27	3 3 1 0 \rightarrow 2 2 1 1	649.653	2352.22	9
		3 3 0 0 \rightarrow 2 2 0 1	632.902	2258.85	9
		4 1 3 0 \rightarrow 3 0 3 1	716.959	1629.36	9
HDCO	0.093	10 10 10 \rightarrow 9 0 9	625.688	136.82	9
		7 0 7 \rightarrow 6 0 6	444.229	134.73	8
		8 1 8 \rightarrow 7 1 7	491.937	129.31	8
HDCS	0.56	13 0 13 \rightarrow 12 0 12	400.766	151.96	8
		11 0 11 \rightarrow 10 0 10	339.646	148.23	7
		14 0 14 \rightarrow 13 0 13	431.218	145.25	8
ND	3.70	10 1 2 \rightarrow 0 1 2 3	491.934	911.92	8
		10 1 2 \rightarrow 0 1 1 2	491.969	384.82	8
		10 1 1 \rightarrow 0 1 2 2	491.917	383.23	8
ND ₃	0.0031	2 1 1 \rightarrow 1 0 0	618.125	4.24	9
		2 1 0 \rightarrow 1 0 0	614.968	4.20	9
		1 0 1 \rightarrow 0 0 0	309.909	1.14	7
NH ₂ D	25.07	1 1 0 1 \rightarrow 0 0 0 0	494.455	8876.12	8
		3 3 0 0 \rightarrow 3 2 2 1	618.142	5010.99	9
		2 2 0 1 \rightarrow 2 1 2 0	475.890	4998.31	8
NHD ₂	0.37	2 1 1 1 \rightarrow 1 0 1 0	709.350	301.28	9
		1 1 0 1 \rightarrow 0 0 0 0	388.652	158.40	8
		3 1 2 1 \rightarrow 2 2 0 0	672.370	40.29	9

The table is limited to species with relative abundances $> 10^{-12}$.

Species detected unambiguously or in a preliminary manner in the specific environments are marked in boldface.

Parameters for line flux calculations: 75 K, 10^5 cm^{-3} , 10^{24} cm^{-2}

* DCN should be observable, but is not listed in CDMS or RADEX, instead calculated RADEX values for HCN are listed.

most abundant at higher temperatures ($\gtrsim 25$ K). Also both ammonia and water (singly- and doubly-deuterated) show high abundances.

Uncertainties for the predicted abundances are factors of ~ 1.5 – 5 for species made of $\lesssim 3$ – 4 atoms and $\gtrsim 1.5$ – 10 for more complex ones. Apart from the estimated abundance and D/H ratio uncertainties due to the errors in the rate coefficients, we also have error bars associated with the exact estimation of physical properties of the observed environment (uncertainties in dust emissivity, temperature, poorly known dust-to-gas mass ratio, etc.) Also, many of the published observed D/H values are based on measurements made from several sources, for which derived physical properties can differ significantly.

We now discuss how our model results compare with assorted observations. van Dishoeck et al. (1995) observed several deuterated species towards the protobinary source IRAS 16293, namely, DCO⁺, DCN, C₂D, HDS, HDCO, NH₂D, detected in the different regions around the protostar. The first region is the warm and dense inner core ($T \gtrsim 80$ K, $n_H \sim 10^7$

cm^{-3}) found to be rich with organic molecules, the second is the circumbinary envelope with $T \sim 40$ K and $n_H \sim 10^6$ – 10^7 cm^{-3} , where molecules such as DCO⁺ and HDCO were found, and the third is the colder, low-density outer part of the envelope with $T \sim 10$ – 20 K and $n_H \sim 10^4$ – 10^5 cm^{-3} with radicals such as CN, C₂H, C₃H₂. We find good agreement between our calculated values and those derived for all observed species. As an example, HDCO shows a D/H ratio of 0.13 in our “Evolution” model compared with the observed value of 0.14, and for DCN the D/H ratio is 0.027 compared with the observed ratio of 0.013. The worst agreement we find is for C₂D and DCO⁺ with a difference of a factor of ~ 5 in the D/H ratios, which is still acceptable agreement. Uncertainties for these species range between factors of 2–5, with largest uncertainties for C₂D and DCN. Considering these uncertainties, our predicted D/H values are in agreement with the IRAS-16293 observations.

Caselli et al. (2003) detected ortho-H₂D⁺ towards the prestellar core L1544, with derived abundances of 7.2×10^{-10} and 3.2×10^{-10} at the peak and off-peak positions, respectively. For our ÒPrimordialÓ model with a core density $n_{H_2} = 10^6 \text{ cm}^{-3}$, a temperature 7 K, and an appropriate equilibrium o/p ratio of 3:1 taken from Walmsley et al. (2004), we find reasonable agreement with calculated abundances of 0.7 – 4.8×10^{-10} in the core (peak position) and 2.3 – 4.2×10^{-10} at the off-peak position, with a lower density, assuming a density of 10^4 – 10^5 cm^{-3} . We however find a higher abundance at the off-peak position; there are several possible reasons for the discrepancy such as incorrect treatment of the ortho-para species in the network or the lack of a detailed physical model. A detailed study is not within the scope of this paper but we note that abundances are within a factor of 2–3 of observed abundances.

Stark et al. (2004) observed H₂D⁺, DCO⁺, HCO⁺, HDO and H₂O toward the protobinary source IRAS 16293 (A and B) as well as the cold prestellar object IRAS 16293 E. They measured the H₂D⁺ abundance to be 2×10^{-9} in the cold, outer envelope with $n_{H_2} = 10^4$ – 10^5 cm^{-3} and $T < 20$ K, where our ÒEvolutionÓ model predicts a similar abundance of $\sim 10^{-9}$. In the inner envelope the temperature is higher, depleting the H₃⁺ isotopologues as CO returns to the gas phase, and the abundance decreases to $\sim 10^{-12} \text{ cm}^{-3}$. The temperature in the inner envelope is not well constrained, but with a central density of $\sim 10^6 \text{ cm}^{-3}$ we find the best agreement at temperatures ≈ 30 K, with an abundance of 1.2×10^{-12} , and the agreement worsens if the temperature is increased, as more CO returns into the gas phase and the overall deuterium fractionation ceases. DCO⁺ and HCO⁺ were observed with abundances 2×10^{-11} and $< 1 \times 10^{-9}$ respectively, which agree with our model values from 17–26 K with DCO⁺ abundances 8.4×10^{-11} – 8.2×10^{-11} and HCO⁺ abundances 4.7×10^{-10} – 1.1×10^{-9} , leading to a D/H ratio of 0.078–0.18. HDO and H₂O were observed with abundances 3×10^{-10} and 3×10^{-7} – 4×10^{-9} respectively, which agree reasonably well with our modeled abundances of 5.9×10^{-12} – 6.3×10^{-11} and 9.9×10^{-10} – 1.7×10^{-8} , respectively. Lastly, HDO, DCO⁺ and HCO⁺ were also observed in the prestellar core object IRAS 16293 E. From estimated temperatures 16–25 K and densities 1.1 – $1.6 \times 10^6 \text{ cm}^{-3}$ we estimate DCO⁺ abundances to be 7.0×10^{-11} – 2.9×10^{-9} and HCO⁺ abundances 8.9×10^{-11} – 1.10×10^{-9} , leading to a D/H ratio 0.26–0.79. This agrees well with the observed abundances of 5.0×10^{-11}

Table 9
Fractional abundances and D/H ratios: deuterated ices.

Dark Clouds			Warm IRDCs			HMPOs		
Species	Abundance	D/H ratio	Species	Abundances	D/H ratios	Species	Abundances	D/H ratios
HDO	3.90×10^{-7}	4.26×10^{-3}	HDO	6.77×10^{-8}	2.94×10^{-3}	HDO	8.68×10^{-7}	1.27×10^{-2}
CH ₃ D	1.41×10^{-7}	8.70×10^{-3}	HDO ₂	4.06×10^{-9}	1.78×10^{-3}	NHDOH	1.73×10^{-7}	9.25×10^{-2}
NH ₂ D	6.75×10^{-8}	6.14×10^{-3}	NH ₂ D	2.48×10^{-9}	7.40×10^{-3}	NH ₂ D	1.68×10^{-7}	2.21×10^{-2}
C ₃ HD	5.38×10^{-9}	9.61×10^{-3}	C ₃ HD	6.62×10^{-10}	7.75×10^{-4}	D ₂ O	1.11×10^{-8}	1.63×10^{-4}
CH ₂ D ₂	1.89×10^{-9}	1.17×10^{-4}	D ₂ O	4.68×10^{-10}	1.15×10^{-5}	HDO ₂	5.01×10^{-9}	7.95×10^{-2}
DNO	1.72×10^{-9}	1.06×10^{-1}	CHDCO	2.77×10^{-10}	1.83×10^{-3}	ND ₂ OH	3.14×10^{-9}	1.68×10^{-3}
D ₂ O	1.05×10^{-9}	1.15×10^{-5}	DCN	2.30×10^{-10}	1.04×10^{-3}	NHD ₂	2.65×10^{-9}	3.29×10^{-4}
HDS	6.72×10^{-10}	1.15×10^{-2}	DCOOH	1.72×10^{-10}	4.31×10^{-2}	C ₃ HD	2.45×10^{-9}	1.25×10^{-2}
NHD ₂	2.48×10^{-10}	2.25×10^{-5}	DNC	1.57×10^{-10}	1.11×10^{-2}	C ₆ HD	9.96×10^{-10}	1.72×10^{-2}
DCN	1.73×10^{-10}	5.90×10^{-3}	CH ₃ D	1.53×10^{-10}	1.09×10^{-1}	D ₂ O ₂	8.15×10^{-10}	1.29×10^{-2}

The table is limited for each environment to 10 species or species with relative abundances $> 10^{-12}$.

Species detected unambiguously or in a preliminary manner in the specific environments are marked in boldface.

Dark clouds 10 K, 10^4 cm^{-3} – Warm IRDCs 25 K, 10^5 cm^{-3} – HMPOs 75 K, 10^5 cm^{-3}

and 1.0×10^{-10} for DCO⁺ and HCO⁺ with a D/H ratio 0.5. We find the same agreement for HDO with an observed abundance 2×10^{-10} comparable to our modeled abundance range of $3.0 - 7.5 \times 10^{-10}$.

Coutens et al. (2012) observed multiple lines of HDO and H₂¹⁸O towards IRAS 16293A with an estimated D/H ~ 0.034 in the hot corino region and D/H ~ 0.005 in the outer envelope, utilizing a standard isotopic ratio of H₂¹⁸O/H₂¹⁶O = 500. In order to reproduce observed line emission, they added an outer absorbing layer with an H₂O column density of $1.23 \times 10^{13} \text{ cm}^{-2}$. Depending on the exact choice of density and temperatures, our models give for the cold envelope ($n_{\text{H}} \sim 10^5 \text{ cm}^{-3}$, $T \lesssim 30 \text{ K}$) D/H ratios of $\sim 0.01 - 0.1$, for both sets of initial abundances, in agreement with observations. For hot cores ($n_{\text{H}} \sim 10^8 \text{ cm}^{-3}$, $T \sim 150 \text{ K}$) the “Primordial” model estimates the D/H ratio to be $0.0001 - 0.001$, while the “Evolution” model predicts that the D/H ratio is $\sim 0.0001 - 0.01$. Although our evolutionary model is a poor solution and does not account for the gradual warm-up of the environment, our predicted D/H ratios from the “Evolution” model are in agreement with those estimated by Coutens et al., albeit only with upper limits of our estimates.

The radical OD was observed for the first time outside of the Solar system by Parise et al. (2012) along the line of sight towards the low-mass protostar IRAS 16293A. They also observed HDO and found a high OD/HDO ratio of $\sim 10 - 100$. Parise et al. compared their observations to the modeled values of OH/H₂O and found their calculated values to be too low. The agreement was slightly better when they implemented a simple evolutionary model with increasing temperature with time, but the result was still lower than observations, with the highest modeled values reaching 5.7. Studying the chemical evolution in our ÓPrimordial modelÓ for temperatures $T < 30 \text{ K}$ and densities $n_{\text{H}} = 10^4 - 10^6 \text{ cm}^{-3}$, we find that the large OD/HDO ratio is mainly due to the efficient reaction $\text{OH} + \text{D} \rightarrow \text{OD} + \text{H}$, as originally suggested by Millar et al. (1989). Via this reaction, the OD/HDO ratios can reach values approximately one order of magnitude larger than OH/H₂O. Furthermore, toward temperatures $\sim 30 \text{ K}$ the OD/HDO ratios can even be as high as two orders of magnitude. Thus, our model is in agreement with the observed OD/HDO ratios from Parise et al. (2012), without the need for a warm-up phase.

4.2. Earlier Models

Roberts & Millar (2000b) and Roberts & Millar (2000a) have investigated the chemical evolution with deuterium fractionation for temperatures $10 - 100 \text{ K}$ and densities $3 \times 10^3 - 3 \times 10^8 \text{ cm}^{-3}$ on a less resolved grid, consisting of only 100 points. They used a time-dependent chemical gas-phase model based on the UMIST’95 database (Millar et al. 1997). Their resulting network consists of ~ 300 species linked by > 5000 reactions, but only includes singly-deuterated species and limited surface chemistry for H₂ and HD. We compared the results between our models for a number of species, including DCO⁺, HDCO, DCN, DNC and DC₅N, looking at the distribution of D/H fractionation ratios and time-dependent abundances at 10^5 yr , and we found good agreement between our models. We also studied the molecular abundances under conditions typical of the TMC-1 environment in our “Primordial” model and under these conditions we found that the quantitative agreement in the D/H ratios is better than an order of magnitude for all species, with the worst agreement for NH₂D where the ratio between the two models is 0.14. The comparison for D/H values is shown in Table 10. The intrinsic uncertainty in the abundance of DC₅N as predicted in our sensitivity analysis is very large, $\sim 1 - 1.5$ orders of magnitude, and is comparable to the difference between our and Roberts’ & Millar’s model. We note however that our modeled D/H ratios show a better agreement with the observations of DC₅N and HC₅N in TMC-1 by MacLeod et al. (1981) than calculated values by Roberts & Millar. In Roberts & Millar (2000a) expanded their study to include doubly-deuterated species, allowed species to freeze onto grains and looked at a different selection of species. We compared their predictions with our results for singly- and doubly- deuterated isotopologues of NH₃, H₂O, H₂CO, and found reasonably good agreement for all singly-deuterated species. In our model, NH₂D shows enhanced D/H ratios ($\sim 10^{-3} - 10^{-1}$) up to temperatures of $30 - 40 \text{ K}$, while the enhanced D/H ratios in the model of Roberts & Millar only appear up to $20 - 30 \text{ K}$. For the doubly-deuterated species D₂O, NHD₂ and D₂CO we predict similar D/H ratios to Roberts & Millar up to temperatures of $\sim 50 \text{ K}$, with values $\sim 10^{-3} - 10^{-1}$, while at larger temperatures our models diverge. Our model predicts a strong decrease in the respective D/H ratios to $\sim 10^{-5}$, while the D/H ratios of Roberts & Millar decrease more smoothly and do not reach the same value until at $\sim 100 \text{ K}$.

Table 10

Comparison of D/H ratios for a TMC1-like environment ($T = 10$ K, $n_H = 10^4$ cm $^{-3}$) between our model and Roberts & Millar (2000b).

Species	Our model	Roberts & Millar	Ratio
NH ₂ D	1.4×10^{-2}	8.4×10^{-2}	0.17
HDCO	1.7×10^{-2}	4.2×10^{-2}	0.40
DCN	2.4×10^{-2}	0.9×10^{-2}	2.7
DNC	2.6×10^{-2}	1.5×10^{-2}	1.7
C ₂ D	1.1×10^{-2}	1.1×10^{-2}	1.0
C ₄ D	1.6×10^{-2}	0.4×10^{-2}	4.0
DCO ⁺	3.9×10^{-2}	1.9×10^{-2}	2.1
N ₂ D ⁺	8.6×10^{-3}	2.5×10^{-2}	0.34
C ₃ HD	1.3×10^{-2}	0.6×10^{-2}	2.2
C ₃ H ₃ D	1.6×10^{-2}	8.3×10^{-2}	0.19
DC ₃ N	9.6×10^{-3}	0.7×10^{-2}	1.4
DC ₅ N	1.2×10^{-2}	2.3×10^{-2}	0.52
HD ₂ S	1.8×10^{-2}	4.0×10^{-2}	1.4

In the study of Roberts et al. (2004), the chemical evolution in a sample of prestellar cores using two subsets of the Rate99 and osu.2003 chemical networks was compared. With the networks limited to include species with six or fewer carbon atoms and no surface chemistry, Roberts et al. used the chemical models to successfully explain observations of the CO depletion, and its relevance to the D₂CO and HDCO fractionation ratios. If we compare the calculated fractionation ratios between the steady state abundances of Roberts et al. (see their Table 5) and our models for a TMC-1 environment, the D/H ratios for the majority of key species such as H₂D⁺, N₂D⁺, DCO⁺ and HDO agree reasonably well. However, we found significant discrepancies for D₂O, HD₂⁺, D₃⁺ and NHD₂. The reason why our D/H ratios for doubly-deuterated species differ from those of Roberts et al. appears to be twofold. First, they have not considered surface chemistry and assumed that all atomic D that freezes out is immediately returned to the gas as HD. In contrast, in our model, the accreted deuterium atoms are incorporated in surface species and do not easily return to the gas phase. Second, they use only steady-state abundances while we use time-dependent abundances at 1 Myr.

Walmsley et al. (2004) studied steady-state chemistry in a completely depleted, low-mass prestellar core, with an emphasis on explaining observations of ortho-H₂D⁺ towards L1544 by Caselli et al. (2003). While our model does not yet include nuclear-spin state chemistry, we compared the calculated abundances of the H₃⁺ isotopologues at densities of $n_H = 10^5, 10^6, 10^7$ cm $^{-3}$, $T = 10$ K assuming a cosmic ray ionization rate $\zeta = 3 \times 10^{-17}$ s $^{-1}$ (Note that at such conditions para-H₂ will be the dominant form of molecular hydrogen and thus fractionation will proceed with a high efficiency as assumed in our model). For both the “Primordial” and “Evolution” models we found good overall agreement for the D/H ratios of the H₃⁺ isotopologues and the electron abundances. The only difference occurs at high densities of $\sim 10^7$ cm $^{-3}$, where the HD₂⁺ and D₃⁺ abundances are one and two orders of magnitude lower in our model, respectively. We could not find out whether this difference increases at higher densities. The likely reason for such a discrepancy is the lack of surface chemistry and the assumption of complete freeze-out in the Walmsley et al. model. Even at such high densities and 10 K, the depletion is not complete in our model, so that the H₃⁺ isotopologues can still be destroyed by ion-molecule reactions in addition to dissociative recombination with elec-

trons or negatively charged grains. Moreover, in our model, atomic D released upon dissociative recombination can stick to a grain and be incorporated in the surface molecules. At $n_H \gtrsim 10^7$ cm $^{-3}$ and after 1 Myr of evolution, a substantial fraction of the gas-phase reservoir of the elemental D can be chemically ‘transferred’ to ices, unable to directly come back to the gas phase. Consequently, it will increase surface fractionation and abundances of deuterated ices.

5. CONCLUSIONS

We present an extended, publicly available chemical network for deuterium fractionation, with the most up-to-date reaction rate coefficients from laboratory measurements and theoretical studies. The new deuterium chemistry model does not yet include nuclear-spin state processes and is better suitable for cold ISM environments, $T \sim 10$ –20 K. In this paper, we have tested this network by performing a benchmarking study of deuterium chemistry under dense ISM conditions with two distinct initial abundance sets. The limits of accuracy of the network have been investigated with a sensitivity analysis. The most problematic reactions for the chemical evolution of H₃⁺, HCO⁺, HOC⁺, HCN, HNC, H₂O, CH₃OH, H₃O⁺, CH₃⁺, C₂H₂⁺ and their isotopologues as well as CO are listed or presented as online material. Ion-neutral and dissociative recombination reactions dominate the list, accompanied by a smaller number of neutral-neutral reactions and the cosmic ray ionization of H₂ and He.

In general, using the 1 σ confidence level, the abundances and column densities of species made of $\lesssim 3$ atoms (e.g., CO, HCO⁺, DCO⁺) are uncertain by factors 1.5–5.0, those for species made of 4–7 atoms are uncertain by a factor of 1.5–7, and those for more complex species made of > 7 atoms are uncertain by a factor of 2–10. For D/H ratios the uncertainties are, for the same different ranges of molecule sizes, a factor of 1.6–5, 1.6–10 and 2.5–10, respectively.

Despite certain limitations of our model, it successfully explains the observed D/H ratios in dark clouds (10 K and 10^4 cm $^{-3}$), prestellar cores ($T \lesssim 10$ K, $n \sim 10^4$ cm $^{-3}$), and protostellar envelopes (cold, $T \sim 30$ K, $n_H \sim 10^5$ cm $^{-3}$ and warm, $T \sim 150$ K, $n_H \sim 10^8$ cm $^{-3}$), for many key species including water, methanol, ammonia and many hydrocarbons. Our results show good agreement with previous model studies by Roberts & Millar (2000a), Roberts & Millar (2000b), Roberts et al. (2004) and Walmsley et al. (2004). We also list the dominant formation and destruction pathways for DCO⁺, DCN and isotopologues of H₃⁺ and water in Appendix B. Finally, in Tables 6–8 we have listed the most abundant, potentially detectable deuterated species in cold cores, and warm IRDCs and HMPOs, which can be searched for with ALMA.

ACKNOWLEDGEMENTS

The research leading to these results has received funding from the European Community’s Seventh Framework Programme [FP7/2007–2013] under grant agreement no. 238258. D.S. acknowledges support by the Deutsche Forschungsgemeinschaft through SPP 1385: “The first ten million years of the solar system – a planetary materials approach” (SE 1962/1-1 and SE 1962/1-2). E. H. wishes to acknowledge the support of the National Science Foundation for his astrochemistry program. He also acknowledges support from the NASA Exobiology and Evolutionary Biology program through a subcontract from Rensselaer Polytechnic Institute.

REFERENCES

- Adams, N. G. & Smith, D. 1985, *ApJ*, 294, L63
- Aikawa, Y. & Herbst, E. 2001, *A&A*, 371, 1107
- Aikawa, Y., Ohashi, N., & Herbst, E. 2003, *ApJ*, 593, 906
- Aikawa, Y., Wakelam, V., Garrod, R. T., & Herbst, E. 2008, *ApJ*, 674, 984
- Aikawa, Y., Wakelam, V., Hersant, F., Garrod, R. T., & Herbst, E. 2012, *ApJ*, 760, 40
- Allen, M., Cesarsky, D. A., & Crutcher, R. M. 1974, *ApJ*, 188, 33
- Alonso-Albi, T., Fuente, A., Crimier, N., et al. 2010, *A&A*, 518, A52
- Anderson, I. M., Caselli, P., Haikala, L. K., & Harju, J. 1999, *A&A*, 347, 983
- André, P., Basu, S., & Inutsuka, S. 2009, *The formation and evolution of prestellar cores*, ed. Chabrier, G. (Cambridge University Press), 254
- Bacmann, A. 2004, *Baltic Astronomy*, 13, 402
- Bacmann, A., Caux, E., Hily-Blant, P., et al. 2010, *A&A*, 521, L42
- Bacmann, A., Lefloch, B., Ceccarelli, C., et al. 2002, *A&A*, 389, L6
- Bacmann, A., Lefloch, B., Ceccarelli, C., et al. 2003, *ApJ*, 585, L55
- Bacmann, A., Lefloch, B., Parise, B., Ceccarelli, C., & Steinacker, J. 2007, in *Molecules in Space and Laboratory*
- Bacmann, A., Taquet, V., Faure, A., Kahane, C., & Ceccarelli, C. 2012, *A&A*, 541, L12
- Bayet, E., Awad, Z., & Viti, S. 2010, *ApJ*, 725, 214
- Bell, M. B., Avery, L. W., Matthews, H. E., et al. 1988, *ApJ*, 326, 924
- Belloche, A., Parise, B., van der Tak, F. F. S., et al. 2006, *A&A*, 454, L51
- Bergin, E. A., Aikawa, Y., Blake, G. A., & van Dishoeck, E. F. 2007, *Protostars and Planets V*, 751
- Bergin, E. A. & Tafalla, M. 2007, *ARA&A*, 45, 339
- Bergman, P., Parise, B., Liseau, R., & Larsson, B. 2011, *A&A*, 527, A39
- Beuther, H., Leurini, S., Schilke, P., et al. 2007, *A&A*, 466, 1065
- Biham, O., Furman, I., Pirronello, V., & Vidali, G. 2001, *ApJ*, 553, 595
- Bonev, B. P., Mumma, M. J., Gibb, E. L., et al. 2009, *ApJ*, 699, 1563
- Brown, P. D., Charnley, S. B., & Millar, T. J. 1988, *MNRAS*, 231, 409
- Brown, P. D. & Millar, T. J. 1989, *MNRAS*, 240, 25P
- Busquet, G., Palau, A., Estalella, R., et al. 2010, *A&A*, 517, L6
- Butner, H. M., Charnley, S. B., Ceccarelli, C., et al. 2007, *ApJ*, 659, L137
- Butner, H. M., Lada, E. A., & Loren, R. B. 1995, *ApJ*, 448, 207
- Cami, J., Bernard-Salas, J., Peeters, E., & Malek, S. E. 2010, *Science*, 329, 1180
- Caselli, P., van der Tak, F. F. S., Ceccarelli, C., & Bacmann, A. 2003, *A&A*, 403, L37
- Caselli, P., Vastel, C., Ceccarelli, C., et al. 2008, *A&A*, 492, 703
- Cazaux, S., Caselli, P., & Spaans, M. 2011, *ApJ*, 741, L34
- Ceccarelli, C. 2002, *Planet. Space Sci.*, 50, 1267
- Ceccarelli, C. & Dominik, C. 2005, *A&A*, 440, 583
- Ceccarelli, C., Loinard, L., Castets, A., et al. 2001, *A&A*, 372, 998
- Cesarsky, D. A., Moffet, A. T., & Pasachoff, J. M. 1973, *ApJ*, 180, L1
- Chabot, M., Tuna, T., Bérroff, K., et al. 2010, *A&A*, 524, A39
- Chapillon, E., Parise, B., Guilloteau, S., & Du, F. 2011, *A&A*, 533, A143
- Charnley, S. B., Tielens, A. G. G. M., & Rodgers, S. D. 1997, *ApJ*, 482, L203
- Chen, H., Liu, S., Su, Y., & Zhang, Q. 2010, *ApJ*, 713, L50
- Coutens, A., Vastel, C., Caux, E., et al. 2012, *A&A*, 539, A132
- Crapsi, A., Caselli, P., Walmsley, C. M., et al. 2005, *ApJ*, 619, 379
- Crapsi, A., Caselli, P., Walmsley, C. M., et al. 2004, *A&A*, 420, 957
- Crowell, K. & Dalgarno, A. 1985, *ApJ*, 289, 618
- Cuppen, H. M., van Dishoeck, E. F., Herbst, E., & Tielens, A. G. G. M. 2009, *A&A*, 508, 275
- Dalgarno, A. & Lepp, S. 1984, *ApJ*, 287, L47
- Demyk, K., Bottinelli, S., Caux, E., et al. 2010, *A&A*, 517, A17
- Druard, C. & Wakelam, V. 2012, *MNRAS*, 426, 354
- Emprechtinger, M., Caselli, P., Volgenau, N. H., Stutzki, J., & Wiedner, M. C. 2009, *A&A*, 493, 89
- Florescu-Mitchell, A. I. & Mitchell, J. B. A. 2006, *Phys. Rep.*, 430, 277
- Flower, D. R. & Pineau-Des-Forêts, G. 1990, *MNRAS*, 247, 500
- Flower, D. R., Pineau Des Forêts, G., & Walmsley, C. M. 2006, *A&A*, 449, 621
- Fontani, F., Caselli, P., Bourke, T. L., Cesaroni, R., & Brand, J. 2008, *A&A*, 477, L45
- Fontani, F., Caselli, P., Crapsi, A., et al. 2006, *A&A*, 460, 709
- Friberg, P. & Hjalmarson, A. 1986, *Highlights of Astronomy*, 7, 513
- Friesen, R. K., Di Francesco, J., Myers, P. C., et al. 2010, *ApJ*, 718, 666
- Garrod, R. T. & Herbst, E. 2006, *A&A*, 457, 927
- Garrod, R. T. & Pauly, T. 2011, *ApJ*, 735, 15
- Garrod, R. T., Wakelam, V., & Herbst, E. 2007, *A&A*, 467, 1103
- Garrod, R. T., Weaver, S. L. W., & Herbst, E. 2008, *ApJ*, 682, 283
- Geiss, J. & Reeves, H. 1981, *A&A*, 93, 189
- Gensheimer, P. D., Mauersberger, R., & Wilson, T. L. 1996, *A&A*, 314, 281
- Geppert, W. D., Hamberg, M., Thomas, R. D., et al. 2006, *Faraday Discussions*, 133, 177
- Gerin, M., Combes, F., Włodarczak, G., Encrenaz, P., & Laurent, C. 1992a, *A&A*, 253, L29
- Gerin, M., Combes, F., Włodarczak, G., et al. 1992b, *A&A*, 259, L35
- Gerlich, D., Herbst, E., & Roueff, E. 2002, *Planet. Space Sci.*, 50, 1275
- Gibb, E. L., Bonev, B. P., Villanueva, G., et al. 2012, *ApJ*, 750, 102
- Giles, K., Adams, N. G., & Smith, D. 1992, *The Journal of Physical Chemistry*, 96, 7645
- Glassgold, A. E., Galli, D., & Padovani, M. 2012, *ApJ*, 756, 157
- Goicoechea, J. R., Pety, J., Gerin, M., Hily-Blant, P., & Le Bourlot, J. 2009, *A&A*, 498, 771
- Graedel, T. E., Langer, W. D., & Frerking, M. A. 1982, *ApJS*, 48, 321
- Guelin, M., Langer, W. D., Snell, R. L., & Wootten, H. A. 1977, *ApJ*, 217, L165
- Guilloteau, S., Piétu, V., Dutrey, A., & Guélin, M. 2006, *A&A*, 448, L5
- Hama, T., Kuwahata, K., Watanabe, N., et al. 2012, *ApJ*, 757, 185
- Hamberg, M., Österdahl, F., Thomas, R. D., et al. 2010a, *A&A*, 514, A83
- Hamberg, M., Zhaunerchyk, V., Vigren, E., et al. 2010b, *A&A*, 522, A90
- Hartogh, P., Lis, D. C., Bockelée-Morvan, D., et al. 2011, *Nature*, 478, 218
- Hasegawa, T. I., Herbst, E., & Leung, C. M. 1992, *ApJS*, 82, 167
- Hatchell, J. 2003, *A&A*, 403, L25
- Hebrard, G. 2006, in *Astronomical Society of the Pacific Conference Series*, Vol. 348, *Astrophysics in the Far Ultraviolet: Five Years of Discovery with FUSE*, ed. G. Sonneborn, H. W. Moos, & B.-G. Andersson, 47
- Heiles, C., McCullough, P. R., & Glassgold, A. E. 1993, *ApJS*, 89, 271
- Herbst, E. 1982, *A&A*, 111, 76
- Herbst, E. 1985, *ApJ*, 291, 226
- Herbst, E., Adams, N. G., Smith, D., & Defrees, D. J. 1987, *ApJ*, 312, 351
- Herbst, E. & Klemperer, W. 1973, *ApJ*, 185, 505
- Hidaka, H., Watanabe, M., Kouchi, A., & Watanabe, N. 2009, *ApJ*, 702, 291
- Hirota, T., Ikeda, M., & Yamamoto, S. 2001, *ApJ*, 547, 814
- Hirota, T., Ikeda, M., & Yamamoto, S. 2003, *ApJ*, 594, 859
- Ho, P. T. P. & Townes, C. H. 1983, *ARA&A*, 21, 239
- Horn, A., Møllendal, H., Sekiguchi, O., et al. 2004, *ApJ*, 611, 605
- Jacq, T., Walmsley, C. M., Henkel, C., et al. 1990, *A&A*, 228, 447
- Jensen, M. J., Bilodeau, R. C., Safvan, C. P., et al. 2000, *ApJ*, 543, 764
- Jørgensen, J. K. & van Dishoeck, E. F. 2010, *ApJ*, 725, L172
- Katz, N., Furman, I., Biham, O., Pirronello, V., & Vidali, G. 1999, *ApJ*, 522, 305
- Kuan, Y.-J., Chuang, H.-E., Charnley, S., & Huang, H.-C. 2008, in *COSPAR, Plenary Meeting*, Vol. 37, 37th COSPAR Scientific Assembly, 1640
- Laas, J. C., Garrod, R. T., Herbst, E., & Widicus Weaver, S. L. 2011, *ApJ*, 728, 71
- Lacour, S., André, M. K., Sonnentrucker, P., et al. 2005, *A&A*, 430, 967
- Larsson, M., Danared, H., Larson, A., et al. 1997, *Phys. Rev. Lett.*, 79, 395
- Launhardt, R., Nutter, D., Ward-Thompson, D., et al. 2010, *ApJS*, 188, 139
- Launhardt, R., Stutz, A. M., Schmiedeke, A., et al. 2013, *A&A*, 551, A98
- Lee, H.-H., Herbst, E., Pineau des Forêts, G., Roueff, E., & Le Bourlot, J. 1996, *A&A*, 311, 690
- Lee, H.-H., Roueff, E., Pineau des Forêts, G., et al. 1998, *A&A*, 334, 1047
- Linsky, J. L. 2003, *Space Sci. Rev.*, 106, 49
- Lis, D. C., Gerin, M., Phillips, T. G., & Motte, F. 2002a, *ApJ*, 569, 322
- Lis, D. C., Roueff, E., Gerin, M., et al. 2002b, *ApJ*, 571, L55
- Liu, F., Parise, B., Kristensen, L., et al. 2011, *A&A*, 527, A19
- Loinard, L., Castets, A., Ceccarelli, C., et al. 2003, in *SFChem 2002: Chemistry as a Diagnostic of Star Formation*, ed. C. L. Curry & M. Fich, 351
- Loinard, L., Castets, A., Ceccarelli, C., et al. 2002, *Planet. Space Sci.*, 50, 1205
- Loren, R. B. & Wootten, A. 1985, *ApJ*, 299, 947
- MacLeod, J. M., Avery, L. W., & Broten, N. W. 1981, *ApJ*, 251, L33
- Mangum, J. G., Plambeck, R. L., & Wootten, A. 1991, *ApJ*, 369, 169
- Marcelino, N., Cernicharo, J., Roueff, E., Gerin, M., & Mauersberger, R. 2005, *ApJ*, 620, 308
- Maret, S., Faure, A., Scifoni, E., & Wiesenfeld, L. 2009, *MNRAS*, 399, 425
- Margulès, L., Huet, T. R., Demaison, J., et al. 2010, *ApJ*, 714, 1120
- Markwick, A. J., Charnley, S. B., Butner, H. M., & Millar, T. J. 2005, *ApJ*, 627, L117
- Markwick, A. J., Millar, T. J., & Charnley, S. B. 2002, *A&A*, 381, 560
- Miettinen, O., Harju, J., Haikala, L. K., & Juvela, M. 2012, *A&A*, 538, A137
- Miettinen, O., Harju, J., Haikala, L. K., Kainulainen, J., & Johansson, L. E. B. 2009, *A&A*, 500, 845
- Millar, T. J., Bennett, A., & Herbst, E. 1989, *ApJ*, 340, 906
- Millar, T. J., Farquhar, P. R. A., & Willacy, K. 1997, *A&AS*, 121, 139
- Minowa, H., Satake, M., Hirota, T., et al. 1997, *ApJ*, 491, L63
- Müller, H. S. P., Schlöder, F., Stutzki, J., & Winnewisser, G. 2005, *Journal of Molecular Structure*, 742, 215
- Müller, H. S. P., Thorwirth, S., Roth, D. A., & Winnewisser, G. 2001, *A&A*, 370, L49
- Nagaoka, A., Watanabe, N., & Kouchi, A. 2005, *ApJ*, 624, L29
- Nielbock, M., Launhardt, R., Steinacker, J., et al. 2012, *A&A*, 547, A11
- Öberg, K. I., Garrod, R. T., van Dishoeck, E. F., & Linnartz, H. 2009a, *A&A*, 504, 891
- Öberg, K. I., Qi, C., Wilner, D. J., & Hogerheijde, M. R. 2012, *ApJ*, 749, 162
- Öberg, K. I., van Dishoeck, E. F., & Linnartz, H. 2009b, *A&A*, 496, 281
- Osamura, Y., Roberts, H., & Herbst, E. 2004, *A&A*, 421, 1101
- Pagani, L., Lesaffre, P., Jorfi, M., et al. 2013, *A&A*, 551, A38
- Pagani, L., Salez, M., & Wannier, P. G. 1992, *A&A*, 258, 479
- Pagani, L., Vastel, C., Hugo, E., et al. 2009, *A&A*, 494, 623
- Parise, B., Belloche, A., Du, F., Güsten, R., & Menten, K. M. 2011, *A&A*, 526, A31
- Parise, B., Castets, A., Herbst, E., et al. 2004, *A&A*, 416, 159
- Parise, B., Caux, E., Castets, A., et al. 2005, *A&A*, 431, 547
- Parise, B., Ceccarelli, C., Tielens, A. G. G. M., et al. 2006, *A&A*, 453, 949

- Parise, B., Ceccarelli, C., Tielens, A. G. G. M., et al. 2002, *A&A*, 393, L49
- Parise, B., Du, F., Liu, F.-C., et al. 2012, *A&A*, 542, L5
- Parise, B., Leurini, S., Schilke, P., Roueff, E., & Thorwirth, S. 2007, in *Molecules in Space and Laboratory*
- Parise, B., Leurini, S., Schilke, P., et al. 2009, *A&A*, 508, 737
- Parise, B., Simon, T., Caux, E., et al. 2003, *A&A*, 410, 897
- Perets, H. B. & Biham, O. 2006, *MNRAS*, 365, 801
- Phillips, T. G., Jefferts, K. B., & Wannier, P. G. 1973, *Astrophys. Lett.*, 15, 17
- Qi, C., Wilner, D. J., Aikawa, Y., Blake, G. A., & Hogerheijde, M. R. 2008, *ApJ*, 681, 1396
- Rathborne, J. M., Jackson, J. M., Zhang, Q., & Simon, R. 2008, *ApJ*, 689, 1141
- Rimmer, P. B., Herbst, E., Morata, O., & Roueff, E. 2012, *A&A*, 537, A7
- Roberts, H., Herbst, E., & Millar, T. J. 2003, *ApJ*, 591, L41
- Roberts, H., Herbst, E., & Millar, T. J. 2004, *A&A*, 424, 905
- Roberts, H. & Millar, T. J. 2000a, *A&A*, 364, 780
- Roberts, H. & Millar, T. J. 2000b, *A&A*, 361, 388
- Roberts, H. & Millar, T. J. 2006, *Royal Society of London Philosophical Transactions Series A*, 364, 3063
- Roberts, H. & Millar, T. J. 2007, *A&A*, 471, 849
- Rodgers, S. D. & Millar, T. J. 1996, *MNRAS*, 280, 1046
- Rodón, J. A., Beuther, H., Megeath, S. T., & van der Tak, F. F. S. 2008, *A&A*, 490, 213
- Rogers, A. E. E., Dudevior, K. A., & Bania, T. M. 2007, *AJ*, 133, 1625
- Roueff, E. & Gerin, M. 2003, *Space Sci. Rev.*, 106, 61
- Roueff, E., Lis, D. C., van der Tak, F. F. S., Gerin, M., & Goldsmith, P. F. 2005, *A&A*, 438, 585
- Roueff, E., Tiné, S., Coudert, L. H., et al. 2000, *A&A*, 354, L63
- Saito, S., Ozeki, H., Ohishi, M., & Yamamoto, S. 2000, *ApJ*, 535, 227
- Sakai, N., Sakai, T., Hirota, T., & Yamamoto, S. 2009, *ApJ*, 702, 1025
- Schilke, P., Walmsley, C. M., Pineau Des Forets, G., et al. 1992, *A&A*, 256, 595
- Schloerb, F. P., Snell, R. L., Langer, W. D., & Young, J. S. 1981, *ApJ*, 251, L37
- Semenov, D., Hersant, F., Wakelam, V., et al. 2010, *A&A*, 522, A42
- Shah, R. Y. & Wootten, A. 2001, *ApJ*, 554, 933
- Sidhu, K. S., Miller, S., & Tennyson, J. 1992, *A&A*, 255, 453
- Sipilä, O., Caselli, P., & Harju, J. 2013, *ArXiv e-prints*
- Sipilä, O., Hugo, E., Harju, J., et al. 2010, *A&A*, 509, A98
- Smith, D., Adams, N. G., & Alge, E. 1982a, *J. Chem. Phys.*, 77, 1261
- Smith, D., Adams, N. G., & Alge, E. 1982b, *ApJ*, 263, 123
- Snow, T. P. & McCall, B. J. 2006, *ARA&A*, 44, 367
- Snow, T. P., Ross, T. L., Destree, J. D., et al. 2008, *ApJ*, 688, 1124
- Solomon, P. M. & Woolf, N. J. 1973, *ApJ*, 180, L89
- Stancil, P. C., Lepp, S., & Dalgarno, A. 1998, *ApJ*, 509, 1
- Stark, R., Sandell, G., Beck, S. C., et al. 2004, *ApJ*, 608, 341
- Stark, R., van der Tak, F. F. S., & van Dishoeck, E. F. 1999, *ApJ*, 521, L67
- Sundstrom, G., Mowat, J. R., Danared, H., et al. 1994, *Science*, 263, 785
- Suzuki, H. 1987, in *IAU Symposium, Vol. 120, Astrochemistry*, ed. M. S. Vardya & S. P. Tarafdar, 199
- Taquet, V., Ceccarelli, C., & Kahane, C. 2012, *ApJ*, 748, L3
- Teanby, N. A., Irwin, P. G. J., de Kok, R., et al. 2009, *Icarus*, 202, 620
- Teixeira, T. C., Devlin, J. P., Buch, V., & Emerson, J. P. 1999, *A&A*, 347, L19
- Tiné, S., Roueff, E., Falgarone, E., Gerin, M., & Pineau des Forêts, G. 2000, *A&A*, 356, 1039
- Turner, B. E. 1990, *ApJ*, 362, L29
- Turner, B. E. 2001, *ApJS*, 136, 579
- Turner, B. E. & Zuckerman, B. 1978, *ApJ*, 225, L75
- van der Tak, F. F. S. 2006, *Royal Society of London Philosophical Transactions Series A*, 364, 3101
- van der Tak, F. F. S., Black, J. H., Schöier, F. L., Jansen, D. J., & van Dishoeck, E. F. 2007, *A&A*, 468, 627
- van der Tak, F. F. S., Müller, H. S. P., Harding, M. E., & Gauss, J. 2009, *A&A*, 507, 347
- van der Tak, F. F. S., Schilke, P., Müller, H. S. P., et al. 2002, *A&A*, 388, L53
- van Dishoeck, E. F. 2006, *Proceedings of the National Academy of Science*, 1031, 12249
- van Dishoeck, E. F. & Blake, G. A. 1998, *ARA&A*, 36, 317
- van Dishoeck, E. F., Blake, G. A., Jansen, D. J., & Groesbeck, T. D. 1995, *ApJ*, 447, 760
- van Dishoeck, E. F., Jonkheid, B., & van Hemert, M. C. 2006, *Faraday Discussions*, 133, 231
- van Dishoeck, E. F., Thi, W., & van Zadelhoff, G. 2003, *A&A*, 400, L1
- Vastel, C., Caselli, P., Ceccarelli, C., et al. 2012, *A&A*, 547, A33
- Vastel, C., Caselli, P., Ceccarelli, C., et al. 2006, *ApJ*, 645, 1198
- Vastel, C., Phillips, T. G., & Yoshida, H. 2004, *ApJ*, 606, L127
- Vasyunin, A. I. & Herbst, E. 2013a, *ApJ*, 762, 86
- Vasyunin, A. I. & Herbst, E. 2013b, *ApJ*, 769, 34
- Vasyunin, A. I., Semenov, D., Henning, T., et al. 2008, *ApJ*, 672, 629
- Vasyunin, A. I., Sobolev, A. M., Wiebe, D. S., & Semenov, D. A. 2004, *Astronomy Letters*, 30, 566
- Vasyunina, T., Linz, H., Henning, T., et al. 2009, *A&A*, 499, 149
- Vasyunina, T., Vasyunin, A. I., Herbst, E., & Linz, H. 2012, *ApJ*, 751, 105
- Villanueva, G. L., Mumma, M. J., Bonev, B. P., et al. 2009, *ApJ*, 690, L5
- Wakelam, V., Herbst, E., Le Bourlot, J., et al. 2010a, *A&A*, 517, A21
- Wakelam, V., Herbst, E., Selsis, F., & Massacrier, G. 2006, *A&A*, 459, 813
- Wakelam, V., Smith, I. W. M., Herbst, E., et al. 2010b, *Space Sci. Rev.*, 156, 13
- Walmsley, C. M., Flower, D. R., & Pineau des Forêts, G. 2004, *A&A*, 418, 1035
- Watson, W. D. 1974, *ApJ*, 188, 35
- Watson, W. D. 1976, *Reviews of Modern Physics*, 48, 513
- Watson, W. D. 1976, *Rev. Mod. Phys.*, 48, 513
- Willacy, K. 2007, *ApJ*, 660, 441
- Wootten, A. 1987, in *IAU Symposium, Vol. 120, Astrochemistry*, ed. M. S. Vardya & S. P. Tarafdar, 311–318

APPENDIX

A. UPDATED AND ADDED REACTIONS TO CHEMICAL NETWORK

In this appendix, we list problematic reactions and rate coefficients (Table A3) identified in our sensitivity analysis for isotopologues and isomers of water, H_3^+ , HCO^+ and HCN , as well as added and updated non-deuterated (Table A1) and deuterated (Table A2) reactions to our network. The added and updated reactions have been collected from several literature references as well as newly announced values (as of 2012-12-26) reported in the Kinetic Database for Astronomy (KIDA; <http://kida.obs.u-bordeaux1.fr/>).

Table A1 Added and updated non-deuterium reactions.

Reaction		α	β	γ	Ref
$\text{C}^+ + \text{H}_2$	$\rightarrow \text{CH}_2^+$	2.00×10^{-16}	-1.30	-23	1
$\text{C}^+ + \text{HCOOH}$	$\rightarrow \text{HCO}^+ + \text{OH} + \text{C}$	8.00×10^{-10}	-0.50	0	5
$\text{C}_2\text{H}_2^+ + \text{H}_2$	$\rightarrow \text{C}_2\text{H}_4^+$	2.90×10^{-14}	-1.50	0	1
$\text{CH}_3^+ + \text{H}_2\text{O}$	$\rightarrow \text{CH}_3\text{OH}_2^+$	5.50×10^{-12}	-1.70	0	3
$\text{CH}_3^+ + \text{H}_2$	$\rightarrow \text{CH}_5^+$	3.78×10^{-16}	-2.30	22	4
$\text{CH}_3\text{O}_2^+ + \text{CH}_3\text{OH}$	$\rightarrow \text{H}_5\text{C}_2\text{O}_2^+ + \text{H}_2\text{O}$	2.00×10^{-9}	-0.50	2810	5
$\text{CH}_3\text{OH}_2^+ + \text{HCOOH}$	$\rightarrow \text{HCOOH}_2^+ + \text{CH}_3\text{OH}$	3.63×10^{-9}	-0.50	685	5
$\text{CH}_5^+ + \text{HCOOH}$	$\rightarrow \text{HCOOH}_2^+ + \text{CH}_4$	3.00×10^{-9}	-0.50	0	5
$\text{H}_2\text{CN}^+ + \text{C}_2\text{H}_2$	$\rightarrow \text{C}_3\text{H}_4\text{N}^+$	3.30×10^{-16}	-2.00	0	4
$\text{H}_2\text{CN}^+ + \text{HCOOH}$	$\rightarrow \text{HCOOH}_2^+ + \text{HCN}$	1.40×10^{-9}	-0.50	0	5
$\text{H}_3^+ + \text{HCOOH}$	$\rightarrow \text{HCO}^+ + \text{H}_2\text{O} + \text{H}_2$	3.90×10^{-9}	-0.50	0	5
$\text{H}_3^+ + \text{O}$	$\rightarrow \text{OH}^+ + \text{H}_2$	7.98×10^{-10}	-0.156	-1.41	1
$\text{H}_3^+ + \text{O}$	$\rightarrow \text{H}_2\text{O}^+ + \text{H}$	3.42×10^{-10}	-0.156	-1.41	1
$\text{H}_3\text{CO}^+ + \text{HCOOH}$	$\rightarrow \text{HCOOH}_2^+ + \text{H}_2\text{CO}$	2.00×10^{-9}	-0.50	0	5
$\text{H}_3\text{O}^+ + \text{C}_2\text{H}_4$	$\rightarrow \text{C}_2\text{H}_5\text{OH}_2^+$	1.90×10^{-14}	-2.80	0.25	4
$\text{H}_3\text{CO}^+ + \text{H}_2\text{CO}$	$\rightarrow \text{H}_5\text{C}_2\text{O}_2^+$	8.15×10^{-15}	-3.00	0	6
$\text{H}_3\text{S}^+ + \text{HCOOH}$	$\rightarrow \text{HCOOH}_2^+ + \text{H}_2\text{S}$	2.00×10^{-9}	-0.50	0	5
$\text{HCOOH}_2^+ + \text{CH}_3\text{OH}$	$\rightarrow \text{CH}_3\text{OH}_2^+ + \text{HCOOH}$	2.29×10^{-9}	-0.50	0	5
$\text{He}^+ + \text{HCOOH}$	$\rightarrow \text{HCO}^+ + \text{OH} + \text{He}$	9.00×10^{-10}	-0.50	0	5
$\text{N}_2\text{H}^+ + \text{HCOOH}$	$\rightarrow \text{HCOOH}_2^+ + \text{N}_2$	1.70×10^{-9}	-0.50	0	5
$\text{C} + \text{O}_2$	$\rightarrow \text{CO} + \text{O}$	1.28×10^{-9}	-0.32	0	4
$\text{C} + \text{OH}$	$\rightarrow \text{CO} + \text{H}$	1.15×10^{-10}	-0.34	0	4
$\text{C}_2 + \text{O}$	$\rightarrow \text{CO} + \text{C}$	2.00×10^{-10}	-0.12	0	1
$\text{C}_2 + \text{OCS}$	$\rightarrow \text{CO} + \text{C}_2\text{S}$	1.00×10^{-10}	0.00	0	4
$\text{C}_2\text{H} + \text{N}$	$\rightarrow \text{C}_2\text{N} + \text{H}$	1.00×10^{-10}	0.18	0	1
$\text{C}_2\text{H} + \text{O}$	$\rightarrow \text{CO} + \text{CH}$	1.00×10^{-10}	0.00	0	1
$\text{C}_3\text{H} + \text{O}$	$\rightarrow \text{C}_2\text{H} + \text{CO}$	1.00×10^{-10}	0.00	0	1
$\text{C}_3\text{O} + \text{O}$	$\rightarrow \text{C}_3 + \text{O}_2$	1.00×10^{-10}	0.00	0	1
$\text{CH} + \text{OCS}$	$\rightarrow \text{H} + \text{CO} + \text{CS}$	4.00×10^{-10}	0.00	0	4
$\text{CH} + \text{SO}$	$\rightarrow \text{H} + \text{OCS}$	1.10×10^{-10}	0.00	0	4
$\text{CH} + \text{SO}$	$\rightarrow \text{CO} + \text{HS}$	9.00×10^{-11}	0.00	0	4
$\text{CH}_2 + \text{H}$	$\rightarrow \text{CH} + \text{H}_2$	2.20×10^{-10}	0.00	0	1
$\text{CH}_4 + \text{CH}$	$\rightarrow \text{C}_2\text{H}_4 + \text{H}$	1.06×10^{-10}	-1.04	0	4
$\text{CN} + \text{N}$	$\rightarrow \text{C} + \text{N}_2$	1.00×10^{-10}	0.00	0	1
$\text{CN} + \text{O}$	$\rightarrow \text{CO} + \text{N}$	2.60×10^{-11}	-0.12	0	1
$\text{CN} + \text{O}_2$	$\rightarrow \text{OCN} + \text{O}$	1.99×10^{-11}	-0.63	0	4
$\text{H}_2 + \text{CH}$	$\rightarrow \text{CH}_2 + \text{H}$	1.20×10^{-9}	0.00	0	4
$\text{HNO} + \text{O}$	$\rightarrow \text{NO} + \text{OH}$	3.77×10^{-11}	-0.08	0	1
$\text{NH} + \text{O}$	$\rightarrow \text{NO} + \text{H}$	6.60×10^{-11}	0.00	0	1
$\text{NH}_2 + \text{O}$	$\rightarrow \text{HNO} + \text{H}$	6.39×10^{-11}	-0.10	0	1
$\text{NH}_2 + \text{O}$	$\rightarrow \text{NH} + \text{OH}$	7.10×10^{-12}	-0.10	0	1
$\text{NH}_3 + \text{CN}$	$\rightarrow \text{HCN} + \text{NH}_2$	2.77×10^{-11}	-0.85	0	1
$\text{O} + \text{C}_2\text{S}$	$\rightarrow \text{CO} + \text{CS}$	1.00×10^{-10}	0.00	0	4
$\text{O} + \text{OCS}$	$\rightarrow \text{CO} + \text{CS}$	1.00×10^{-10}	0.00	0	4
$\text{O} + \text{OH}$	$\rightarrow \text{O}_2 + \text{H}$	4.00×10^{-11}	0.00	0	4
$\text{S} + \text{C}_2\text{O}$	$\rightarrow \text{CO} + \text{CS}$	1.00×10^{-10}	0.00	0	4
$\text{S} + \text{HCO}$	$\rightarrow \text{H} + \text{OCS}$	8.00×10^{-11}	0.00	0	4
$\text{S} + \text{HCO}$	$\rightarrow \text{CO} + \text{HS}$	4.00×10^{-11}	0.00	0	4
$\text{C}_3\text{H}^+ + \text{e}^-$	$\rightarrow \text{C}_2 + \text{CH}$	6.00×10^{-9}	-0.50	0	2
$\text{C}_3\text{H}^+ + \text{e}^-$	$\rightarrow \text{C}_2\text{H} + \text{C}$	9.90×10^{-8}	-0.50	0	2
$\text{C}_3\text{H}^+ + \text{e}^-$	$\rightarrow \text{C}_3 + \text{H}$	1.95×10^{-7}	-0.50	0	2
$\text{C}_3\text{H}_2^+ + \text{e}^-$	$\rightarrow \text{C}_2 + \text{CH}_2$	1.44×10^{-8}	-0.50	0	2
$\text{C}_3\text{H}_2^+ + \text{e}^-$	$\rightarrow \text{C}_2\text{H} + \text{CH}$	1.44×10^{-8}	-0.50	0	2
$\text{C}_3\text{H}_2^+ + \text{e}^-$	$\rightarrow \text{C}_2\text{H}_2 + \text{C}$	8.64×10^{-8}	-0.50	0	2
$\text{C}_3\text{H}_2^+ + \text{e}^-$	$\rightarrow \text{C}_3\text{H} + \text{H}$	1.66×10^{-7}	-0.50	0	2
$\text{C}_3\text{H}_2^+ + \text{e}^-$	$\rightarrow \text{C}_3 + \text{H}_2$	8.28×10^{-8}	-0.50	0	2
$\text{C}_4\text{H}^+ + \text{e}^-$	$\rightarrow \text{C}_4 + \text{H}$	1.74×10^{-7}	-0.50	0	2
$\text{C}_4\text{H}^+ + \text{e}^-$	$\rightarrow \text{C}_3\text{H} + \text{C}$	7.80×10^{-8}	-0.50	0	2
$\text{C}_4\text{H}^+ + \text{e}^-$	$\rightarrow \text{C}_2\text{H} + \text{C}_2$	4.80×10^{-8}	-0.50	0	2
$\text{C}_5^+ + \text{e}^-$	$\rightarrow \text{C}_4 + \text{C}$	3.90×10^{-8}	-0.50	0	2
$\text{C}_5^+ + \text{e}^-$	$\rightarrow \text{C}_3 + \text{C}_2$	2.61×10^{-7}	-0.50	0	2
$\text{C}_6^+ + \text{e}^-$	$\rightarrow \text{C}_5 + \text{C}$	1.80×10^{-7}	-0.30	0	2
$\text{C}_6^+ + \text{e}^-$	$\rightarrow \text{C}_4 + \text{C}_2$	2.20×10^{-7}	-0.30	0	2
$\text{C}_6^+ + \text{e}^-$	$\rightarrow \text{C}_3 + \text{C}_3$	1.60×10^{-6}	-0.30	0	2
$\text{C}_7^+ + \text{e}^-$	$\rightarrow \text{C}_6 + \text{C}$	2.30×10^{-8}	-0.30	0	2

Table A1 Added and updated non-deuterium reactions.

Reaction		α	β	γ	Ref
$C_7^+ + e^- \rightarrow C_5 + C_2$		4.37×10^{-7}	-0.30	0	2
$C_7^+ + e^- \rightarrow C_4 + C_3$		1.84×10^{-6}	-0.50	0	2
$C_8^+ + e^- \rightarrow C_7 + C$		6.00×10^{-8}	-0.30	0	2
$C_8^+ + e^- \rightarrow C_6 + C_2$		2.00×10^{-8}	-0.30	0	2
$C_8^+ + e^- \rightarrow C_5 + C_3$		1.80×10^{-6}	-0.30	0	2
$C_8^+ + e^- \rightarrow C_4 + C_4$		1.20×10^{-7}	-0.30	0	2
$C_9^+ + e^- \rightarrow C_7 + C_2$		1.20×10^{-7}	-0.30	0	2
$C_9^+ + e^- \rightarrow C_6 + C_3$		1.32×10^{-6}	-0.30	0	2
$C_9^+ + e^- \rightarrow C_5 + C_4$		5.60×10^{-7}	-0.30	0	2
$C_{10}^+ + e^- \rightarrow C_9 + C$		2.00×10^{-8}	-0.30	0	2
$C_{10}^+ + e^- \rightarrow C_8 + C_2$		2.00×10^{-8}	-0.30	0	2
$C_{10}^+ + e^- \rightarrow C_7 + C_3$		1.40×10^{-6}	-0.30	0	2
$C_{10}^+ + e^- \rightarrow C_6 + C_4$		6.00×10^{-8}	-0.30	0	2
$C_{10}^+ + e^- \rightarrow C_5 + C_5$		5.00×10^{-7}	-0.30	0	2
$CNC^+ + e^- \rightarrow C_2 + N$		2.00×10^{-8}	-0.60	0	1
$CNC^+ + e^- \rightarrow CN + C$		3.80×10^{-7}	-0.60	0	1
$H_3^+ + e^- \rightarrow H + H + H$		5.44×10^{-8}	-0.50	0	3
$H_3^+ + e^- \rightarrow H_2 + H$		1.36×10^{-8}	-0.50	0	3
$H_2CO^+ + e^- \rightarrow CH_2 + O$		2.50×10^{-8}	-0.70	0	1
$H_2CO^+ + e^- \rightarrow CO + H + H$		2.50×10^{-7}	-0.70	0	1
$H_2CO^+ + e^- \rightarrow CO + H_2$		7.50×10^{-8}	-0.70	0	1
$H_2CO^+ + e^- \rightarrow HCO + H$		1.50×10^{-7}	-0.70	0	1
$HC_5NH^+ + e^- \rightarrow C_5N + H_2$		8.00×10^{-8}	-0.70	0	1
$HC_5NH^+ + e^- \rightarrow HC_3N + C_2H$		1.20×10^{-7}	-0.70	0	1
$HC_5NH^+ + e^- \rightarrow HC_5N + H$		9.20×10^{-7}	-0.70	0	1
$HC_5NH^+ + e^- \rightarrow HCN + C_4H$		4.40×10^{-7}	-0.70	0	1
$HC_5NH^+ + e^- \rightarrow HNC + C_4H$		4.40×10^{-7}	-0.70	0	1
$HCNH^+ + e^- \rightarrow CN + H + H$		9.06×10^{-8}	-0.65	0	1
$HCNH^+ + e^- \rightarrow HCN + H$		9.62×10^{-8}	-0.65	0	1
$HCNH^+ + e^- \rightarrow HNC + H$		9.62×10^{-8}	-0.65	0	1
$C_2H + CRPHOT \rightarrow C_2 + H$		5.27×10^{-14}	0.00	0	2
$C_2H + CRPHOT \rightarrow C + CH$		1.24×10^{-14}	0.00	0	2
$C_3H + CRPHOT \rightarrow C_2H + C$		2.15×10^{-14}	0.00	0	2
$C_3H + CRPHOT \rightarrow C_2 + CH$		1.30×10^{-15}	0.00	0	2
$C_3H + CRPHOT \rightarrow C_3 + H$		4.23×10^{-14}	0.00	0	2
$C_3H_2 + CRPHOT \rightarrow C_3H + H$		2.99×10^{-14}	0.00	0	2
$C_3H_2 + CRPHOT \rightarrow C_3 + H_2$		1.56×10^{-14}	0.00	0	2
$C_3H_2 + CRPHOT \rightarrow C_2H_2 + C$		1.50×10^{-14}	0.00	0	2
$C_3H_2 + CRPHOT \rightarrow C_2H + CH$		2.60×10^{-15}	0.00	0	2
$C_3H_2 + CRPHOT \rightarrow C_2 + CH_2$		1.95×10^{-15}	0.00	0	2
$C_4 + CRPHOT \rightarrow C_3 + C$		1.00×10^{-14}	0.00	0	2
$C_4 + CRPHOT \rightarrow C_2 + C_2$		2.99×10^{-15}	0.00	0	2
$C_4H + CRPHOT \rightarrow C_4 + H$		3.77×10^{-14}	0.00	0	2
$C_4H + CRPHOT \rightarrow C_3H + C$		1.69×10^{-14}	0.00	0	2
$C_4H + CRPHOT \rightarrow C_2H + C_2$		1.04×10^{-14}	0.00	0	2
$C_5 + CRPHOT \rightarrow C_4 + C$		1.69×10^{-15}	0.00	0	2
$C_5 + CRPHOT \rightarrow C_3 + C_2$		1.13×10^{-14}	0.00	0	2
$C_6 + CRPHOT \rightarrow C_5 + C$		1.17×10^{-15}	0.00	0	2
$C_6 + CRPHOT \rightarrow C_4 + C_2$		1.43×10^{-15}	0.00	0	2
$C_6 + CRPHOT \rightarrow C_3 + C_3$		1.04×10^{-14}	0.00	0	2
$C_7 + CRPHOT \rightarrow C_6 + C$		1.30×10^{-16}	0.00	0	2
$C_7 + CRPHOT \rightarrow C_5 + C_2$		2.47×10^{-15}	0.00	0	2
$C_7 + CRPHOT \rightarrow C_4 + C_3$		1.04×10^{-14}	0.00	0	2
$C_8 + CRPHOT \rightarrow C_7 + C$		3.9×10^{-16}	0.00	0	2
$C_8 + CRPHOT \rightarrow C_6 + C_2$		1.30×10^{-16}	0.00	0	2
$C_8 + CRPHOT \rightarrow C_5 + C_3$		1.17×10^{-15}	0.00	0	2
$C_8 + CRPHOT \rightarrow C_4 + C_4$		7.80×10^{-16}	0.00	0	2
$C_9 + CRPHOT \rightarrow C_7 + C_2$		7.80×10^{-16}	0.00	0	2
$C_9 + CRPHOT \rightarrow C_6 + C_3$		8.58×10^{-15}	0.00	0	2
$C_9 + CRPHOT \rightarrow C_5 + C_4$		3.64×10^{-15}	0.00	0	2
$CH + PHOTON \rightarrow CH^+ + e^-$		7.60×10^{-10}	0.00	3.80	4
$CH + PHOTON \rightarrow C + H$		9.20×10^{-10}	0.00	1.72	4
$C_2H + PHOTON \rightarrow C_2 + H$		8.10×10^{-10}	0.00	1.7	2
$C_2H + PHOTON \rightarrow CH + C$		1.90×10^{-10}	0.00	1.7	2
$C_3H + PHOTON \rightarrow C_3 + H$		6.50×10^{-10}	0.00	1.7	2
$C_3H + PHOTON \rightarrow C_2H + C$		3.30×10^{-10}	0.00	1.7	2
$C_3H + PHOTON \rightarrow C_2 + CH$		2.00×10^{-11}	0.00	1.7	2
$C_3H_2 + PHOTON \rightarrow C_2H_2 + C$		1.33×10^{-9}	0.00	1.7	2
$C_3H_2 + PHOTON \rightarrow C_2H + CH$		1.16×10^{-10}	0.00	1.7	2
$C_3H_2 + PHOTON \rightarrow CH_2 + C_2$		1.16×10^{-10}	0.00	1.7	2
$C_3H_2 + PHOTON \rightarrow C_3H + H$		1.33×10^{-9}	0.00	1.7	2
$C_3H_2 + PHOTON \rightarrow C_3 + H_2$		6.67×10^{-10}	0.00	1.7	2
$C_4 + PHOTON \rightarrow C_3 + C$		3.08×10^{-10}	0.00	1.7	2
$C_4 + PHOTON \rightarrow C_2 + C_2$		9.02×10^{-11}	0.00	1.7	2
$C_4H + PHOTON \rightarrow C_3H + C$		5.20×10^{-10}	0.00	1.7	2
$C_4H + PHOTON \rightarrow C_4 + H$		1.16×10^{-9}	0.00	1.7	2
$C_4H + PHOTON \rightarrow C_2H + C_2$		3.20×10^{-9}	0.00	1.7	2
$C_5 + PHOTON \rightarrow C_3 + C_2$		8.70×10^{-12}	0.00	1.7	2
$C_5 + PHOTON \rightarrow C_4 + C$		1.30×10^{-12}	0.00	1.7	2

Table A1 Added and updated non-deuterium reactions.

Reaction		α	β	γ	Ref
C ₆ + PHOTON	→ C ₅ + C	9.00 x 10 ⁻¹¹	0.00	1.7	2
C ₆ + PHOTON	→ C ₄ + C ₂	1.10 x 10 ⁻¹⁰	0.00	1.7	2
C ₆ + PHOTON	→ C ₃ + C ₃	8.00 x 10 ⁻¹⁰	0.00	1.7	2
C ₇ + PHOTON	→ C ₆ + C	1.00 x 10 ⁻¹¹	0.00	1.7	2
C ₇ + PHOTON	→ C ₅ + C ₂	1.90 x 10 ⁻¹⁰	0.00	1.7	2
C ₇ + PHOTON	→ C ₄ + C ₃	8.00 x 10 ⁻¹⁰	0.00	1.7	2
C ₈ + PHOTON	→ C ₇ + C	3.00 x 10 ⁻¹¹	0.00	1.7	2
C ₈ + PHOTON	→ C ₆ + C ₂	1.00 x 10 ⁻¹¹	0.00	1.7	2
C ₈ + PHOTON	→ C ₅ + C ₃	9.00 x 10 ⁻¹⁰	0.00	1.7	2
C ₈ + PHOTON	→ C ₄ + C ₄	6.00 x 10 ⁻¹¹	0.00	1.7	2
C ₉ + PHOTON	→ C ₇ + C ₂	6.00 x 10 ⁻¹¹	0.00	1.7	2
C ₉ + PHOTON	→ C ₆ + C ₃	6.60 x 10 ⁻¹⁰	0.00	1.7	2
C ₉ + PHOTON	→ C ₅ + C ₄	2.80 x 10 ⁻¹⁰	0.00	1.7	2
C ₁₀ + PHOTON	→ C ₉ + C	1.14 x 10 ⁻¹¹	0.00	1.7	2
C ₁₀ + PHOTON	→ C ₈ + C ₂	1.14 x 10 ⁻¹¹	0.00	1.7	2
C ₁₀ + PHOTON	→ C ₇ + C ₃	7.98 x 10 ⁻¹⁰	0.00	1.7	2
C ₁₀ + PHOTON	→ C ₆ + C ₄	3.42 x 10 ⁻¹¹	0.00	1.7	2
C ₁₀ + PHOTON	→ C ₅ + C ₅	2.50 x 10 ⁻¹⁰	0.00	1.7	2
Removed reactions					
CH ₃ OH ₂ ⁺ + H ₂ CO	→ H ₇ C ₂ O ₂ ⁺	—	—	—	7
H ₃ CO ⁺ + CH ₄	→ CH ₃ OCH ₄ ⁺	—	—	—	4
HCO ⁺ + CH ₄	→ CH ₃ CH ₂ O ⁺	—	—	—	4
C ₄ H ⁺ + e ⁻	→ C ₃ + CH	—	—	—	2
C ₆ ⁺ + e ⁻	→ C ₈ + C	—	—	—	2
C ₉ + PHOTON	→ C ₈ + C	—	—	—	2
C ₉ + CRPHOT	→ C ₈ + C	—	—	—	2
HNO + O	→ NO ₂ + H	—	—	—	1
O + NH	→ OH + N	—	—	—	1
NH ₂ + O	→ NO + H ₂	—	—	—	1
NH ₃ + CN	→ NH ₂ CN + H	—	—	—	1

Cosmic ray-induced photoionization: $k = \alpha \zeta_{\text{CR}}$ Photoreactions: $k = \alpha e^{-\gamma A_V}$ Ion-neutral reactions (Kooji formula): $k = \alpha(T/300)^\beta e^{-\gamma/T}$

(1) Wakelam et al. (2010b); (2) Chabot et al. (2010); (3) Roberts et al. (2004)

(4) KIDA database; (5) Laas et al. (2011); (6) Garrod & Herbst (2006)

(7) Horn et al. (2004)

Table A2 Added and updated deuterium reactions.

Reaction		α	β	γ	Refs.
$C_2D + H \rightarrow C_2H + D$		5.00×10^{-11}	0.50	832	9
$C_2H + D \rightarrow C_2D + H$		5.00×10^{-11}	0.50	250	9
$C_2H_2^+ + HD \rightarrow C_2HD^+ + H_2$		1.00×10^{-9}	0.00	0	5
$C_2HD^+ + H_2 \rightarrow C_2H_2^+ + HD$		2.50×10^{-9}	0.00	550	5
$CH_3^+ + D_2 \rightarrow CH_2D^+ + HD$		4.40×10^{-10}	0.00	0	3
$CH_3^+ + D_2 \rightarrow CHD_2^+ + H_2$		6.60×10^{-10}	0.00	0	3
$CH_3^+ + HD \rightarrow CH_2D^+ + H_2$		1.30×10^{-9}	0.00	0	3
$CH_2D^+ + H_2 \rightarrow CH_3^+ + HD$		8.70×10^{-10}	0.00	370	3
$CH_2D^+ + HD \rightarrow CHD_2^+ + H_2$		1.60×10^{-9}	0.00	0	3
$CH_2D^+ + HD \rightarrow CH_3^+ + D_2$		4.40×10^{-10}	0.00	400	3
$CH_2D^+ + D_2 \rightarrow CHD_2^+ + HD$		1.20×10^{-9}	0.00	0	3
$CHD_2^+ + H_2 \rightarrow CH_2D^+ + HD$		1.60×10^{-9}	0.00	370	3
$CHD_2^+ + H_2 \rightarrow CH_3^+ + D_2$		6.60×10^{-10}	0.00	400	3
$CHD_2^+ + HD \rightarrow CD_3^+ + H_2$		1.50×10^{-9}	0.00	0	3
$CHD_2^+ + HD \rightarrow CH_2D^+ + D_2$		1.20×10^{-9}	0.00	400	3
$CD_3^+ + H_2 \rightarrow CHD_2^+ + HD$		1.50×10^{-9}	0.00	370	3
$D^+ + H \rightarrow H^+ + D$		1.00×10^{-9}	0.00	0	6
$D^+ + H_2 \rightarrow H^+ + HD$		2.10×10^{-9}	0.00	0	3
$D_3^+ + H \rightarrow HD_2^+ + D$		2.00×10^{-9}	0.00	655	4
$D_3^+ + H_2 \rightarrow H_2D^+ + D_2$		7.00×10^{-10}	0.00	341	2
$D_3^+ + H_2 \rightarrow HD_2^+ + HD$		2.00×10^{-10}	0.00	234	15
$D_3^+ + HD \rightarrow HD_2^+ + D_2$		8.70×10^{-10}	0.00	159	2
$DCN + H \rightarrow HCN + D$		1.00×10^{-10}	0.50	500	9*
$DCO^+ + H \rightarrow HCO^+ + D$		2.20×10^{-9}	0.00	796	7
$H^+ + D \rightarrow D^+ + H$		1.00×10^{-9}	0.00	41	6
$H^+ + HD \rightarrow D^+ + H_2$		1.00×10^{-9}	0.00	464	3
$H_2D^+ + H \rightarrow H_3^+ + D$		1.00×10^{-9}	0.00	632	7
$H_2D^+ + H_2 \rightarrow H_3^+ + HD$		3.50×10^{-9}	0.00	220	15
$H_3^+ + D \rightarrow H_2D^+ + H$		1.00×10^{-9}	0.00	0	7*
$H_3^+ + D_2 \rightarrow H_2D^+ + HD$		3.50×10^{-10}	0.00	0	2
$H_3^+ + D_2 \rightarrow HD_2^+ + H_2$		1.10×10^{-9}	0.00	0	2
$H_3^+ + HD \rightarrow H_2D^+ + H_2$		3.50×10^{-10}	0.00	0	15
$H_2D^+ + D \rightarrow HD_2^+ + H$		2.00×10^{-9}	0.00	0	4
$H_2D^+ + HD \rightarrow H_3^+ + D_2$		3.50×10^{-10}	0.00	63	2
$H_2D^+ + HD \rightarrow HD_2^+ + H_2$		2.60×10^{-10}	0.00	0	15
$H_2D^+ + D_2 \rightarrow HD_2^+ + HD$		7.00×10^{-10}	0.00	0	2
$H_2D^+ + D_2 \rightarrow D_3^+ + H_2$		7.00×10^{-10}	0.00	0	2
$HCN + D \rightarrow DCN + H$		1.00×10^{-10}	0.50	500	9*
$HCO^+ + D \rightarrow DCO^+ + H$		1.00×10^{-9}	0.00	0	7
$HD_2^+ + D \rightarrow D_3^+ + H$		2.00×10^{-9}	0.00	0	4
$HD_2^+ + H \rightarrow H_2D^+ + D$		2.00×10^{-9}	0.00	550	4
$HD_2^+ + D_2 \rightarrow D_3^+ + HD$		8.70×10^{-10}	0.00	0	2
$HD_2^+ + H_2 \rightarrow H_3^+ + D_2$		1.10×10^{-9}	0.00	251	2
$HD_2^+ + H_2 \rightarrow H_2D^+ + HD$		2.60×10^{-10}	0.00	187	15
$HD_2^+ + HD \rightarrow H_2D^+ + D_2$		7.00×10^{-10}	0.00	107	2
$HD_2^+ + HD \rightarrow D_3^+ + H_2$		2.00×10^{-10}	0.00	0	15
$N_2H^+ + D \rightarrow N_2D^+ + H$		1.00×10^{-9}	0.00	0	7
$N_2D^+ + H \rightarrow N_2H^+ + D$		2.20×10^{-9}	0.00	550	7
$OH + D \rightarrow OD + H$		1.30×10^{-10}	0.50	0	8
$OD + H \rightarrow OH + D$		1.30×10^{-10}	0.50	810	8
$C_2HD^+ + H_2 \rightarrow C_2H_3D^+$		3.39×10^{-14}	-1.50	0	12
$CH_3^+ + D_2 \rightarrow CH_3D_2^+$		3.50×10^{-14}	-1.00	0	12
$CH_3^+ + D_2O \rightarrow CH_3OD_2^+$		1.65×10^{-11}	-1.70	0	12
$CH_3^+ + HDO \rightarrow CH_3OHD^+$		1.10×10^{-11}	-1.70	0	12
$CH_2D^+ + D_2O \rightarrow CH_2DOD_2^+$		2.20×10^{-11}	-1.70	0	12
$CH_2D^+ + H_2 \rightarrow CH_4D^+$		2.00×10^{-14}	-1.00	0	12
$CH_2D^+ + H_2O \rightarrow CH_2DOH_2^+$		1.10×10^{-11}	-1.70	0	12
$CH_2D^+ + HDO \rightarrow CH_2DOHD^+$		1.65×10^{-11}	-1.70	0	12
$CH_2D^+ + HD \rightarrow CH_3D_2^+$		3.50×10^{-14}	-1.00	0	12
$CHD_2^+ + D_2O \rightarrow CHD_2OD_2^+$		2.75×10^{-11}	-1.70	0	12
$CHD_2^+ + H_2 \rightarrow CH_3D_2^+$		3.50×10^{-14}	-1.00	0	12
$CHD_2^+ + H_2O \rightarrow CHD_2OH_2^+$		1.65×10^{-11}	-1.70	0	12
$CHD_2^+ + HDO \rightarrow CHD_2OHD^+$		2.20×10^{-11}	-1.70	0	12
$CD_3^+ + D_2 \rightarrow CD_3OD_2^+$		2.75×10^{-11}	-1.70	0	12
$CD_3^+ + H_2 \rightarrow CH_2D_3^+$		6.30×10^{-14}	-1.00	0	12
$CD_3^+ + H_2O \rightarrow CD_3OH_2^+$		2.20×10^{-11}	-1.70	0	12
$CD_3^+ + HDO \rightarrow CD_3OHD^+$		2.75×10^{-11}	-1.70	0	12
$CD_3OCD_4^+ + e^- \rightarrow CD_3OCD_3 + D$		8.50×10^{-8}	-0.70	0	14
$CD_3OCD_4^+ + e^- \rightarrow CD_3OD + CD_3$		9.18×10^{-7}	-0.70	0	14
$CD_3OCD_4^+ + e^- \rightarrow CD_3 + CD_4 + O$		6.97×10^{-7}	-0.70	0	14
$D_3^+ + e^- \rightarrow D_2 + D$		5.40×10^{-9}	-0.50	0	12
$D_3^+ + e^- \rightarrow D + D + D$		2.16×10^{-8}	-0.50	0	12
$H_2D^+ + e^- \rightarrow D + H + H$		4.38×10^{-8}	-0.50	0	10
$H_2D^+ + e^- \rightarrow H_2 + D$		4.20×10^{-9}	-0.50	0	10
$H_2D^+ + e^- \rightarrow HD + H$		1.20×10^{-8}	-0.50	0	10
$HD_2^+ + e^- \rightarrow D + D + H$		4.38×10^{-8}	-0.50	0	11
$HD_2^+ + e^- \rightarrow D_2 + H$		1.20×10^{-8}	-0.50	0	11
$HD_2^+ + e^- \rightarrow HD + D$		4.20×10^{-9}	-0.50	0	11
$DCNH^+ + e^- \rightarrow DCN + H$		2.33×10^{-7}	-0.50	0	13
$DCNH^+ + e^- \rightarrow HNC + D$		1.16×10^{-7}	-0.50	0	13

Table A2 Added and updated deuterium reactions.

Reaction			α	β	γ	Refs.
$\text{HCND}^+ + \text{e}^-$	\rightarrow	$\text{DNC} + \text{H}$	2.33×10^{-7}	-0.50	0	13
$\text{HCND}^+ + \text{e}^-$	\rightarrow	$\text{HCN} + \text{D}$	1.16×10^{-7}	-0.50	0	13
$\text{HDCN}^+ + \text{e}^-$	\rightarrow	$\text{NHD} + \text{C}$	1.75×10^{-7}	-0.50	0	13
$\text{HDNC}^+ + \text{e}^-$	\rightarrow	$\text{HNC} + \text{D}$	0.58×10^{-7}	-0.50	0	13
$\text{HDNC}^+ + \text{e}^-$	\rightarrow	$\text{DNC} + \text{H}$	1.16×10^{-7}	-0.50	0	13
Removed reactions						
$\text{C}_2\text{H}_2^+ + \text{HD}$	\rightarrow	$\text{C}_2\text{H}_3\text{D}^+$	—	—	—	11
$\text{CH}_3^+ + \text{HD}$	\rightarrow	CH_4D^+	—	—	—	11
$\text{CH}_2\text{D}^+ + \text{D}_2$	\rightarrow	CH_2D_3^+	—	—	—	11
$\text{CHD}_2^+ + \text{HD}$	\rightarrow	CH_2D_3^+	—	—	—	11

* Estimate

Cosmic ray-induced photoionization: $k = \alpha \zeta_{\text{CR}}$ Photoreactions: $k = \alpha e^{-\gamma A_V}$ Ion-neutral reactions (Kooji formula): $k = \alpha(T/300)^\beta e^{-\gamma/T}$

(1) Ceccarelli & Dominik (2005); (2) Giles et al. (1992); (3) Smith et al. (1982a,b)

(4) Walmsley et al. (2004); (5) Herbst et al. (1987); (6) Watson (1976)

(7) Adams & Smith (1985); (8) Croswell & Dalgarno (1985); (9) Schilke et al. (1992)

(10) Sundstrom et al. (1994); (11) Roberts et al. (2004); (12) Larsson et al. (1997)

(13) Roueff et al. (2005); (14) Hamberg et al. (2010a); (15) Gerlich et al. (2002)

Table A3 Problematic reactions that show correlation coefficients > 0.05 and strong chemical ties to any of the following species, including their isotopologues and isomers: water, H_3^+ , HCO^+ and HCN. An asterisk alongside the uncertainty signifies a reaction resulting from cloning the network.

Reaction	Uncertainty	Reaction	Uncertainty
<i>Problematic reactions connected to all species</i>			
$\text{H}_2 + \text{CRP} \rightarrow \text{H}_2^+ + \text{e}^-$	2.00	$\text{He} + \text{CRP} \rightarrow \text{He}^+ + \text{e}^-$	2.00
<i>H_3^+ isotopologues</i>			
$\text{H}_3^+ + \text{e}^- \rightarrow \text{H} + \text{H} + \text{H}$	2.00	$\text{H}_2\text{D}^+ + \text{e}^- \rightarrow \text{D} + \text{H} + \text{H}$	2.00
$\text{HD}_2^+ + \text{e}^- \rightarrow \text{D} + \text{D} + \text{H}$	2.00	$\text{H}_3^+ + \text{HD} \rightarrow \text{H}_2\text{D}^+ + \text{H}_2$	1.25
$\text{H}_2\text{D}^+ + \text{HD} \rightarrow \text{HD}_2^+ + \text{H}_2$	1.25	$\text{HD}_2^+ + \text{HD} \rightarrow \text{D}_3^+ + \text{H}_2$	1.25
$\text{H}_2\text{D}^+ + \text{H}_2 \rightarrow \text{H}_3^+ + \text{HD}$	2.00	$\text{HD}_2^+ + \text{H}_2 \rightarrow \text{H}_2\text{D}^+ + \text{HD}$	2.00
$\text{D}_3^+ + \text{H}_2 \rightarrow \text{HD}_2^+ + \text{HD}$	2.00	$\text{H}_3^+ + \text{D}_2 \rightarrow \text{HD}_2^+ + \text{H}_2$	2.00
$\text{H}_2\text{D}^+ + \text{D}_2 \rightarrow \text{D}_3^+ + \text{H}_2$	2.00	$\text{H}_3^+ + \text{D} \rightarrow \text{H}_2\text{D}^+ + \text{H}$	2.00
$\text{H}_2\text{D}^+ + \text{D} \rightarrow \text{HD}_2^+ + \text{H}$	2.00	$\text{HD}_2^+ + \text{D} \rightarrow \text{D}_3^+ + \text{H}$	2.00
$\text{H}_3^+ + \text{CO} \rightarrow \text{HCO}^+ + \text{H}_2$	1.25	$\text{H}_2\text{D}^+ + \text{CO} \rightarrow \text{DCO}^+ + \text{H}_2$	1.25*
$\text{HD}_2^+ + \text{CO} \rightarrow \text{DCO}^+ + \text{HD}$	1.25*	$\text{D}_3^+ + \text{CO} \rightarrow \text{DCO}^+ + \text{D}_2$	1.25*
$\text{H}_3^+ + \text{OH} \rightarrow \text{H}_2\text{O}^+ + \text{H}_2$	2.00	$\text{H}_2\text{D}^+ + \text{OH} \rightarrow \text{H}_2\text{O}^+ + \text{HD}$	2.00
$\text{H}_3^+ + \text{OD} \rightarrow \text{H}_2\text{O}^+ + \text{HD}$	2.00		
<i>HCO^+ isotopologues</i>			
$\text{H}_3^+ + \text{CO} \rightarrow \text{HCO}^+ + \text{H}_2$	1.25	$\text{H}_3^+ + \text{CO} \rightarrow \text{HOC}^+ + \text{H}_2$	1.25
$\text{H}_2\text{D}^+ + \text{CO} \rightarrow \text{DCO}^+ + \text{H}_2$	1.25	$\text{H}_2\text{D}^+ + \text{CO} \rightarrow \text{DOC}^+ + \text{H}_2$	1.25
$\text{HCO}^+ + \text{e}^- \rightarrow \text{CO} + \text{H}$	1.25	$\text{HOC}^+ + \text{e}^- \rightarrow \text{CO} + \text{H}$	1.25
$\text{DCO}^+ + \text{e}^- \rightarrow \text{CO} + \text{D}^*$	1.25	$\text{DOC}^+ + \text{e}^- \rightarrow \text{CO} + \text{D}$	1.25*
$\text{HOC}^+ + \text{H}_2 \rightarrow \text{HCO}^+ + \text{H}_2$	2.00	$\text{HCO}^+ + \text{D} \rightarrow \text{DCO}^+ + \text{H}$	2.00
$\text{DOC}^+ + \text{H}_2 \rightarrow \text{DCO}^+ + \text{H}_2$	2.00	$\text{DOC}^+ + \text{H}_2 \rightarrow \text{HCO}^+ + \text{HD}$	2.00
$\text{HCO}^+ + \text{OH} \rightarrow \text{H}_2\text{O}^+ + \text{CO}$	2.00	$\text{H}^+ + \text{D} \rightarrow \text{D}^+ + \text{H}$	2.00
<i>HCN isotopologues</i>			
$\text{H}_2\text{CN}^+ + \text{e}^- \rightarrow \text{HCN} + \text{H}$	2.00	$\text{H}_2\text{CN}^+ + \text{e}^- \rightarrow \text{HNC} + \text{H}$	2.00
$\text{HDCN}^+ + \text{e}^- \rightarrow \text{HCN} + \text{D}$	2.00*	$\text{HDCN}^+ + \text{e}^- \rightarrow \text{DCN} + \text{H}$	2.00*
$\text{HDCN}^+ + \text{e}^- \rightarrow \text{HNC} + \text{D}$	2.00	$\text{HDCN}^+ + \text{e}^- \rightarrow \text{DNC} + \text{H}$	2.00*
$\text{H}_2\text{CN}^+ + \text{e}^- \rightarrow \text{CN} + \text{H} + \text{H}$	2.00	$\text{HDCN}^+ + \text{e}^- \rightarrow \text{CN} + \text{H} + \text{D}$	2.00
$\text{C}^+ + \text{HNC} \rightarrow \text{H}_2\text{CN}^+ + \text{H}_2\text{O}$	2.00*	$\text{C}^+ + \text{HCN} \rightarrow \text{C}_2\text{N}^+ + \text{H}$	2.00
$\text{C}^+ + \text{DNC} \rightarrow \text{C}_2\text{N}^+ + \text{D}$	2.00*	$\text{C}^+ + \text{DCN} \rightarrow \text{C}_2\text{N}^+ + \text{D}$	2.00*
$\text{C}^+ + \text{HCN} \rightarrow \text{CNC}^+ + \text{H}$	2.00	$\text{C}^+ + \text{NH}_2 \rightarrow \text{HCN}^+ + \text{H}$	2.00
$\text{C}^+ + \text{NH}_3 \rightarrow \text{H}_2\text{CN}^+ + \text{H}$	2.00	$\text{NH}_2 + \text{O} \rightarrow \text{HNO} + \text{H}$	2.00
$\text{N} + \text{CN} \rightarrow \text{C} + \text{N}_2$	2.00		
<i>H_2O isotopologues</i>			
$\text{H}_3\text{O}^+ + \text{e}^- \rightarrow \text{H}_2\text{O} + \text{H}$	1.25*	$\text{H}_2\text{DO}^+ + \text{e}^- \rightarrow \text{HDO} + \text{H}$	1.25*
$\text{HD}_2\text{O}^+ + \text{e}^- \rightarrow \text{D}_2\text{O} + \text{H}$	1.25*	$\text{H}_3\text{O}^+ + \text{e}^- \rightarrow \text{OH} + \text{H} + \text{H}$	1.25
$\text{H}_2\text{DO}^+ + \text{e}^- \rightarrow \text{OH} + \text{D} + \text{H}$	1.25*	$\text{HD}_2\text{O}^+ + \text{e}^- \rightarrow \text{OD} + \text{D} + \text{H}$	1.25*
$\text{H}_3^+ + \text{H}_2\text{O} \rightarrow \text{H}_3\text{O}^+ + \text{H}_2$	1.25	$\text{H}_3^+ + \text{HDO} \rightarrow \text{H}_3\text{O}^+ + \text{HD}$	1.25*
$\text{H}_3^+ + \text{HDO} \rightarrow \text{H}_2\text{DO}^+ + \text{H}_2$	1.25*	$\text{H}_3^+ + \text{O} \rightarrow \text{H}_2\text{O}^+ + \text{H}$	1.40
$\text{HCO}^+ + \text{H}_2\text{O} \rightarrow \text{H}_3\text{O}^+ + \text{CO}$	1.50	$\text{HCO}^+ + \text{HDO} \rightarrow \text{H}_2\text{DO}^+ + \text{CO}$	1.50*
$\text{DCO}^+ + \text{H}_2\text{O} \rightarrow \text{H}_2\text{DO}^+ + \text{CO}$	1.50*	$\text{DCO}^+ + \text{HDO} \rightarrow \text{HD}_2\text{O}^+ + \text{CO}$	1.50*
$\text{HCO}^+ + \text{D}_2\text{O} \rightarrow \text{HD}_2\text{O}^+ + \text{CO}$	1.50*		

B. DOMINANT FORMATION AND DESTRUCTION PATHWAYS FOR DEUTERATED SPECIES

In this Appendix, we list the dominant pathways identified for isotopologues and isomers of the selected species H_3^+ , HCO^+ , HCN, H_2O as well as species involved in the formation of these essential species. The intention is to help with future comparisons with our model.

Table B1
Most essential formation and destruction pathways for H_3^+ , H_2D^+ , HD_2^+ and D_3^+ .

Reaction	α	β	γ	Accuracy	Ref	Estimated by
$\text{H}_3^+ + \text{HD} \rightarrow \text{H}_2\text{D}^+ + \text{H}_2$	1.70E-09	0.00E+00	0.00E+00	<i>factor 2</i>	(1)	T
$\text{H}_3^+ + \text{D} \rightarrow \text{H}_2\text{D}^+ + \text{H}$	1.00E-09	0.00E+00	0.00E+00	<i>factor 2</i>	(2)	T
$\text{H}_2\text{D}^+ + \text{HD} \rightarrow \text{HD}_2^+ + \text{H}_2$	8.10E-10	0.00E+00	0.00E+00	$\pm 15\%$	(3)	M
$\text{H}_2\text{D}^+ + \text{D} \rightarrow \text{HD}_2^+ + \text{H}$	2.00E-09	0.00E+00	0.00E+00	<i>factor 2</i>	(4)	T
$\text{H}_3^+ + \text{D}_2 \rightarrow \text{HD}_2^+ + \text{H}_2$	1.10E-09	0.00E+00	0.00E+00	$\pm 15\%$	(3)	M
$\text{HD}_2^+ + \text{HD} \rightarrow \text{D}_3^+ + \text{H}_2$	6.40E-10	0.00E+00	0.00E+00	$\pm 15\%$	(3)	M
$\text{HD}_2^+ + \text{D} \rightarrow \text{D}_3^+ + \text{H}$	2.00E-09	0.00E+00	0.00E+00	<i>factor 2</i>	(4)	T
$\text{H}_2\text{D}^+ + \text{D}_2 \rightarrow \text{D}_3^+ + \text{H}_2$	7.00E-10	0.00E+00	0.00E+00	$\pm 15\%$	(3)	M
$\text{H}_2\text{D}^+ + \text{CO} \rightarrow \text{DCO}^+ + \text{H}_2$	5.37E-10	0.00E+00	0.00E+00	$< 25\%$	(5)	C
$\text{H}_2\text{D}^+ + \text{CO} \rightarrow \text{HCO}^+ + \text{HD}$	1.07E-09	0.00E+00	0.00E+00	$< 25\%$	(5)	C
$\text{HD}_2^+ + \text{CO} \rightarrow \text{DCO}^+ + \text{HD}$	1.07E-09	0.00E+00	0.00E+00	$< 25\%$	(5)	C
$\text{HD}_2^+ + \text{CO} \rightarrow \text{HCO}^+ + \text{D}_2$	5.37E-10	0.00E+00	0.00E+00	$< 25\%$	(5)	C
$\text{D}_3^+ + \text{CO} \rightarrow \text{DCO}^+ + \text{D}_2$	1.61E-09	0.00E+00	0.00E+00	$< 25\%$	(5)	C
$\text{D}_3^+ + \text{e}^- \rightarrow \text{D} + \text{D} + \text{D}$	2.16E-08	-0.50E+00	0.00E+00	$< 25\%$	(5)	C

T, Theoretical/Calculated

C, Cloned

Ion-neutral reactions (Kooji formula): $k = \alpha(T/300)^\beta e^{-\gamma/T}$

Pathways extracted at 1 Myr from four points with $T = 10$ or 100 K and densities = 10^4 and 10^8 cm^{-3} in the ÒPrimordialÓ model

(1) Sidhu et al. (1992); (2) Adams & Smith (1985); (3) Giles et al. (1992); (4) Walmsley et al. (2004)

(5) OSU www.physics.ohio-state.edu/~eric/

Table B2
Most essential formation and destruction pathways for HCO^+ , HOC^+ , DCO^+ and DOC^+ .

Reaction	α	β	γ	Accuracy	Ref	Estimated by
$\text{H}_3^+ + \text{CO} \rightarrow \text{HCO}^+ + \text{H}_2$	1.61E-09	0.00E+00	0.00E+00	$< 25\%$	(1)	M
$\text{H}_3^+ + \text{CO} \rightarrow \text{HOC}^+ + \text{H}_2$	9.44E-11	0.00E+00	0.00E+00	$< 25\%$	(1)	M
$\text{HOC}^+ + \text{H}_2 \rightarrow \text{HCO}^+ + \text{H}_2$	1.00E-11	0.00E+00	0.00E+00	<i>factor 2</i>	(1)	?
$\text{CH}_3^+ + \text{O} \rightarrow \text{HCO}^+/\text{HOC}^+ + \text{H}_2$	2.05E-10	0.00E+00	0.00E+00	<i>factor 2</i>	(1)	?
$\text{HCO}^+ + \text{SO} \rightarrow \text{HSO}^+ + \text{CO}$	3.30E-09	-0.50E+00	0.00E+00	<i>factor 2</i>	(1)	?
$\text{HCO}^+ + \text{e}^- \rightarrow \text{CO} + \text{H}$	2.80E-07	-0.69E+00	0.00E+00	$< 25\%$	(1)	?
$\text{HCO}^+ + \text{C} \rightarrow \text{CH}^+ + \text{CO}$	1.10E-09	0.00E+00	0.00E+00	<i>factor 2</i>	(1)	?
$\text{H}_2\text{D}^+ + \text{CO} \rightarrow \text{DCO}^+ + \text{H}_2$	5.37E-10	0.00E+00	0.00E+00	$< 25\%$	(1)	M
$\text{HCO}^+ + \text{D} \rightarrow \text{DCO}^+ + \text{H}$	1.00E-09	0.00E+00	0.00E+00	<i>factor 2</i>	(2)	M
$\text{D}_3^+ + \text{CO} \rightarrow \text{DCO}^+ + \text{D}_2$	1.61E-09	0.00E+00	0.00E+00	$< 25\%$	(1)	C
$\text{DOC}^+ + \text{H}_2 \rightarrow \text{DCO}^+ + \text{H}_2$	3.33E-12	0.00E+00	0.00E+00	$< 50\%$	(1)	C
$\text{CH}_2\text{D}^+ + \text{O} \rightarrow \text{DCO}^+ + \text{H}_2$	6.83E-11	0.00E+00	0.00E+00	$< 25\%$	(1)	C
$\text{DCO}^+ + \text{e}^- \rightarrow \text{CO} + \text{D}$	2.40E-07	-0.69E+00	0.00E+00	$< 25\%$	(1)	C
$\text{DCO}^+ + \text{SO} \rightarrow \text{DSO}^+ + \text{CO}$	3.30E-09	-0.50E+00	0.00E+00	<i>factor 2</i>	(1)	C
$\text{DCO}^+ + \text{H} \rightarrow \text{HCO}^+ + \text{D}$	2.20E-09	0.00E+00	7.69E+02	<i>factor 2</i>	(2)	M
$\text{DCO}^+ + \text{C} \rightarrow \text{CD}^+ + \text{CO}$	1.10E-09	0.00E+00	0.00E+00	<i>factor 2</i>	(1)	C
$\text{DCO}^+ + \text{HCN} \rightarrow \text{HDCN}^+ + \text{CO}$	7.30E-09	-0.50E+00	0.00E+00	<i>factor 2</i>	(1)	C
$\text{DCO}^+ + \text{HNC} \rightarrow \text{HDCN}^+ + \text{CO}$	6.63E-09	-0.50E+00	0.00E+00	<i>factor 2</i>	(1)	C

T, Theoretical/Calculated

M, Laboratory measurements

C, Cloned

?, No listing for estimation method, most likely theoretical

Ion-neutral reactions (Kooji formula): $k = \alpha(T/300)^\beta e^{-\gamma/T}$

Pathways extracted at 1 Myr from four points with $T = 10$ or 100 K and densities = 10^4 and 10^8 cm^{-3} in the ÒPrimordialÓ model

(1) OSU www.physics.ohio-state.edu/~eric/; (2) KIDA: <http://kida.obs.u-bordeaux1.fr/>

Table B3
Most essential formation and destruction pathways for HCN, HNC, DCN and DNC.

Reaction		α	β	γ	Accuracy	Ref	Estimated by
$\text{H}_2\text{CN}^+ + \text{e}^- \rightarrow \text{HCN} + \text{H}$		9.62E-08	-0.65E+00	0.00E+00	factor 2	(1)	M
$\text{H}_2\text{CN}^+ + \text{e}^- \rightarrow \text{HNC} + \text{H}$		1.85E-07	-0.65E+00	0.00E+00	< 25%	(2)	?
$\text{H}_2\text{NC}^+ + \text{e}^- \rightarrow \text{HNC} + \text{H}$		1.80E-07	-0.50E+00	0.00E+00	< 25%	(2)	?
$\text{CH}_2 + \text{N} \rightarrow \text{HCN} / \text{HNC} + \text{H}$		3.95E-11	-0.17E+00	0.00E+00	< 25%	(2)	T
$\text{HNC} + \text{H}^+ \rightarrow \text{HCN} + \text{H}^+$		2.78E-08	-0.50E+00	0.00E+00	factor 2	(2)	?
$\text{NH (ice)} + \text{C (ice)} \rightarrow \text{HCN (ice)}$		1.00	0.00	0.00	–	(3)	
$\text{CN (ice)} + \text{H (ice)} \rightarrow \text{HCN (ice)}$		1.00	0.00	0.00	–	(3)	
$\text{ND (ice)} + \text{C (ice)} \rightarrow \text{DCN (ice)}$		1.00	0.00	0.00	–	(3)	C
$\text{CN (ice)} + \text{D (ice)} \rightarrow \text{DCN (ice)}$		1.00	0.00	0.00	–	(3)	C
$\text{HDCN}^+ + \text{e}^- \rightarrow \text{DCN} + \text{H}$		2.33E-07	-0.50E+00	0.00E+00	<i>factor 2</i>	(4)	T
$\text{D}_2\text{CN}^+ + \text{e}^- \rightarrow \text{DCN/DNC} + \text{D}$		1.85E-07	-0.65E+00	0.00E+00	<i>factor 2</i>	(2)	C
$\text{HDNC}^+ + \text{e}^- \rightarrow \text{DNC} + \text{H}$		1.66E-07	-0.50E+00	0.00E+00	<i>factor 2</i>	(4)	T
$\text{HCN} + \text{D} \rightarrow \text{DCN} + \text{H}$		1.00E-10	0.50E+00	5.00E+02	<i>factor 2</i>	(5)	T
$\text{CHD} + \text{N} \rightarrow \text{DCN} + \text{H}$		1.98E-11	1.67E-01	0.00E+00	< 50%	(5)	T
$\text{DCN} + \text{H}_3^+ \rightarrow \text{HDCN}^+ + \text{H}_2$		8.50E-09	-0.50E+00	0.00E+00	< 25%	(2)	C
$\text{DCN} + \text{H}_3^+ \rightarrow \text{H}_2\text{CN}^+ + \text{HD}$		8.50E-09	-0.50E+00	0.00E+00	< 25%	(2)	C
$\text{DCN} + \text{HCO}^+ \rightarrow \text{HDCN}^+ + \text{CO}$		7.30E-09	-0.50E+00	0.00E+00	factor 2	(2)	C
$\text{DCN} + \text{H}^+ \rightarrow \text{DCN}^+ + \text{H}$		1.39E-08	-0.50E+00	0.00E+00	factor 2	(2)	C
$\text{DCN} + \text{H} \rightarrow \text{HCN} + \text{D}$		1.00E-10	0.50E+00	5.00E+02	<i>factor 2</i>	(5)	C
$\text{DCN} + \text{H}_3\text{O}^+ \rightarrow \text{HDCN}^+ + \text{H}_2\text{O}$		4.10E-09	-0.50E+00	0.00E+00	< 25%	(2)	C
$\text{DCN} + \text{H}_3\text{O}^+ \rightarrow \text{H}_2\text{CN}^+ + \text{HDO}$		4.10E-09	-0.50E+00	0.00E+00	< 25%	(2)	C
$\text{DCN} + \text{D}_3\text{O}^+ \rightarrow \text{D}_2\text{CN}^+ + \text{D}_2$		8.20E-09	-0.50E+00	0.00E+00	< 25%	(2)	C

T, Theoretical/Calculated

C, Cloned

?, No listing for estimation method, most likely theoretical

Ion-neutral reactions (Kooji formula): $k = \alpha(T/300)^\beta e^{-\gamma/T}$

Pathways extracted at 1 Myr from four points with $T = 10$ or 100 K and densities = 10^4 and 10^8 cm^{-3} in the ÒPrimordialÓ model

(1) Wakelam et al. (2010b); (2) OSU www.physics.ohio-state.edu/~eric/; (3) Garrod & Herbst (2006); (4) Roueff et al. (2005)

(5) Schilke et al. (1992)

Table B4
Most essential formation and destruction pathways for H₂O, HDO and D₂O.

Reaction		α	β	γ	Accuracy	Ref	Estimated by
H ₃ O ⁺ + e ⁻	→ H ₂ O + H	1.10E-07	-0.50E+00	0.00E+00	< 25%	(1)	M
H ₃ O ⁺ + HCN	→ H ₂ O + H ₂ CN ⁺	8.20E-09	-0.50E+00	0.00E+00	< 25%	(2)	?
H ₃ O ⁺ + HNC	→ H ₂ O + H ₂ NC ⁺	7.42E-09	-0.50E+00	0.00E+00	factor 2	(2)	?
OH (ice) + H (ice)	→ H ₂ O (ice)	1.00	0.00	0.00	--	(3)	
OD (ice) + H (ice)	→ HDO (ice)	1.00	0.00	0.00	--	(3)	C
OH (ice) + D (ice)	→ HDO (ice)	1.00	0.00	0.00	--	(3)	C
H ₂ O + H ⁺	→ H ₂ O ⁺ + H	7.30E-09	-0.50E+00	0.00E+00	< 25%	(2)	?
H ₂ O + H ₃ ⁺	→ H ₃ O ⁺ + H ₂	4.50E-09	-0.50E+00	0.00E+00	< 25%	(2)	?
H ₂ DO ⁺ + e ⁻	→ HDO + H	7.33E-08	-0.50E+00	0.00E+00	< 25%	(2)	C
HD ₂ O ⁺ + e ⁻	→ HDO + D	7.33E-08	-0.50E+00	0.00E+00	< 25%	(2)	C
H ₂ DO ⁺ + HCN	→ HDO + H ₂ CN ⁺	4.10E-09	-0.50E+00	0.00E+00	< 25%	(2)	C
H ₂ DO ⁺ + HNC	→ HDO + H ₂ CN ⁺	3.71E-09	-0.50E+00	0.00E+00	factor 2	(2)	C
H ₂ + OD	→ HDO + H	5.60E-13	0.00E+00	1.04E+03	factor 2	(2)	C
HDO + HCO ⁺	→ H ₂ DO ⁺ + CO	2.10E-09	-0.50E+00	0.00E+00	< 50%	(2)	C
HDO + H ₃ ⁺	→ H ₂ DO ⁺ + H ₂	2.70E-09	-0.50E+00	0.00E+00	< 25%	(2)	C
HDO + H ₃ ⁺	→ H ₃ O ⁺ + HD	1.80E-09	-0.50E+00	0.00E+00	< 25%	(2)	C
HDO + C ⁺	→ HOC ⁺ /DOC ⁺ + H	9.00E-10	-0.50E+00	0.00E+00	< 25%	(2)	C
HDO + C ⁺	→ HCO ⁺ /DCO ⁺ + H	4.45E-10	-0.50E+00	0.00E+00	< 25%	(2)	C
HD ₂ O ⁺ + e ⁻	→ D ₂ O + H	3.67E-08	-0.50E+00	0.00E+00	< 25%	(2)	C
D ₃ O ⁺ + e ⁻	→ D ₂ O + D	1.10E-07	-0.50E+00	0.00E+00	< 25%	(2)	C
HD ₂ O ⁺ + HCN	→ D ₂ O + H ₂ CN ⁺	1.37E-09	-0.50E+00	0.00E+00	< 25%	(2)	C
HD ₂ O ⁺ + HNC	→ D ₂ O + H ₂ CN ⁺	1.24E-09	-0.50E+00	0.00E+00	factor 2	(2)	C
HD + OD	→ D ₂ O + H	2.80E-13	1.00E+00	1.04E+03	factor 2	(2)	C
OD (ice) + D (ice)	→ D ₂ O (ice)	1.00	0.00	0.00	--	(3)	C
D ₂ O + C ⁺	→ DOC ⁺ + D	1.80E-09	-0.50E+00	0.00E+00	< 25%	(2)	C
D ₂ O + C ⁺	→ DCO ⁺ + D	8.90E-10	-0.50E+00	0.00E+00	< 25%	(2)	C
D ₂ O + H ₃ ⁺	→ HD ₂ O ⁺ + H ₂	1.35E-09	-0.50E+00	0.00E+00	< 25%	(2)	C
D ₂ O + H ₃ ⁺	→ H ₂ DO ⁺ + HD	2.70E-09	-0.50E+00	0.00E+00	< 25%	(2)	C
D ₂ O + H ₃ ⁺	→ H ₃ O ⁺ + D ₂	4.50E-10	-0.50E+00	0.00E+00	< 25%	(2)	C
D ₂ O + H ⁺	→ D ₂ O ⁺ + H	2.43E-09	-0.50E+00	0.00E+00	< 25%	(2)	C
D ₂ O + H ⁺	→ HDO ⁺ + D	4.87E-09	-0.50E+00	0.00E+00	< 25%	(2)	C

M, Laboratory measurement

C, Cloned

?, No listing for estimation method, but most likely theoretical

Ion-neutral reactions (Kooji formula): $k = \alpha(T/300)^\beta e^{-\gamma/T}$

Pathways extracted at 1 Myr from four points with T = 10 or 100 K and densities = 10⁴ and 10⁸ cm⁻³ in the ÒPrimordialÓ model

(1) Jensen et al. (2000); (2) OSU www.physics.ohio-state.edu/~eric/; (3) Garrod & Herbst (2006)

Table B5Important reactions for species involved in the main pathways of the assorted deuterated species; H_2D^+ , HD_2^+ , D_3^+ , HDO , D_2O , DCO^+ and DCN .

Formation of species:	Reaction		α	β	γ	Accuracy	Ref	Estimated by
H_2^+	$\text{H}_2 + h\nu_{\text{CR}} \rightarrow \text{H}_2^+ + \text{e}^-$		9.30E-01	0.00E+00	0.00E+00	factor 2	(1)	T
CH_3^+	$\text{H}_3^+ + \text{C} \rightarrow \text{CH}^+ + \text{H}_2$		2.00E-09	0.00E+00	0.00E+00	factor 2	(1)	?
isotopologues	$\text{CH}^+ + \text{H}_2 \rightarrow \text{CH}_2^+ + \text{H}$		1.20E-09	0.00E+00	0.00E+00	< 25%	(1)	?
	$\text{CH}_2^+ + \text{H}_2 \rightarrow \text{CH}_3^+ + \text{H}$		1.20E-09	0.00E+00	0.00E+00	< 25%	(1)	?
	$\text{CH}_3^+ + \text{HD} \rightarrow \text{CH}_2\text{D}^+ + \text{H}_2$		1.30E-09	0.00E+00	0.00E+00	factor 2	(2)	M
	$\text{CH}_2\text{D}^+ + \text{HD} \rightarrow \text{CHD}_2^+ + \text{H}_2$		6.60E-10	0.00E+00	0.00E+00	factor 2	(2)	M
	$\text{CHD}_2^+ + \text{HD} \rightarrow \text{CD}_3^+ + \text{H}_2$		6.60E-10	0.00E+00	0.00E+00	factor 2	(2)	M
	$\text{D}_3^+ + \text{CH}_2 \rightarrow \text{CD}_3^+ + \text{H}_2$		5.19E-11	-0.50E+00	0.00E+00	factor 2	(1)	C
H_2CN^+	$\text{H}_3^+ + \text{HCN} \rightarrow \text{H}_2\text{CN}^+ + \text{H}_2$		1.70E-08	-0.50E+00	0.00E+00	< 25%	(1)	?
HDCN^+	$\text{DCO}^+ + \text{HCN} \rightarrow \text{HDCN}^+ + \text{CO}$		7.30E-09	-0.50E+00	0.00E+00	factor 2	(1)	C
	$\text{DCO}^+ + \text{HNC} \rightarrow \text{HDCN}^+ + \text{CO}$		6.63E-09	-0.50E+00	0.00E+00	factor 2	(1)	C
HDNC^+	$\text{CH}_2\text{D}^+ + \text{N} \rightarrow \text{HDNC}^+ + \text{H}$		4.47E-11	0.00E+00	0.00E+00	< 25%	(1)	C
D_2CN^+	$\text{HD}_2^+ + \text{HCN} \rightarrow \text{D}_2\text{CN}^+ + \text{H}_2$		2.83E-09	-0.50E+00	0.00E+00	factor 2	(1)	C
	$\text{HD}_2^+ + \text{HNC} \rightarrow \text{D}_2\text{CN}^+ + \text{H}_2$		2.50E-09	-0.50E+00	0.00E+00	factor 2	(1)	C
CH_2	$\text{C} + \text{H}_2 \rightarrow \text{CH}_2$		1.00E-17	0.00E+00	0.00E+00	factor 10	(1)	?
	$\text{CH} + \text{H}_2 \rightarrow \text{CH}_2 + \text{H}$		1.20E-09	0.00E+00	0.00E+00	factor 10	(1)	?
CHD	$\text{HD} + \text{C} \rightarrow \text{CHD}$		1.20E-17	0.00E+00	0.00E+00	factor 10	(1)	C
OH	$\text{H}_2\text{DO}^+ + \text{e}^- \rightarrow \text{OD} + \text{H} + \text{H}$		2.60E-10	-5.00E-01	0.00E+00	factor 2	(1)	C
OD^+	$\text{H}_2\text{D}^+ + \text{O} \rightarrow \text{OD}^+ + \text{H}_2$		2.67E-10	0.00E+00	0.00E+00	factor 2	(3)	C
	$\text{H}^+ + \text{OD} \rightarrow \text{OD}^+ + \text{H}$		8.00E-09	-0.50E+00	0.00E+00	factor 2	(1)	C
HDO^+	$\text{OD}^+ + \text{H}_2 \rightarrow \text{HDO}^+ + \text{H}$		7.33E-10	0.00E+00	0.00E+00	< 25%	(1)	C
	$\text{H}_3^+ + \text{OD} \rightarrow \text{HDO}^+ + \text{H}_2$		4.75E-09	-0.50E+00	0.00E+00	factor 2	(1)	C
	$\text{H}_2\text{D}^+ + \text{O} \rightarrow \text{HDO}^+ + \text{H}$		2.28E-10	-1.56E-01	-1.41E+00	factor 2	(3)	C
H_2DO^+	$\text{HDO}^+ + \text{H}_2 \rightarrow \text{H}_2\text{DO}^+ + \text{H}$		4.57E-10	0.00E+00	0.00E+00	< 25%	(1)	C
	$\text{HD}_2^+ + \text{O} \rightarrow \text{D}_2\text{O}^+ + \text{H}$		1.14E-10	-1.56E+00	-1.41E+00	factor 2	(3)	C
	$\text{D}_2\text{O}^+ + \text{H}_2 \rightarrow \text{HD}_2\text{O}^+ + \text{H}$		3.05E-10	0.00E+00	0.00E+00	< 25%	(1)	C

M, Laboratory measurement

T, Theoretical/Calculated

(L) Literature

C, Cloned

?, No listing for estimation method, but most likely theoretical

Ion-neutral reactions (Kooji formula): $k = \alpha(T/300)^\beta e^{-\gamma/T}$ Pathways extracted at 1 Myr from four points with $T = 10$ or 100 K and densities = 10^4 and 10^8 cm^{-3} in the ÒPrimordialÓ model(1) OSU www.physics.ohio-state.edu/~eric/; (2) Smith et al. (1982a,b); (3) Wakelam et al. (2010b)

C. LISTING OF OBSERVED D/H RATIOS IN DENSE INTERSTELLAR ENVIRONMENTS

We have collected and generated an updated listing of observed deuterated species and D/H ratios.

Table C1 Listings of observed interstellar deuterated species.

Species	Sources		Spatial scale Beam size ["]	Refs	Model
	Class -I	Class O/I			
D / H	$< 4 \times 10^{-4}$		1.8°	1	$10^{-3} - 10^{-2}$
--	$\leq 2.7 \times 10^{-5}$			2	--
--	2.2×10^{-5}		14°	3	--
--	≤ 0.14			4	--
HD / H ₂	$0.74 - 8.6 \times 10^{-6}$		30x30	5	$< 10^{-4}$
--	$1.32 - 14.83 \times 10^{-6}$			6	--
ND / NH		0.3 - 1.0	41(ND), 22(NH)	7	$10^{-4} - 10^0$
OD / OH	$\leq 2.5 \times 10^{-3}$		1.8°	8	$10^{-2} - 10^0$
C ₂ D / C ₂ H	0.01		33	9	$10^{-3} - 10^{-2}$
--	0.01	0.18	20	10	--
D ₂ O / H ₂ O		5×10^{-5}	1.5x1.5	11	$< 10^{-5} - 10^{-3}$
DCN / HCN	0.008-0.015			12	$10^{-3} - 10^{-1}$
--	0.012 - 0.11			13	--
--	0.013		20	10	--
--	0.023			14	--
--		0.005 - 0.02		15	$< 10^{-5} - 10^{-3}$
DCO ⁺ / HCO ⁺	0.007 - 0.081			13	$10^{-2} - 10^0$
--	0.02 - 0.18		20	16	--
--	0.006 - 0.04		25-57	17	--
--	0.0086 - 0.015		20	10	--
--	0.031 - 0.059		30-96	18	--
--	≤ 0.03			4	--
--		0.04 - 1×10^{-2}	13 ^b	19	$10^{-4} - 10^{-2}$
DNC / HNC	< 0.014		10 - 30	20	$10^{-3} - 10^{-1}$
--	0.02 - 0.09		~ 20	21	--
--	0.008 - 0.122		17-20 ^a	22	--
--	0.015 - 0.03		20	10	--
H ₂ D ⁺ / H ₃ ⁺		$< 3 \times 10^{-3}$	13 ^b	19	$10^{-4} - 10^{-2}$
HDO / H ₂ O		0.014 - 0.058		23	$10^{-3} - 10^{-2}$
--		≥ 0.01	10-30	24	--
--		$\geq 6 \times 10^{-4}$	3.1×2.5	25	--
--		2.94×10^{-5}	1.5x1.5	11	--
--		0.03	10-33	26	--
--		$0.6 - 5 \times 10^{-4}$		27	--
--		≥ 0.01	20	28	--
HDO / H ₂ O (solid)		0.005 - 0.02		29	$10^{-3} - 10^{-1}$
--		$8 \times 10^{-4} - 10^{-2}$		30	--
HDS / H ₂ S	0.05 - 0.15		20	10	$10^{-2} - 10^{-1}$
N ₂ D ⁺ / N ₂ H ⁺	0.016 - 0.051		~ 30	31	$10^{-2} - 10^0$
--	0.01 - 0.16		10-20	32	--
--	0.03 - 0.04		26.4 ^a	33	--
--	0.11		44	34	--
--	0.08 - 0.14		18 ^a	35	--
--	0.02 - 0.52		11 ^a	36	--
--	~ 0.1		9-26 ^a	37	--
--	0.08 - 0.35		20	16	--
--		0.005 - 0.014	11-26 ^a	38	$10^{-4} - 10^{-2}$
--		0.033 - 0.271	11-16	39	--
--		0.003 - 0.027	9-26 ^a	40	--
D ₂ CO / H ₂ CO	0.11 - 0.19		27 ^a	41	$10^{-3} - 10^{-2}$
--	0.40			42	--
--	0.01 - 0.1		17	43	--
--	≤ 0.07		22	44	--
--	$2.05 - 3.3 \times 10^{-2}$		20-60	45	--
--		0.01 - 0.04	20-60	46	--
--		0.022 - 1.04	10-30	47	$10^{-5} - 10^{-3}$
--		0.02 - 0.4		48	--
--		0.03 - 0.16		49	--
D ₂ CS / H ₂ CS	0.333			50	$10^{-3} - 10^{-1}$
HDCO / H ₂ CO	0.092 - 0.122		27 ^a	41	$10^{-3} - 10^{-1}$
--	0.015		20	10	--
--		0.07 - 4.3	10-30	47	$10^{-4} - 10^{-2}$
--		0.09 - 2.6	20-60	45	--
HDCS / H ₂ CS	0.333			42	$10^{-2} - 10^{-1}$
--	0.015 - 0.025		> 60	51	$10^{-2} - 10^{-1}$
ND ₃ / NH ₃	$1.1 - 65 \times 10^{-4}$		22 ^b	52	$< 10^{-5} - 10^{-3}$
--	8×10^{-4}		25	53	--
--		9.35×10^{-4}	25	54	$< 10^{-5} - 10^{-4}$
NH ₂ D / NH ₃	0.1 - 0.8		7	55	$10^{-3} - 10^{-1}$

Species	Sources		Spatial scale Beam size ["]	Refs	Model
	Class -I	Class O/I			
--	0.07 - 0.42		22 ^b	52	--
--	0.02 - 0.1		20	16	--
--	0.025 - 0.18		18	56	--
--	< 0.02		20	10	--
--		< 0.1	7	55	10 ⁻⁴ - 10 ⁻²
--		0.071	~ 20	57	--
--		0.06 - 0.1	22	44	--
--		0.04 - 0.33	37	58	--
--		0.06 - 0.1	20	10	--
--		0.06	20	28	--
--		2.6 - 17.3 × 10 ⁻²	20-60	45	--
NHD ₂ / NH ₃	0.03 - 0.27		22 ^b	52	10 ⁻⁴ - 10 ⁻¹
--	~ 5 × 10 ⁻³		22	44	--
--		0.02 - 0.4		59	< 10 ⁻⁵ - 10 ⁻³
C ₃ HD / C ₃ H ₂	0.05 - 0.15		1.7 ^a ^b	60	10 ⁻³ - 10 ⁻¹
C ₄ D / C ₄ H	4.30 × 10 ⁻³		1.7 ^a ^b	61	10 ⁻³ - 10 ⁻²
--		0.0043-0.023	17-28	62	--
C ₄ HD / C ₄ H ₂		0.013 - 0.051	17-28	62	10 ⁻³ - 10 ⁻¹
CD ₃ OH / CH ₃ OH		0.001 - 0.028	15	63	< 10 ⁻⁵ - 10 ⁻²
C ₃ H ₃ D / C ₃ H ₄	0.04 - 0.18		40-60	64	10 ⁻³ - 10 ⁻¹
--	0.1 - 0.22		40	65	--
--	0.05 - 0.06		27 ^a	66	--
CH ₂ DCN / CH ₃ CN		≥ 0.01	27 ^a	67	10 ⁻² - 10 ⁻¹
CH ₂ DOH / CH ₃ OH		0.01 ± 0.73	17-28	62	10 ⁻³ - 10 ⁻²
--		0.05 - 0.30		68	--
--		0.05 - 0.95	10-30	47	--
--		0.60 - 1.2	11-30	69	--
CH ₃ OD / CH ₃ OH		0.008 - 0.076	10-30	44	10 ⁻⁴ - 10 ⁻²
--		0.02 - 0.06	11-30	69	--
--		≤ 0.1	20	10	--
CHD ₂ OH / CH ₃ OH		0.06 - 0.051	10-30	47	10 ⁻³ - 10 ⁰
--		0.1 - 0.3	11-30	69	--
DC ₃ N / HC ₃ N	0.010 - 0.020			70	10 ⁻³ - 10 ⁻²
DC ₃ N / HC ₃ N		0.02 - 0.045	17-28	62	10 ⁻⁴ - 10 ⁻³
DC ₅ N / HC ₅ N	0.006 - 0.016			71	10 ⁻³ - 10 ⁻²
DC ₅ N / HC ₅ N		0.018 - 0.036	17-28	62	10 ⁻⁵ - 10 ⁻³
--	0.013 - 0.019			72	--
DCOOCH ₃ / HCOOCH ₃	0.02 - 0.06			73	10 ⁻³ - 10 ⁻¹
--	~ 0.15		9-33	71	--

Young stellar object IR classification -I: Prestellar objects, O/I: Embedded/revealed protostellar sources

(a) Half-power beam width (HPBW)

(b) Full-width half-maximum (FWHM)

(c) LWRS

- (1) Cesarsky et al. (1973); (2) Hébrard (2006); (3) Rogers et al. (2007); (4) Heiles et al. (1993); (5) Lacour et al. (2005)
(6) Snow et al. (2008); (7) Bacmann et al. (2010); (8) Allen et al. (1974); (9) Friberg & Hjalmarson (1986); (10) van Dishoeck et al. (1995)
(11) Butner et al. (2007); (12) Parise et al. (2007); (13) Lis et al. (2002a); (14) Wootten (1987); (15) Mangum et al. 1991)
(16) Tiné et al. (2000); (17) Anderson et al. (1999); (18) Butner et al. (1995); (19) Stark et al. (1999); (20) Goicoechea et al. (2009)
(21) Hirota et al. (2003); (22) Hirota et al. (2001); (23) Coutens et al. (2012); (24) Liu et al. (2011); (25) Jørgensen & van Dishoeck (2010)
(26) Parise et al. (2005); (27) Gensheimer et al. (1996); (28) Jacq et al. (1990); (29) Parise et al. (2003); (30) Teixeira et al. (1999)
(31) Chen et al. (2010); (32) Friesen et al. (2010); (33) Miettinen et al. (2009); (34) Fontani et al. (2008); (35) Belloche et al. (2006)
(36) Crapsi et al. (2005); (37) Crapsi et al. (2004); (38) Alonso-Albi et al. (2010); (39) Emprechtinger et al. (2009); (40) Fontani et al. (2006)
(41) Bergman et al. (2011); (42) Marcelino et al. (2005); (43) Bacmann et al. (2003); (44) Roueff et al. (2000); (45) Turner (1990)
(46) Roberts & Millar (2007); (47) Parise et al. (2006); (48) Loinard et al. (2002); (49) Ceccarelli et al. (2001); (50) Marcelino et al. (2005)
(51) Minowa et al. (1997); (52) Roueff et al. (2005); (53) Lis et al. (2002b); (54) van der Tak et al. (2002); (55) Busquet et al. (2010)
(56) Saito et al. (2000); (57) Shah & Wootten (2001); (58) Hatchell (2003); (59) Loinard et al. (2003); (60) Bell et al. (1988)
(61) Sakai et al. (2009); (62) Suzuki (1987); (63) Parise et al. (2004); (64) Markwick et al. (2005); (65) Markwick et al. (2002)
(66) Gerin et al. (1992a); (67) Gerin et al. (1992b); (68) Bacmann et al. (2007); (69) Parise et al. (2002); (70) Suzuki (1987)
(71) MacLeod et al. (1981); (72) Schloerb et al. (1981); (73) Margulès et al. (2010)